AERODYNAMIC AND STRUCTURAL OPTIMIZATION OF VERTICAL AXIS WIND TURBINE

BY

Ali Salman Alhamaly

A Thesis Presented to the

DEANSHIP OF GRADUATE STUDIES

KING FAHD UNIVERSITY OF PETROLEUM & MINERALS

DHAHRAN, SAUDI ARABIA

In Partial Fulfillment of the
Requirements for the Degree of

MASTER OF SCIENCE

In

MECHANICAL ENGINEERING

May 2018

KING FAHD UNIVERSITY OF PETROLEUM & MINERALS

DHAHRAN- 31261, SAUDI ARABIA

DEANSHIP OF GRADUATE STUDIES

This thesis, written by **Ali Salman Alhamaly** under the direction of his thesis advisor and approved by his thesis committee, has been presented and accepted by the Dean of Graduate Studies, in partial fulfillment of the requirements for the degree of **MASTER OF SCIENCE IN MECHANICAL ENGINEERING.**

Dr.Zuhair M. Gasem
Department Chairman

Dr. Ahmet Sahin
(Advisor)

Dr. Salam A. Zummo
Dean of Graduate Studies

Dr. Farooq Saeed
(Member)

10/5/13

Date:

Dr. Hassen Ouakad
(Member)

Dedication

This thesis is dedicated to my family who has continuously supported and encouraged me throughout my master program journey

ACKNOWLEDGMENTS

I would like to start by thanking my thesis committee members for their great effort, guidance, and contribution to this thesis. I would like to thank my advisor, Dr. Sahin for his guidance and encouragement throughout my research journey at KFUPM. I have definitely enjoyed the discussions we had both in class and out of class. I would like as well to thank Dr. Ouakad for his enthusiasm and kind words about my work and his kind words. I learned a lot from him during the short period of time that we get to know each other. Special thanks go to Dr. Saeed for his instrumental and influential role in this research. I would like to thank him for all time he has spent in developing the ideas that led to the framework of this research. I learned a lot of insights about the aerodynamics of vertical axis turbine throughout the numerous discussions we had during his time at KFUPM and latter at IAU. I certainly have enjoyed his mentorship throughout my graduate school time.

The final thank goes to my family and close friends who have been a continuous source of encouragement to me during my graduate studies. They have given me the motivation to continue my endeavors in the research at toughest of times.

TABLE OF CONTENTS

LIST OF TABLES

LIST OF FIGURES

LIST OF ABBREVIATIONS

HAWT	:	horizontal axis wind turbine
VAWT	:	vertical axis wind turbine
AEP	:	annual energy production
DMST	:	double multiple stream tube
LCOE	:	levelized cost of energy
COE	:	cost of energy
AC	:	actuator cylinder
TSR	:	tip speed ratio
DLC	:	design load case
MW	:	mega watt
hr	:	hour

ABSTRACT

Full Name : Ali S. Alhamaly

Thesis Title : Aerodynamic and Structural Optimization of Vertical Axis Wind Turbine

Major Field : Mechanical Engineering

Date of Degree : May 2018

The scope of this thesis is to develop a method for the aerodynamic and structural optimization of vertical axis wind turbine (VAWT) and implement it in the design of a multi-megawatt VAWT that yields low cost of energy. Determination of the optimum design requires a delicate balance between maximizing the energy produced from the turbine and minimizing the amount of material used to build the turbine. Thus, a coupled analysis that combines both aerodynamics and structural mechanics of the turbine is needed to discover this delicate balance. State of the art simulation tools are used to simulate the coupled aerodynamic and structural response of the turbine in the time domain. These tools include HAWC2 and BECAS codes developed at the Denmark Technical University, Department of Wind Energy (DTU Wind Energy). These simulation tools are interfaced with MATLAB numerical optimization routines to find the shape and internal structural makeup of the turbine rotor that gives the optimum cost based on a defined objective function and constraints. Several optimum designs are obtained using the present optimization framework. Some designs are obtained by coupling the aerodynamic and structural variables employing a single multi-disciplinary objective function. Other designs were obtained by sequentially varying the aerodynamic and structural variables by employing a sequence of single discipline objective functions. Final results show that the coupled

approach results in lower cost of energy, while the sequential approach gives higher annual energy production at slightly higher cost.

ملخص الرسالة

الاسم الكامل:علي سلمان الحمالي

عنوان الرسالة: التحسين الهوائي والهيكلي لتوربينات الرياح ذات المحور الرأسي

التخصص: الهندسة الميكانيكة

تاريخ الدرجة العلمية: شعبان 1439

نطاق هذه الأطروحة هو تطوير إطار عددي لتحسين تصميم توربين الرياح ذات المحورالرأسي. هدف هذه الأطروحة هو الوصول لتصميم توربين يخفض تكلفة الطاقة. يتطلب تحديد التصميم الأمثل توازناً دقيقاً بين إنتاج أقصى كمية من الطاقة المنتجة من التوربين وتقليل كمية المواد المستخدمة لبناء التوربين. وبالتالي ، هناك حاجة إلى إجراء تحليل مزدوج يجمع بين الديناميكيات الهوائية والميكانيكية الهيكلية للتوربين لاكتشاف هذا التوازن الدقيق.في هذه الأطروحة تستخدم أدوات محاكاة حديثة لمحاكاة الديناميكية الهوائية والهيكلية للتوربين. هذه الأدوات المستخدمة تم تطويرها في جامعة الدنمارك التقنية ، قسم طاقة الرياح. أدوات المحاكاة هذه تم دمجها مع هيكلية التحسين الرقمي لإيجاد الشكل والتركيب الهيكلي الداخلي للتوربين الذي يعطي التكلفة المثلى على أساس الهدف المحدد والقيود. تم الحصول على العديد من التصاميم المثلى باستخدام إطار التحسين الحالي. تم الحصول على بعض التصاميم من خلال اقتران المتغيرات الديناميكية والهيكلية باستخدام هدف متعدد التخصصات. تم الحصول على تصميمات أخرى عن طريق تغيير المتغيرات الإيروديناميكية والهيكلية بالتسلسل عن طريق استخدام سلسلة من الأهداف الفردي. تشير النتائج النهائية إلى أن الهدف متعدد التخصصات يؤدي إلى تصاميم ذات التكلفة الأقل ، بينما يعطي النهج المتسلسل إنتاجًا سنويًا أعلى من الطاقة بتكلفة أعلى قليلاً من الهدف متعدد التخصصات.

CHAPTER 1

INTRODUCTION

Wind energy is one of the most important renewable energy sources available today. At the end of 2017, the total power capacity added from wind energy alone accounted for 52 GW. This is equivalent to 33% of all capacity added from renewable sources excluding large hydro projects[1]. Also, the total added wind energy capacity accounted for 20.2% of all power generation capacity in 2017 [1]. The global wind power capacity at the end of 2017 was about 539 GW, a 45.8% increase compared with the end of 2014[2]. It is also projected that the total installed capacity of wind power by 2020 could reach between 639 – 879 GW [3]. The magnitude of wind energy capacity installation indicates how wind energy is becoming an essential energy source for green energy. In terms of cost, the onshore wind power at the end of 2017 had the least global average levelized cost of electricity (LCOE) for a renewable source at $67 per MWh. This is a reduction of 27% compared with the cost in 2009 [1]. Also. The capital cost of wind power is expected to decrease by 35% and 26% for offshore and onshore respectively by 2025 [3]. The expected capacity growth and cost reduction of wind power require active research and development in the area of wind turbine design to produce wind turbines with high energy production at a low cost of ownership.

Wind turbines are devices used to convert wind energy into useful power by means of converting the kinetic energy in the wind into rotational energy in the turbine rotor. There are two main types of wind turbines: the horizontal axis wind turbine (HAWT) in which the axis

of rotation is parallel with the direction of the wind, and vertical axis wind turbine (VAWT) in which the axis of rotation is perpendicular to the direction of the wind.

Comparing the magnitude of wind turbine installation between HAWT and VAWT, it can be seen that HAWT is the main turbine configuration adopted by the industry and is almost the only installed type for utility-scale power generation. On the other hand, VAWT industrial focus and academic research almost disappeared in the mid-1990s when FloWind Company closed its doors due to financial issues [4]. In addition, almost all of the US DOE-sponsored research for VAWT was terminated [4]. From that time onwards VAWTs fell out-of-favor within the wind turbine community, and commercial VAWTs were not pursued past basic research.

The interest in VAWT has been renewed lately in the research community because of the need to exploit off-shore wind resources. VAWT has potential advantages over HAWT in off-shore applications. These advantages make it possible to reduce the life cycle cost of an off-shore VAWT wind farm compared to HAWT [4]–[8]. Some of these advantages includes: low center of gravity of VAWT due to placement of drive train and generator at the bottom, the simple rotor design, the elimination of yaw actuator due to the insensitivity to wind directions, the elimination of pitch actuator in the blade, and the ability to scale the rotor without necessarily increasing the maximum radius [4]–[6]. A pictorial comparison between HAWT and VAWT configurations and their cost implication is shown in Figure 1.1 [5].

Lately, several research projects were undertaken to exploit the advantages of VAWT in off-shore applications such as DeepWind, S4VAWT, Aerogenerator, and Nenuphar [9]–[11].

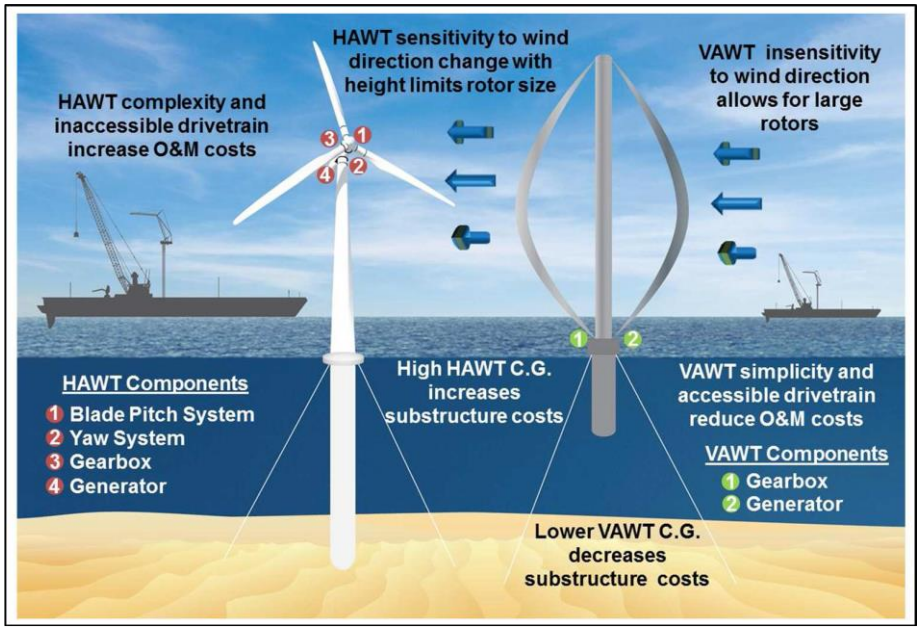

Figure 1.1: Comparison between VAWT and HAWT in off-shore applications and the cost implication of each configuration [5].

The significant growth of wind energy capacity globally and the need to produce wind turbines with minimum cost provides the primary motivation for this research. The aim of this research is to devalop an optimization framework for VAWT that produce designs with low cost of energy. The cost of energy is assessed in this work by comparing the annual energy production (AEP) with the blade mass. VAWT optimum designs are obtained based on choosing the variables affecting the performance and blade mass, using simulation tools that take into account the effect of these variables on the performance and blade mass, and then suitably finding the combination of these variables that achieve the design objectives through numerical optimization.

This thesis is organized as follows. CHAPTER 2 begins with a literature review on HAWT and VAWT optimization. State of the art optimization techniques used by researchers are identified in the literature review in an attempt to implement best practices of wind turbine optimization in this work. The chapter concludes with learning outcomes from the literature review and comparison between the level of complexity between HAWT and VAWT optimization

studies. CHAPTER 3 discusses the aerodynamic and structural analysis tools used for VAWT. The chapter gives a general overview of the available codes for VAWT and describes in details the analysis tools used for this thesis. CHAPTER 4 describes the optimization framework used to find optimum VAWT designs. The chapter describes in details the objective functions, constraints, design variables, and optimization workflow. CHAPTER 4 discusses how the different analysis tools are combined with the numerical optimizer to evaluate the objective function and constraints. CHAPTER 5 presents the results of the optimization in terms of several optimum designs that are obtained for different objective functions and different parameters. The chapter discusses the results and highlights the trends in the optimum designs. CHAPTER 6 concludes the work of this thesis, suggests several improvements to the current work, and provide recommendations for further research in the area of VAWT optimization.

CHAPTER 2

LITERATURE REVIEW

This chapter presents a comprehensive literature review on horizontal axis wind turbine (HAWT) and vertical axis wind turbine (VAWT) optimization studies. In the literature researchers use several optimization techniques, objective functions, constraints, design variables, and simulation tools to perform optimization. This chapter aims to give a broad overview and summary of research litriture to gain insights for use in this research work. The chapter starts by reviewing optimization studies on HAWT followed by studies on VAWT and will conclude with a section on the learning outcomes from this literature review.

2.1 HAWT Optimization Studies

Ning et al. [12], [13] presented a critical evaluation of the objectives and constraints that are used in HAWT optimization studies. The work focuses mainly on three different type of objectives to optimize HAWT and their implication on the final results. The three objectives are: maximizing the annual energy production (AEP), minimizing the ratio of turbine mass to annual energy production, and minimizing the cost of energy (COE). A set of structural constraints accompanies these objectives. The objective is to understand how different choices of simulation models impact the quality of the solutions, how various optimization objectives are appropriate, when specific objectives and constraint are necessary, and what their limitations are.

The aerodynamic analysis of the turbine in Ning et al. [12], [13] is carried out using a new technique for the Blade Element Momentum (BEM) method. The new technique ensures that the solution is continuously differentiable, a feature which is an essential consideration when using gradient-based optimizer. The model considers annual wind speed distribution based on a Rayleigh distribution with 10 m/s mean wind speed.

The structural analysis of the turbine used by Ning et al. [12], [13] is based on beam finite element analysis code called pBEAM (polynomial beam element analysis module). The National Wind Technology Center's PreComp code [14] is used to estimate the cross-sectional properties of composite blades such as inertia and stiffness. Simplistic edgewise gravity load is used to estimate fatigue loading on the root section of the blade. This simplistic approach is added to limit the minimum chord length at the chord of the blade.

The basis of the cost model used by Ning et al. [12], [13] is the work of Fingersh et al. [15] but with modification to the tower mass and balance of station models. The reference wind turbine used for comparison is the NREL-5MW wind turbine [16]. Five chord lengths, four twist angles, and three spar cap thicknesses parametrize the rotor geometry. The specific optimizer used is thr MATLAB built-in function *fmincon*. The constraints of the optimization problem are maximum strain on the blade, spar cap buckling limit, maximum tip deflection, the maximum blade passing frequency, and maximum fatigue loading on the root section. The design variables used during optimization are chord length (at five locations), twist angle (at four locations), spar cap thickness (at three locations), tip speed ratio, rotor diameter, and power rating of the turbine.

Several objective functions are considered by Ning et al. [12], [13]. The first objective is AEP maximization achived by changing chord lengths, twist angles, and the tip speed ration with constraints related only to the blade mass. Once AEP is maximized, the blade mass is

minimized by changing the thickness of the spar cap while using the previously mentioned structural constraints. The second objective is to minimize the whole blade mass first by changing chord length, and spar cap thickness subjected to the structural constraints and then maximizing AEP by changing the twist distribution and the tip speed ratio while constraining the maximum blade tip speed. The third and last objective is to minimize COE by changing chord length, twist angles, spar cap thickness, and the tip speed ratio subjected to the structural constraints. In all of the above three objectives, the rotor diameter and all subcomponents are kept fixed. The results indicate that maximizing AEP first and minimizing COE afterwords lead to increase in AEP and decrease in COE compared to the reference turbine. Minimizing the mass first leads to decrease in both COE and AEP. Between AEP and COE objectives, minimizing COE yields better overall results although AEP increase is slightly lower compared to AEP objective.

Another objective function motivated by the first three objectives is to minimize the ratio of total turbine mass to AEP. Several designs are obtained using this new objective with different rotor diameters. The results of this objective are compared with COE objective. Design with a minimum ratio of total turbine mass to AEP objective gave COE values that are higher than minimum COE objective at all rotor diameters that are larger than the reference diameter. This is because minimizing the ratio of total turbine mass to AEP objective overemphasizes the tower mass over other turbine subcomponents. However, the tower cost is only a small portion of the total turbine cost. Hence reducing the tower mass does not lead to significant overall turbine cost reduction. The study suggests that minimizing the ratio of total turbine mass to AEP while fixing the tower and nacelle masses is better objective function since it removes the incentive of the optimizer to minimize the tower mass, especially when comparing designs at different diameters.

In summary, maximizing AEP without some constraints on the blade mass lead to a design with high COE. The reason for the high COE is that similar optimum aerodynamic performance can be achieved using different rotor masses. Minimizing the blade mass and then optimizing airfoil section and twist distribution is not much advantageous than maximizing AEP alone. COE is a superior objective function that leads to balanced designs in terms of both aerodynamic and structural considerations.

Xudong et al. [17] studied cost optimization of horizontal axis wind turbine by changing the main shape of the turbine rotor. The objective was to minimize the cost of energy (COE) based solely on the rotor cost. The aerodynamic model used is a 1-D blade element momentum (BEM) with tip loss correction. An aero-elastic code was used to model the blade flapwise and edgewise deflection in addition to rotor axial displacement. The cost of the rotor is modeled relative to the reference case rotor in which blade mass determines the relative increase or decrease in rotor cost. Three reference turbines are chosen for optimization. For each optimization, the rotor diameter, rotor speed, and rotor airfoil remained unchanged from the base rotor. The design variables are the chord length, twist angle, tip pitch angle, and relative thickness. These variables have bound constraints that are derived based on the reference rotor. Also, maximum thrust and torque are limited by the maximum thrust and torque of the reference rotor. The annual wind speed distribution is calculated using Rayleigh distribution. From the calculated annual wind speed, AEP is calculated. The optimizer used is the gradient-based MATLAB function *fmincon*. Results of optimization for all the three rotors indicate a reduction in annual energy production compared with the reference case. However, the cost of energy for all three rotors decreased which is the desired outcome.

Fuglsang and Thomsen [18] reported cost optimization of horizontal axis wind turbine placed in an off-shore wind farm. The aerodynamic and aeroelastic analysis [19] accommodates turbulent wind flow based on the actual site of the wind farm. The objective function is to

minimize COE for a wind turbine in an off-shore wind farm. The cost of the turbine is based on the different component masses which are obtained relative to the reference turbine by simple linear scaling. The design variables used in cost optimization are: hub height, rotor speed, rotor diameter, and rated power. Optimization of the cost is carried out for two locations: standalone onshore turbine, and offshore turbine placed in the middle of a densely spaced farm. Results of optimization show COE reduction of 3.3 % and 11% for the onshore and offshore turbine respectively relative to the reference turbine. Optimization results indicate an increase in rotor diameter and a decrease in rotor speeds. Also, the capital cost of each optimized turbine is increased, but the increase in annual energy production outweigh the capital cost increase leading to designs with a lower overall cost of energy. It is worth noting that the optimized onshore turbine achieves a lower cost of energy compared with the optimized offshore turbine. In an effort to lower the COE for the offshore turbine, the authors perform optimization for a turbine placed in a loosely spaced farm. Results show that this turbine achieves COE similar to the onshore turbine at the same rated maximum power. The reason for this additional decrease in cost is the reduced fatigue load on the turbine placed in loosely spaced farm due to operation in a mild turbulent wake.

Yu et al. [20] describe a method for aerodynamic shape optimization of HAWT considering aeroelastic deformation effects. The aerodynamic analysis is carried out using 3D CFD simulation of the rotor, and the aeroelastic analysis is based on a second-order nonlinear isotropic Euler-Bernoulli cantilevered beam undergoing deformation with each beam having 15 degrees of freedom. The aerodynamic and aeroelastic analyses are coupled such that the deformation of the blade is taken into account when aerodynamic forces are calculated. The objective of optimization is to maximize the lift to drag ratio of a 2-D sectional airfoil along the span of the blade by changing the shape of the airfoil itself. Nine different shape parameters are used to describe the airfoil shape using PARSEC shape function (PARSEC is a method to

parameterize the airfoil contour using shape functions). The parameters of PARSEC shape functions are used as the design variables for the optimizer. Three design constraints are imposed: airfoil thickness and drag are not allowed to decrease below the reference airfoil values, and the area of the airfoil are held fixed with respect to the reference airfoil. The optimization process is divided into two parts: coupled 3D aerodynamics and aeroelastic analysis and a 2D CFD sectional airfoil optimization. The coupled 3D analysis gives the inflow condition at the selected design sections along the span; then the 2D analysis uses the inflow condition as an input flow field to find the shape of the airfoil that gives the maximum lift to drag ratio. The optimization is carried out for two turbines at one wind and rotor speeds. The two turbines are NREL phase VI rotor blade and NREL 5MW reference rotor blade. Results of optimization for both turbines show an increase in torque compared with the reference cases. The bending moment and thrust force also show an increase compared with the reference. The unusual thing is that the optimized rotors yield higher performance in off-design conditions as well.

Ashuri et al. [21] present multidisciplinary optimization of an offshore HAWT. The optimization integrates the aerodynamic and structural analysis of the rotor and turbine tower. The objective of optimization is to minimize the COE. The base case used for comparison is the 5MW NREL wind turbine [16]. The rotor is optimized by varying 18 design variables. These are: the four chord lengths, two twist angles, three spar thicknesses, four shell thicknesses, three web thicknesses, rotor rotational speed, and blade length. The tower is optimized by varying five design variables: tower diameter at the bottom (interface) and top (connection to nacelle), tower thickness at the bottom and top, and tower height. To enable smooth interpolation of the design variables along the span of the blade, some geometric properties of the blade are held constant. Design constraints include maximum flapwise tip deflection, maximum flapwise and edgewise ultimate and fatigue stresses. The computational

tools used in aerodynamic, structural and cost analysis are NREL open-source wind turbine design tools: AeroDyn [22] and FAST [23]. The cost of different components of the turbine is calculated using the mass models of Fingresh et al. [15]. The optimization is carried out in a bi-level fashion in which two sequential optimizations are performed. In the first level, the blade length, tower height, and rotational speed are varied while other variables remained constant. In the second level, only the variables in the first level are held constant while all other variables are varied. A gradient-based optimization algorithm is used in both levels. Note that since the objective function is minimizing the COE, this necessitates a multidisciplinary optimization since COE depends on the mass of all turbine components as well as on the aerodynamic performance. The results of optimization indicate a reduction of 2.3% in the levelized cost of energy compared with 5MW NREL case. The optimized design has 3.6% longer blade, 4.2% heavier rotor, 2.5 % higher rated rotational speed, 5.7% higher tip speed, and more massive and taller tower. The results reveal that the most important driving design constraints are the tip deflection and the rotor and tower fatigue stresses.

Zahle et al. [24] present a multidisciplinary HAWT optimization framework that aims to maximize the AEP of a turbine without increasing its blade mass nor significantly increasing the ultimate and fatigue loads on various turbine components. The authors developed HAWTOpt2, which is an aero-structural optimization framework and used it to carry out the optimization problem and to interface with various analysis tools such as HAWC2 [25] and BECAS [26]. The design variables used to optimize the blade include chord, twist, and airfoil thickness distribution along the blade length, total blade length, blade per bend and pre-cone, tip speed ratio, and internal composite layup thickness. The study uses a total of 60 design variables. Constraints used in the optimization are mainly structural and are used to limit the blade mass, bending moments at blade root and tower bottom, and the ultimate strain failure. The reference blade used to compare the optimized design is the DTU 10MW RWT blade [27].

Results of the multidisciplinary optimization show that the optimized blade achieves an increase in AEP of 8.7% relative to the reference blade. Also, all extreme and lifetime loads of the optimized blade were within 5% from the reference blade except for the blade root torsion fatigue which increased by 15%. The increase in AEP was achieved mainly by the increase in the blade radius. An interesting takeaway from this study is the ability of the optimizer to aeroelastically tailor the blade to have lower torsional stiffness near the tip of the blade which is essential in unloading the tip at higher wind speeds to satisfy the structural constraints. The critical point here is that no information was given to the optimizer to figure out aeroelastic tailoring. It is the multidisciplinary design approach which aims to maximize the objective function and satisfy the constraints that led to such automatic tailoring as a mean to achieve an optimal design.

The studies presented above for HAWT optimization do not comprise an exhaustive list for all the major work in the field but give a glimpse on the state of the art of HAWT optimization. Details of other optimization studeis on HAWTs can be found in [28]–[30].

2.2 VAWT Optimization Studies

Carrigan et al. [31] studied torque optimization of VAWT by changing the airfoil shape and solidity at a constant tip speed ratio of one. The airfoil shape family that the optimizer chooses from is NACA 4 digit series. The optimization considers both symmetrical and cambered airfoils. The airfoil shape was parametrized using three parameters. The aerodynamic analysis was done using 2-D CFD simulation of the turbine. Spalart-Allmaras turbulence model was used with second-order implicit time integration in the CFD solver. Stochastic direct search optimization method is the algorithm of choice for this study. Optimization is carried out at both constant and variable solidity. In both cases, the tip speed ratio is kept at one. Results using constant solidity indicated a cambered airfoil with a thickness lower than the reference

case (reference case is NACA 0015). On the other hand, results with variable solidity lead to a symmetrical airfoil that has higher thickness than NACA 0015. Although the optimization was done at tip speed ratio of one, analysis of the optimized designs at several tip speed ratios indicated that higher performance isachieved at tip speed ratio higher than one.

Paulsen et al. [32] studied mass and stiffness optimization of VAWT blade for a large 5-MW offshore turbine. No actual optimization is performed, but the study investigates variations in airfoil section and chord length along the length of the blade. The results suggest that, compared with constant chord case (the reference case), variation in the chord and airfoil produce designs with lower blade mass and also lower loads.

Kumar et al. [33] studied low Reynolds number VAWT for application on Mars. Kumar et al. designed and optimized the rotor based on maximum power coefficient constrained by a minimum power at design wind speed. Aerodynamic analysis was done using CARDAAV code which is based on the double multiple stream tube (DMST) model. CFD simulation with transition model was used to predict the lift and drag coefficients for the NACA 0018 airfoil. The design variables used are rotor solidity and radius to height ratio. The design is also constrained to minimize the swept area, but the study gives no details on how this constraint is achieved. The number of blades is fixed at 2. Different optimum designs are produced at tip speed ratios equal to (3, 3.5, and 4). NACA 0018 airfoil is used throughout the blade for all designs. The optimization is done in sequential order: first, radius to height ratio is optimized at two different solidities. Second, at the optimal radius to height ratio, the solidity is varied to find the optimum solidity that maximized the power coefficient.

Bedon et al. [34] studied the optimization of small vertical axis wind turbine using chord length, rotor speed, and airfoil thickness as design variables. The aerodynamic analysis is carried out using blade element momentum (BEM) method that is based on double multiples stream tube

(DMST) theory. The optimizer used is a multi-objective genetic algorithm implemented in MATLAB by using the function *gamultiobj*. The study considered symmetrical airfoils with arbitrary thickness. Aerodynamic characteristic of arbitrary thickness symmetrical airfoil is obtained by interpolating existing airfoil data at various thicknesses. The study considers four different objective functions. These objectives are: (1)maximizing power coefficient at fixed rotor speed for a range of wind speed, (2)maximizing power coefficient at fixed rotor and wind speed, (3)multi-objective maximization of both power and power coefficient using variable rotor speed at several wind speed, and (4)maximizing annual energy production using variable rotor speed and wind speed distribution described by Weibull distribution. The study uses the 2-meter diameter Sandia VAWT as a reference. The experimental data for the reference turbine is obtained from Sheldahl [35]. In all optimization, the airfoil chord and thickness are varied (wind and rotor speed also depending on the optimization) while keeping the original Sandia rotor dimensions and number of blades. The study demonstrates the capability of the optimizer to produce designs with better performance compared with the original Sandia reference turbine. In general, the optimized turbine uses airfoils with higher thickness and longer chord length compared with reference turbine. Also, the study shows that the optimum designs for maximum power at a given wind speed range and maximum annual energy production are different due to differences in the objective function.

In a later work, Bedon et al. [36] extended their previous paper by considering optimization based on chord and thickness distributions along the span of the blade instead of just optimizing a single value throughout the blade span. The analysis method is precisely the same as in Bedon et al. [34]. The study considers a multi-objective function which attempts to maximize both power coefficient at 9 m/s and total power at 12 m/s. The results of the optimization show that both power coefficient and overall AEP of the optimized turbine has increased compared with the reference design.

In another study by Bedon et al.[37], the authors perform a numerical investigation of the aerodynamic performance of FP7 DeepWind rotor. The authors study the effects of varying the number of blades, blade airfoils, and the chord distribution. The rotor configuration for the DeepWind rotor is the one reported by Paulsen et al. [32] which is an improved rotor from the 1st baseline FP7 DeepWind. The study uses a code based on DMST for the aerodynamic analysis. Increasing the number of blades from the base rotor (two blades) lead to significant enhancement regarding smoothing the variation of the tangential force with turbine rotation. The normal force variation with turbine rotation is also reduced in the case of four blades. However, the three blade case gives rise to more normal force variation compared with the reference rotor. The study investigates the effect of changing the airfoil type using four different NACA airfoils (0015, 0018 (reference), 0021, and 0025). Using NACA 0015 gives rise to an enhancement in the power generation compared to all the other airfoil. NACA 0021 and 0025 led to a reduction in the amount of power generation but they are advantageous from the cyclic loading, since using these airfoils gives rise to a significant reduction in the normal and tangential force variation. The original airfoil (NACA 0018) performance is very similar to the NACA 0015 with slightly lower power production. The optimal chord distribution was found using genetic algorithm optimization aiming at maximizing the energy production for wind speeds around 14 m/s. The optimization considers the base rotor initial parameters except for the chord which is varied. Results of optimization indicate larger chord everywhere along the span the blade. The resulting optimized rotor gave 66.3% increase in the maximum power compared to the base rotor. It is worth noting here that the resulting optimized rotor is subjected to significantly higher normal and tangential forces both in terms of their mean and cyclic values.

Paraschivoiu et al. [38] presented power optimization of a straight bladed VAWT by using variable pitch. The aerodynamic analysis was done using CARDAAV code which is based on

DMST. A genetic algorithm was used to optimize the pitch angle sequence. The blade pitch angle curve is parameterized in terms of three parameters. These parameters are the design variables that the optimizer changes to achieve an optimum solution. The objective function used is to maximize the power at one wind and rotor speed corresponding to a tip speed ratio of 5.3. Results of optimizing the blade pitch sequence indicate an increase of about 21% in power compared to the case of zero pitch (reference case). The study shows that the enhanced performance does not extend far beyond the design point (tip speed ratio of 5.3) and falls off rapidly for higher wind. Nevertheless, results show an increase in AEP of 30% compared with reference case. AEP is calculated with Rayleigh distribution of wind speed with a mean of 6 m/s.

Song et al. [39] presented optimization of a novel drag-based VAWT. The optimization focuses on three different shape parameters of the blade. These parameters are the radius of curvature, the installation angle, and the central angle of the small arc. The intent is to maximize the power coefficients at a fixed wind and rotor speed by changing the shape parameters mentioned above. 2-D CFD simulations were used to obtain the aerodynamic performance of the turbine. Orthogonal experiment design was used to explore the influence of the three shape parameters on the turbine performance. Each shape parameter is given three level values (low, medium, and high). An orthogonal table is constructed to evaluate 27 different cases for the purpose of reaching optimum design. Results of the orthogonal experimental design show that the central angle of the small arc parameter has the most significant effect on performance followed by the radius of curvature and then the installation angle.

Bianchini et al. [40] performed numerical analysis and design space exploration for VAWT aimed at optimizing the annual energy production (AEP) of the turbine. The design variables that extensively explored were: turbine aspect ratio, solidity, turbine swept area, airfoil type, and wind speed distribution. Six different wind speed distributions were considered in which

the average wind speed was increased by one m/s from 3 to 8 m/s. Rayleigh distribution was used for all wind speeds. Four different airfoils were considered, namely: NACA 0012, 0015, 0018, and 4415. The aerodynamic performance simulations were done using VARDAR code which is based on a modification of DMST. Optimization of AEP was done manually by considering several values of the design variables (the study considers 21,600 different permutations of the design variables) and then finding the set of variables that give the maximum AEP. The effect of three primary constraints on the optimum value of the design variables is examined, namely: no constraint case, limiting the maximum cut-out speed based on centrifugal stress, and limiting both the maximum centrifugal stress and parasite torque due to the supporting struts. Results show that the optimum value of the design variables depend on whether constraints are imposed. For instance, including the parasite torque on the rotor due to the struts affects the outcome of the results significantly. Also, the study shows the capability to produce different optimum VAWT designs for different wind distribution including distribution with low wind speeds.

Jafaryar et al.[41] presents torque optimization of VAWT by varying the shape of the airfoil. Three main parameters are used to characterize NACA 4 digit airfoil shape which are: max camber height, max camber location, and max airfoil thickness. Computational fluid dynamics simulation is used to obtain the aerodynamic performance of the turbine. A second-order polynomial fit function is used to characterize the torque of the turbine as a function of the airfoil shape parameters mentioned above. The fit function is obtained using response surface methodology. This fit function was constructed for constant wind speed and several rotor speeds. The quadratic fit of the torque is used to find the optimum shape of the airfoil which gives the highest torque.

Shires [42] presented structural and aerodynamic optimization of a novel offshore VAWT based on the Aerogenerator concept. The optimization aims to produce a low-stress VAWT

design that minimizes the manufacturing and maintenance cost, rotor mass, and aerodynamic overturning moments. The Aerogenerator concept has a "V" shape with tilted blades along the span of the V arm. The study chooses configuration shape such as arm and blade span, chord length, and positions of the blades and their struts as design variables. The objective function chosen is to minimize the mass of the whole rotor. The constraints used are mainly structural and include limits on the maximum overturning moment, maximum blade and strut length, and rated power of 10MW. Several designs are obtained by optimizing the design variables, and the final optimum design achieves 3% reduction in rotor mass and 11% reduction in overturning moment compared to the reference Aerogenerator turbine. The final design is also optimized aerodynamically to achieve the desired power curve. In this case, only blade twist and thickness are optimized. The final optimum structural and aerodynamic design was a two arms design with a titled blade in each arm.

Schelbergen [43] presents a detailed optimization for Darrius and straight bladed VAWT. The ultimate optimization goal is to come up with VAWT designs that have a low cost of energy. The objective function used is the mass of the blade divided by the frontal area of the turbine. This objective function given the assumption presented in the study represents a surrogate for the cost of energy. The design is constrained using ultimate, fatigue, and buckling failures in additions to simple bound constraints on the design variables. Constant solidity and tip speed ratio are also used to simplify the design space and reduce the computational cost. The design variables used are rotor radius, the internal material thickness of the blade, and strut geometry (only for straight blade VAWT). The aerodynamic loads applied to the blade are determined independently from the optimization by calculating the angle of attack the blade sees under the condition of constant solidity and tip speed ratio. The force per unit chord is then scaled by the length of the chord. The chord length itself is determined as an outcome of the optimization. The structural analysis is carried out using the finite element code MSC Nastran. MATLAB

fmincon is used to perform the optimization. The results show that the optimization algorithm can reduce the objective function for both Darrius and straight bladed turbines from the reference case. The resulting design for the Darrius and straight bladed VAWT are different in terms of overall size and also the value of the objective function. The study concludes by presenting scaling trends for optimized VAWT designs.

Roscher [44] and Roscher et al. [45] presented detailed optimization of Darrius VAWT that is based on Schelbergen [43] work. The study shows improvements in the previous result by Schelbergen [43] that are attributed to the smooth transition of the blade cross-section, a variable blade section height, and relaxation of local buckling constraints.

2.3 Lessons Learned from Previous Studies

The literature review presented in the previous two sections serves the purpose of identifying the trends in wind turbine optimization. The review is also used to gain insight into performing the optimization for this thesis. Several observations can be learned from the literature review regarding wind turbine optimization studies. These observations are as follows. First, in regards to the quantity of published research, it is noticed in general that there is more research effort on HAWT than on VAWT. This is attributed to the fact that HAWT is by far the most used type of wind turbine for power generation. Thus, research funding and effort is heavily concentrated on HAWT due to their majority share in commercial use. This focus on HAWT has led to a large number of optimization studies and resulted in far better understanding of the HAWT optimization problem compared to VAWT. In addition, several approaches to HAWT optimization in terms of analysis tools, objective functions, constraints, and design variables have already been implemented and as a result facilitated good comparison between these different approaches. Unfortunately, such variety of approaches for VAWT optimization are

currently not available and most studies use more or less the same variables and objective function.

VAWT optimization studies are focused more on pure aerodynamic objective functions like the power coefficient or the maximum power. Usually, these objective functions are evaluated at a single wind speed which puts a limitation on the optimum designs when analyzed at various off-design wind speeds. In addtion, these optimum designs are commonly obtained without any structural constraints which means that the aerodynamic benefits proposed by the optimum design might suffer from a massive increase in structural loads on the rotor or a significant increase in total mass of the rotor leading to unrealistic or unrealizable designs. This thesis will address some of these drawbacks in optimization formulation.

The ultimate goal of all wind turbine optimizations is to achieve designs that produce maximum amount of energy at the lowest cost possible, i.e., achieve the lowest possible levelized cost of energy (LCOE). Realizing that minimizing LCOE requires a multi-disciplinary analysis of the wind turbine, it becomes clear that the wind turbine optimization is inherently a multi-disciplinary optimization (MDO) problem. MDO requires multi-disciplinary analysis codes that capture the coupling between various disciplines into the objective function and constraints. Doing this in principle is more complicated than performing a single discipline optimization, but there are potential benefits that encourage a more multi-disciplinary approach. For instance, we learn from HAWT MDO studies that designs achieved using MDO tend to be more optimum if judged by LCOE objective, which is the ultimate goal. Also, MDO designs satisfy the constraints in all discipline and hence eliminate the need to perform another optimization on top of an optimum design to satisfy constraints. Furthermore, if constrained well enough and given proper degrees of freedom, MDO can give insights that are not straightforward. These insights seem to be lost if sequential optimizations are performed since

sequential optimizations tend to produce sub-optimum designs when judged by the end goal of optimization.

The computational cost of wind turbine optimization is a very challenging problem especially for expensive to compute objective functions that arise in MDO. The primary driver for the computational cost of wind turbine optimization is that the objective function and constraints are derived from a simulation, and usually this simulation is costly to evaluate.

CHAPTER 3

AERODYNAMIC AND STRUCTURAL ANALYSIS TOOLS FOR VAWT

This chapter presents a brief description of the analysis tools used in this thesis to obtain the aerodynamic and structural response of the turbine. The chapter starts by describing the capabilities needed form the analysis tools to capture the desired outputs, followed by examples of available codes that calculate the performance of VAWT. Finally, brief descriptions of the simulation tools used in this thesis are presented.

3.1 Capabilities Desired in Analysis Codes

To be able to optimize a turbine for a specific objective, the effects of the turbine design and wind conditions on the objective function need to be known. In another word, the effects of changing the turbine parameters and wind conditions on the main performance aspects of the turbine need to be quantified. For instance, the aerodynamic response of turbine needs to be calculated for different blade geometry, airfoil type, rotor shape, rotor speed, and wind speed. In addition to the aerodynamic response, the structural response of the turbine needs to be calculated as well. For example, stress, deflection, stiffness, mass, and vibration data for different parts of the turbine need to be obtained when changing the design of the turbine. From the aerodynamic response, the performance of the turbine can be evaluated in terms of the

maximum power, annual energy production (AEP), and aerodynamic efficiency. On the other hand, the structural response gives information about the mass, maximum stress, fatigue life, maximum deflections, maximum vibrations, and is used to assess the stability of the structure. From above, we can see that the aerodynamic response is important when the amount of power or energy production need to be optimized. The structural response, on the other hand, is essential when the mass, safety constraints, and cost of the turbine need to be optimized. Hence, for turbine optimization, it is essential to evaluate both the aerodynamic and structural responses of the turbine to capture both the amount of energy and also the mass and cost of the turbine. Evaluation of both the aerodynamic and structural responses is essential because an optimal turbine design needs the balance between the amount of energy produced and the cost of producing the turbine parts. For this reason, the analysis tool used in optimization needs to have the capability of capturing both the aerodynamic and structural response of the turbine. This thesis uses analysis tools that have both aerodynamic and structural response capabilities as will be shown later in this chapter. Before we discuss the analysis tools used in this thesis, the next section introduces a short description of some of the available analysis tools for VAWT.

3.2 Available Analysis Codes for VAWT

There are various codes for VAWT analysis that differ in terms of formulation, fidelity, and computational cost. Here, we divide these codes into two broad categories. The first is VAWT aerodynamic codes, and the second is VAWT aero-elastic codes which combine aerodynamic and structural response of VAWT.

VAWT aerodynamic codes:

1. CARDAAV: is a double multiple stream tube theory (DMST) code [46], [47].

2. UMPM: Unsteady Multibody Panel Method, which is a 3D vortex panel method with free vortex wake developed at TU Delft [48].
3. U2DiVA: Unsteady Two-Dimensional Vorticity Aerodynamics model, which is a 2D unsteady multibody free vortex wake panel code developed at TU Delft [49].
4. CACTUS: Code for Axial and Cross-flow TUrbine Simulation, which is a 3D lifting line with free vortex wake [50].

VAWT aeroelastic codes:

1. QBLADE: aeroelastic code that can handle both HAWT and VAWT. The aerodynamic formulation is a 3D lifting line with free vortex wake. The structural analysis is based on multibody formulation with Euler beams. The code is developed at TU Berlin [51], [52].
2. OWENS: Offshore Wind Energy Numerical Simulation tool. OWENS is a combination of several analysis codes that are coupled to produce an aeroelastic solver. Its aerodynamic solver is CACTUS, and it uses the multibody formulation with Timoshenko beams as for its structural solver [5], [53].
3. VAEMPS: Vertical axis wind turbine AeroElast Multibody Panel Solver. VAEMPS ss a combination of the aerodynamic code UMPM and the structural solver of OWENS [44].
4. HAWC2: aeroelastic code that can handle both HAWT and VAWT. The aerodynamic formulation uses actuator cylinder model, and the structural solver uses the multibody formulation with Timoshenko beams. The code is developed by the Department of Wind Energy at Technical University of Denmark (DTU) [54], [55].

Comparison between the above codes regarding accuracy and computational cost is outside the scope of this work, but the interested reader can refer to [8], [44], [49], [56] for comparison between the codes.

This thesis uses HAWC2 aeroelastic code as the primary analysis code. The reason for choosing HAWC2 is its superior capabilities in calculating the coupled aerodynamic and structural response of VAWT, low computational cost, and commercial availability of the code. The next section of this chapter examines more closely the codes used in this thesis.

3.3 Aero-Servo-Elastic Code (HAWC2)

HAWC2 (Horizontal Axis Wind turbine simulation Code 2nd generation) code is used as the primary simulation tool in this study. HAWC2 is an aeroelastic code intended for calculating wind turbine response in time domain. HAWC2 can simulate any arbitrary wind turbine configurations and blade geometry. In addition, HAWC2 is capable of finding the response of the turbine due to realistic wind conditions which include wind shear, skew, and turbulence [25]. Although HAWC2 was initially used only to analyze HAWT, it has been extended for the analysis of VAWT recently [55]. The VAWT aerodynamic module of HAWC2 uses actuator cylinder (AC) flow model to represent the aerodynamic forces on the blades and to find the induction velocity field. The structural module of HAWC2 is based on a multibody formulation where each body is an assembly of Timoshenko beam elements [54]. The HAWC2 structural module is used to calculate the internal forces and moments and deflections for different turbine components like the blades and the tower. The internal forces and moments are the results of the applied aerodynamic, centrifugal, and gravity forces on the entire turbine. HAWC2 has also the ability to perform modal analysis of the turbine and to determine the mode shapes and frequencies of the whole turbine.

The AC model uses 2D cylinders (circles) to represent the effect of the rotor on the flow field. Several 2D cylinders are used to cover the whole span of the blade the 2D cylinders act on the flow using normal and tangential volumetric forces as shown in Figure 3.1. The AC model is based on a modified linear solution to Euler and mass continuity equations. The modification itself is based on the induction factor and thrust coefficient [40]. HAWC2 uses dynamic stall models to account for the unsteady variation in the angle of attack on the blade airfoil. Dynamic stall models are needed when there is an unsteady variation of the local flow and also due to significant changes in angle of attack for VAWT blade especially at low tip speed ratio (TSR).

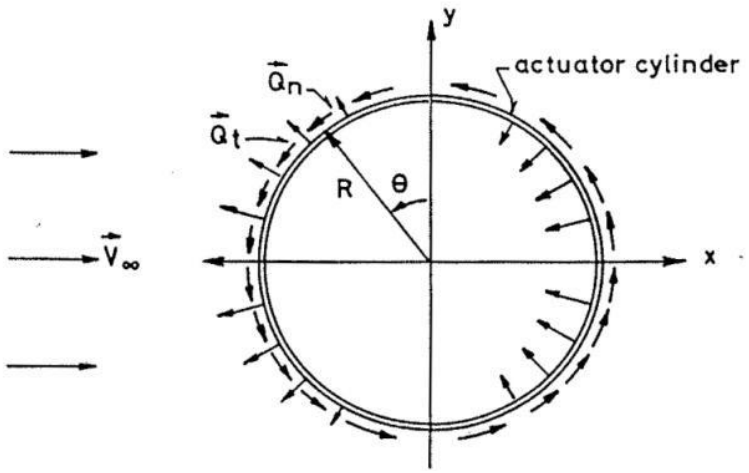

Figure 3.1: The AC model representation of a 2D VAWT with the tangential (Qt) and normal (Qn) volumetric forces [55].

HAWC2 uses a multibody formulation which is a general coupling method that can couple rigid and flexible structures**.**. Using this formulation, HAWC2 can account for large rotation and translations at the coupling point between bodies [57]. For each main body (like a blade), HAWC2 allows the definition of several sub-bodies within this main body. Example of this construction is shown in Figure 3.2. Each body is divided into a set of Timoshenko beam elements with 6 degrees of freedom. The Timoshenko beam elements account for the flexibility of the bodies. Beam elements have also mass and inertia. In the context of a blade, this means

that flapwise, edgewise and torsional flexibility are accounted for [57]. Figure 3.3 shows an example of VAWT and HAWT discretization to several main bodies.

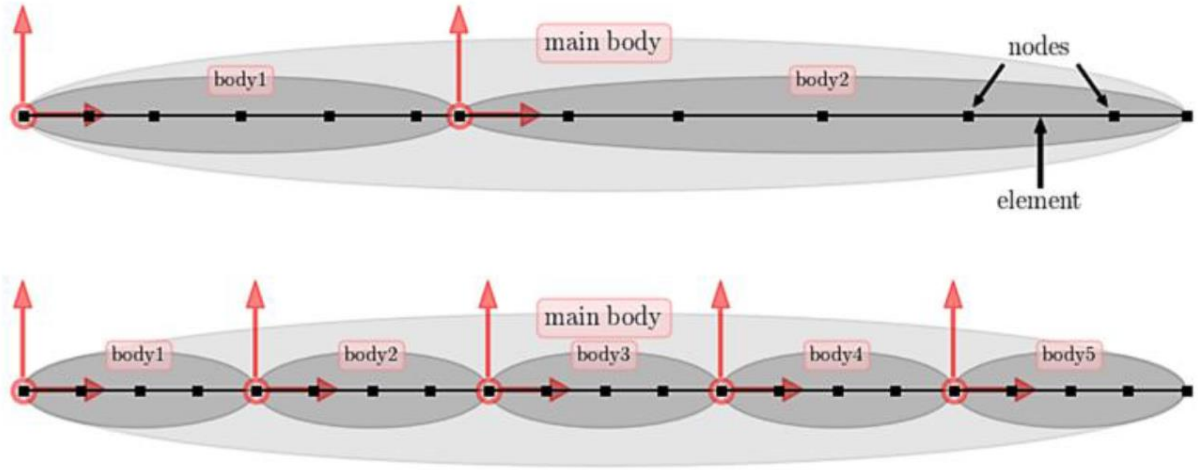

Figure 3.2: discretization of a main body into several sub-bodies. Each sub-body consists of multiple Timoshenko beam elements [57].

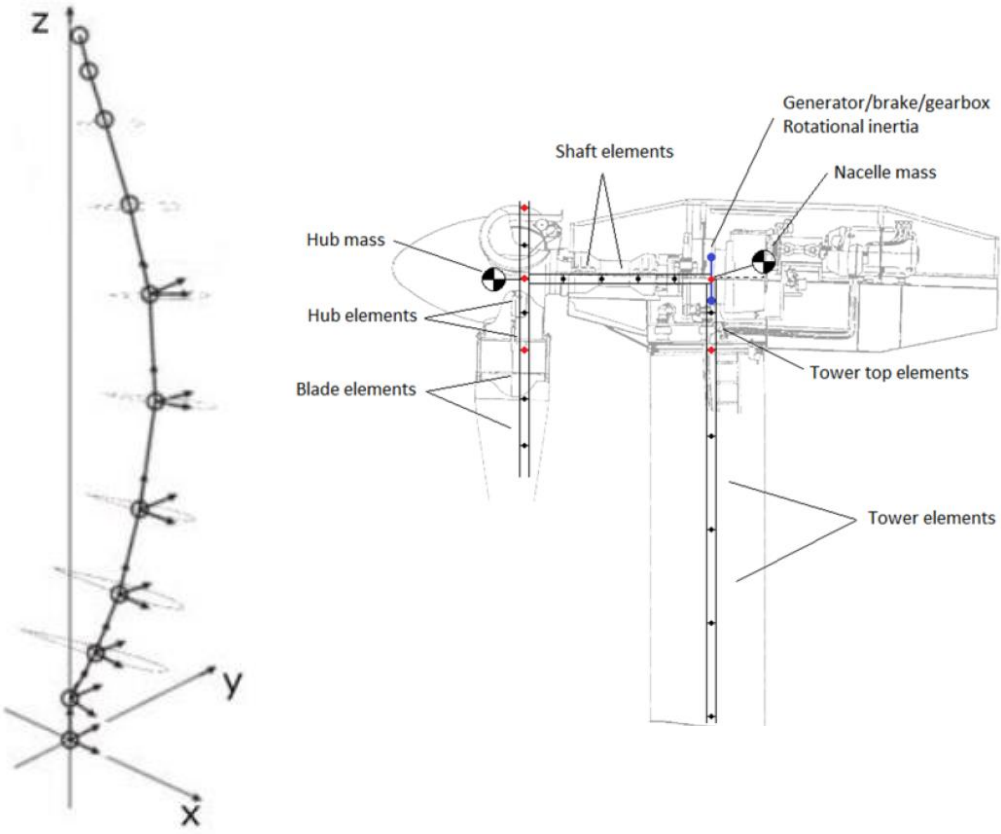

Figure 3.3: discretization of a VAWT (left) and HAWT (right) in HAWC2 structural solver [57].

HAWC2 structural solver uses Timoshenko beam elements to represent flexible bodies which means that the various beam cross-sectional properties like mass and stiffness need to be calculated for all flexible bodies. The question here is: how is it possible to come up with beam cross-sectional properties from a physical design of the different turbine components with the possibilities that these components are made from anisotropic materials? In this thesis, BECAS code is used to calculate the needed beam cross-sectional properties for HAWC2. [57]

3.4 Beam Analysis Code (BECAS)

BECAS [26], [58]–[60] (BEam Cross-section Analysis Software) is a general purpose cross-section analysis code that determines cross section stiffness and mass properties using a finite element based approach. BECAS determines the cross section stiffness properties while accounting for all the geometrical and material induced couplings. BECAS is used as a pre-processor for HAWC2 to determine the required stiffness and mass properties of the blades. In addition to being pre-processor for HAWC2, It can also be used as a post-processor for HAWC2 to find the stresses and failure criteria in the blades or any other body modeled as Timoshenko beam. Finding the stresses and failure criteria is achieved by using HAWC2 internal forces and moments that are computed from an aeroelastic simulation of the turbine to calculate the local 3D stresses for each cross-section of the blade. Figure 3.4 shows an example of how BECAS is used as pre-processor. Figure 3.5 shows an example of stress calculation results using BECAS.

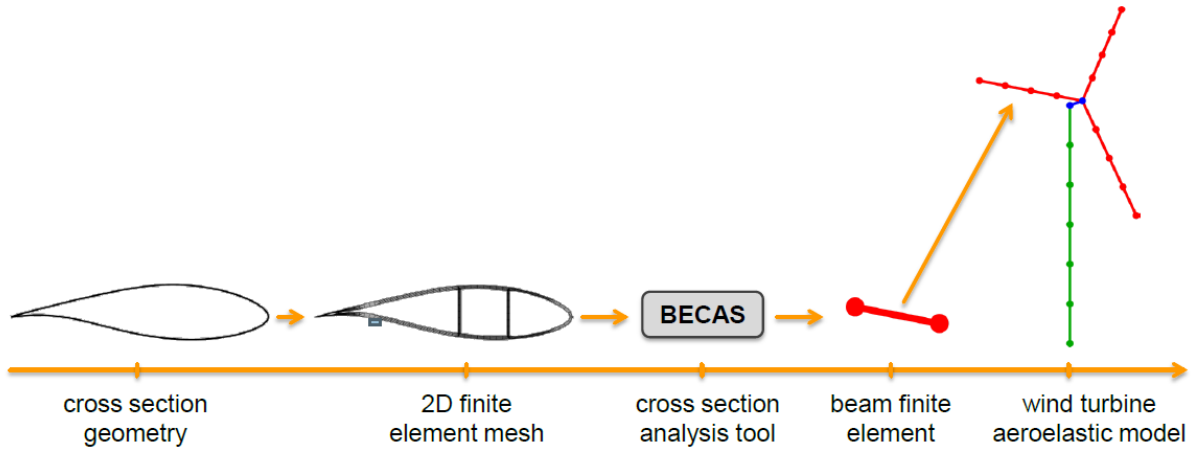

Figure 3.4: Example of using BECAS as a pre-processor for HAWC2 [26].

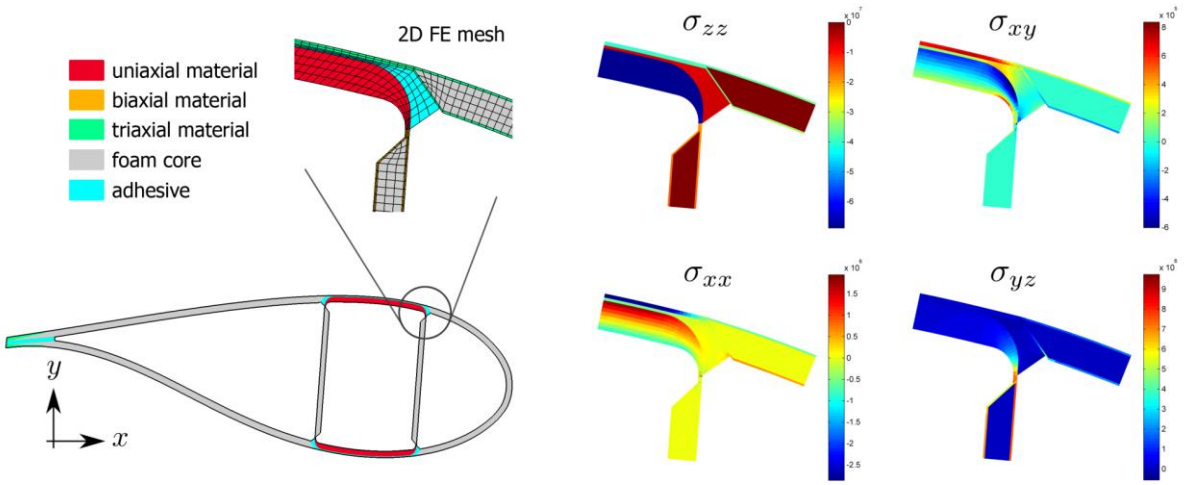

Figure 3.5: Example of using BECAS to find the stress in the blade by applying the beam moments and forces that are computed from HAWC2 aeroelastic simulation [26].

3.5 Optimizer and Data Analysis (MATLAB)

Results from HAWC2 and BECAS constitute the analysis module of the optimization framework. There is a need for management software that can handle the optimization problem and the data flow between the different analysis module codes. In addition, software needs to

take the results from HAWC2 and BECAS and produce useful quantities. Such quantities are the objective functions and constraints for the optimization problem. The software used in this thesis for managing and performing the optimization is MATLAB.

MATLAB is used to transfer data between HAWC2 and BECAS as needed to formulate the objective function and the necessary constraints. MATLAB has another significant role, which is performing the optimization and finding the optimum design based on the predefined objective function. Built-in functions in MATLAB Optimization Toolbox are employed to perform the optimization. Different optimization algorithms are available in MATLAB such as the gradient-based optimizer *fmincon*, the direct search optimizer *patternsearch*, and genetic algorithm optimizer *ga*, to name a few. The choice of the optimizer depends on the objective functions, constraints, and the number of variables. In this work, the optimization results were obtained using the gradient-based optimizer *fmincon*.

CHAPTER 4

TURBINE OPTIMIZATION FORMULATION

This chapter outlines the optimization problem employed in this thesis. First, a generic formulation of the optimization problem is presented. Next, the objective functions used in this work to optimize the turbine along with the appropriate constraints are presented. After that, a description of the turbine parameterization that defines the internal structure and the outside shape of the rotor is explained in terms of both the aerodynamic and structural design variables. Next, the optimization workflow is presented which is a description of how the different analysis tools are fitted together to perform the optimization and minimize the objective function. Finally, the optimization cases that are analyzed are described.

4.1 Problem Formulation

In generic terms, the optimization problem handled in this study is a non-linear constrained optimization which means that the objective function and constraints are non-linear functions of the design variables. The non-linear optimization problem can be defined as:

$$\begin{aligned} &Minimize \quad f(\boldsymbol{x}, \boldsymbol{p}) \;\; with\, respect\, to\, \boldsymbol{x} \\ &Subject\, to \quad \boldsymbol{g}(\boldsymbol{x}, \boldsymbol{p}) \leq \boldsymbol{0} \end{aligned} \tag{4.1}$$

where the scalar function, f, is the objective function that is minimized. The vector function, $\boldsymbol{g}$, is a set of nonlinear constraints that describe the conditions of feasible designs. Both the

objective function and the constraint function depend on a vector of design variables, $\boldsymbol{x}$, and a vector of constant parameters, $\boldsymbol{p}$. The design variables are the degrees of freedom that the optimizer can use to change the design and reach an optimum one. The design variables are divided into aerodynamic and structural variables. Aerodynamic variables control the outside shape of the turbine and also its rotational speed. Examples of aerodynamic variables are the blade chord length, maximum radius, maximum height, and the rotor speed. On the other hand, structural variables control the internal material thickness inside the blade.

The constant parameters are fixed quantities that affect the overall design but cannot be changed by the optimizer. The parameters affect the final design by limiting the design space that the optimizer can choose from. Along with the design variables, the fixed parameters are essential to describe the turbine operation and geometry adequately. The parameters are held constant mainly for convenience and simplicity, namely, to reduce the computational time in performing the optimization problem.

Note that although all objective functions, constraints, and design variables are defined as dimensional and unscaled quantities, they are defined as non-dimensional and scaled quantity to the optimizer to have all variables and functions on the same scale. Scaling helps in avoiding premature stopping of the optimization iterations, better convergence, and better estimate of gradients. For instance, the objective functions are scaled following Parkinson et al. [61]:

$$f_{scaled} = \frac{f_{unscaled} - Allowable}{Allowable - Indifference} \tag{4.2}$$

Considering minimization problems, the $Allowable$ is the maximum expected objective function value (could be also the starting value of the non-optimum design), the $Indifference$ is the desired objective function value (or what is aimed from the optimizer to achieve). When scaled according to equation (4.2), the optimum value for the scaled objective function should

is near –1. The constraints are also scaled using equation (4.2). The design variables are scaled following Parkinson et al. [61] notation:

$$x_{scaled} = \frac{x_{unscaled} - C_1}{C_2} \tag{4.3}$$

$$C_1 = \frac{Max + Min}{2} \tag{4.4}$$

$$C_2 = \frac{Max - Min}{2} \tag{4.5}$$

x_{scaled} is any design variable after scaling, $x_{unscaled}$ is any design variable before scaling, and Max and Min are the upper and lower limits on any unscaled design variable respectively.

4.2 Objective Functions

The objective function determines how the design evolves, influences the choice of design variables, and dictates the outcome of the design. The objective function also determines the computational cost of the optimization problem and the level of coupling between aerodynamic and structural variables if any. This study considres the following three objective functions:

- Annual Energy Production (AEP)
- Blade mass (m_b)
- Blade mass over AEP $\left(\frac{m_b}{AEP}\right)$

AEP objective involves only aerodynamic variables while m_b objective involves only structural variables. AEP and m_b objectives are used in sequential optimization in which the turbine is first optimized aerodynamically to maximize AEP, then the resulting optimized turbine is optimized structurally to minimize m_b. On the other hand, $m_b/AEP$is a coupled objective that involves both aerodynamic and structural variables simultaneously. This objective is used in the coupled optimization formulation.

The reason for carrying out both sequential and coupled optimization is to examine which optimization method gives the lower cost of energy (COE). In this study, the cost of energy is assessed using quantity m_b/AEP. Hence, it is desired to see which optimization method gives lower m_b/AEP, a sequential optimization or an integrated coupled optimization? Notice that using m_b/AEP as a proxy and surrogate for the cost of energy, is motivated, as mentioned by Ning et.al [13], by examining a simplified version of the cost of energy equation [15]:

$$COE = \frac{(FCR * ICC) + O\&M}{AEP} \tag{4.6}$$

In which FCR is the fixed charge rate, ICC is the initial capital cost, and O&M is the operation and maintenance cost. Using equation (4.6), we assume that the initial capital cost will be proportional to the turbine blade mass, while the operational cost is a fixed rate that will increase the COE by a fixed amount independent of the turbine design. So in light of this assumption, m_b/AEP objective approximate the COE objective very well, and this is the reason why this study judges design by m_b/AEP metric. Mathematically:

$$m_b \propto (FCR * ICC) + O\&M \tag{4.7}$$

AEP is calculated by finding the aeroelastic response of the turbine using HAWC2 from cut-in to cut-out wind speeds. For each wind speed, the power as a function of time is obtained from HAWC2 and then the revolution averaged power is calculated. The revolution averaged power at each wind speed V_i is the function $P(V_i)$. From $P(V_i)$, AEP is calculated using:

$$AEP = 8760 * \int_{V_{cut-in}}^{V_{cut-out}} p(V) * P(V) dV \tag{4.8}$$

Where $p(V)$ is the probability density function of wind speed. In this study, $p(V)$ is calculated using Weibull distribution with a shape parameter $k = 2$ and annual mean wind speed $\bar{V} = 7.5\ m/s$ so that explicitly, $p(V)$ is given by:

$$p(V) = \frac{\pi}{2\bar{V}^2} V\ exp\left[-\pi\left(\frac{V}{2\bar{V}}\right)^2\right] \tag{4.9}$$

The integral in equation (4.8) is evaluated using the trapezoidal rule with cut-in and cut-out speeds of 5 m/s and 25 m/s respectively and a 2 m/s speed increment. All the results in this study have been evaluated using deterministic wind with no wind shear effect. Figure 4.1 shows a plot of the Weibull wind probability distribution that is used in this study.

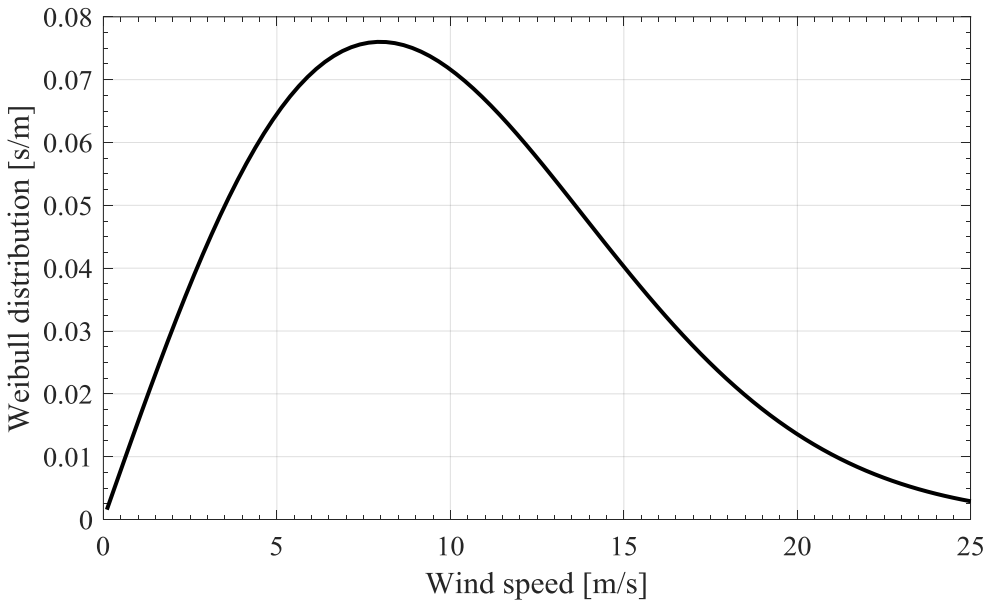

Figure 4.1: Weibull distribution with a shape parameter $\boldsymbol{k = 2}$ and annual mean wind speed $\boldsymbol{\bar{V} = 7.5\ m/s}$

The blade mass m_b is calculated using the output of BECAS. BECAS gives the mass per unit length based on the material internal thickness and the chord length of a particular section along the length of the blade. From BECAS output, the mass per unit length can be calculated as a function of blade length and then the resulting distribution can be integrated with blade length

to give the total blade mass. More details about the mass per unit length and internal thickness distributions can be found in section 4.3.

4.3 Constraints

Constraints are used to limit the optimizer from choosing design variables that lead to infeasible or unrealistic design. Constraints can be related to structural, aerodynamic, and operational variables. This work uses three main constraints:

- Maximum allowable ultimate stress.
- Maximum power.
- Bound constraints on all design variables.

The maximum allowable ultimate stress constraint is written as:

$$\boldsymbol{g_{ult}} = \left(\left| \frac{\gamma_m \boldsymbol{\sigma}_j}{\boldsymbol{\sigma}_{ult\,j}} \right| \right)_i - 1 \tag{4.10}$$

σ_j is the j^{th} stress component in the material coordinate, $\sigma_{ult\,j}$ is the j^{th} ultimate (maximum or minimum) stress component in the material coordinate. The index j goes from 1 to 6, since there are in general 6 stress components. For example, σ_1 is the stress in the fiber direction (tensile or compression), σ_2 is the stress perpendicular to the fiber direction (tensile or compression), and σ_3 is the in-plane shear stress of the composite laminate. The material coordinate can be defined by the fiber plane angle α and fiber angle β as can be seen in Figure 4.2. The subscript i in equation (4.10) refers to the location along the blade in which $\boldsymbol{g_{ult}}$ is calculated. γ_m is the partial safety factor for materials and was set to 2.2. The material used for the blade is glass fiber reinforced plastic (GFRP) and hence $\sigma_{ult\,j}$ corresponds to the values of GFRP.

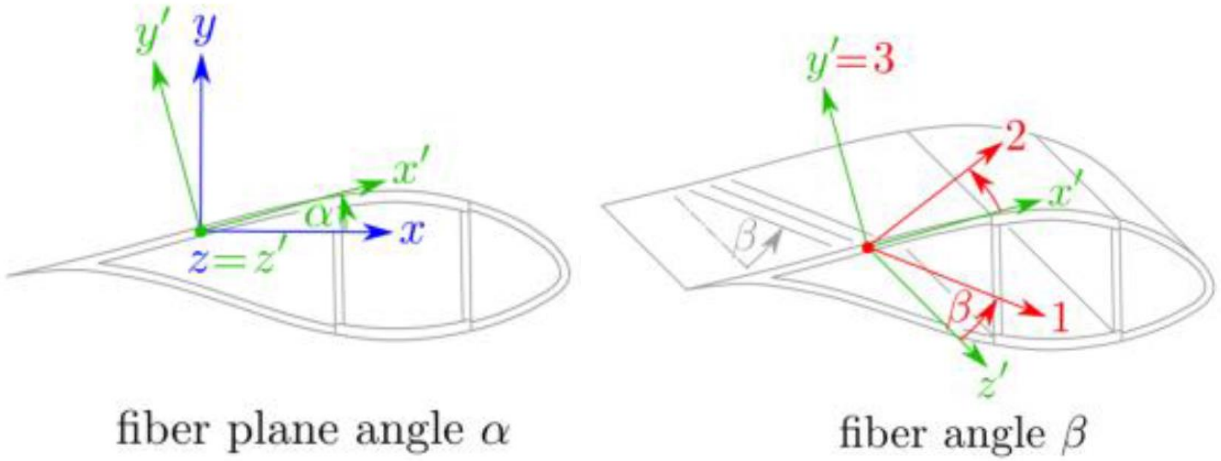

Figure 4.2: Definition of material coordinate system used by BECAS [57].

Internal forces and moments from HAWC2 simulation are passed to MATLAB as time series in a process to find the maximum stress components at any location along the blade. The times at which each moment component (flapwise, edgewise, and torsion) achieve a maximum or minimum are analyzed as a potential to cause the maximum failure in the blade. Figure 4.3 shows an example of a VAWT with stress analysis location designated by a solid circle. The figure also shows the flapwise moment time series at single wind speed and for a specific blade location.

There will be a total of six total times that need to be analyzed for each blade location and each wind speed. So for example, if the total location along the blade to be analyzed is n and the total wind speeds analyzed is m, then there will be total of $6 * (6 * n * m)$ ultimate stress constraints in the vector $\boldsymbol{g_{ult}}$. Note that the "6" outside the parentheses is there because there are 6 stress components.

It should be emphasized here that the ultimate stress calculation is based on load resulting from the turbine operating at power production mode only which corresponds to Design Load Case

(DLC) 1.1 in IEC 61400-1 standard. The exception being that the wind used is deterministic and not turbulent. The reason for considering DLC 1.1 alone without the other DLC as suggested by IEC standard is that previous study by Galinos [7] showed that loads emerging from DLC 1.1 for VAWT give rise to the maximum ultimate stress. Galinos [7] also mentioned that in contrast to HAWT, VAWT is less affected by turbulence when it comes to finding the ultimate load. VAWT maximum ultimate stress insensitivity to turbulence is because of its structural and aerodynamic response has natural large unsteady variation even without turbulence. The unsteadiness added by turbulence is deemed to be small especially when the ultimate load on the blade is the concerned.

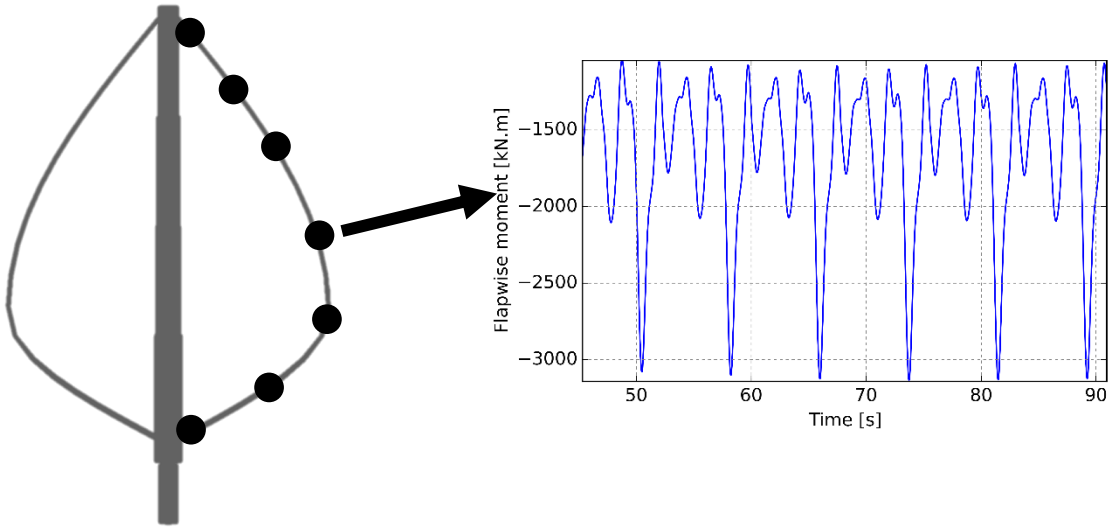

Figure 4.3: Example of a VAWT with stress analysis location designated by solid circle. The time series is for the flapwise bending moment in the blade.

The maximum power constraints can be written as:

$$\boldsymbol{g_{power}} = \boldsymbol{P}(\boldsymbol{V_i}) - P_{rated} \tag{4.11}$$

P_{rated} is the rated power of the turbine and in this study, it is set to 5.4 MW. The power constraints applies only at above rated wind speed. This constraint is not handled by the optimizer directly as a non-liner constraint, but instead, it is handled internally by a simple iterative scheme in MATLAB that mimics the design of a speed controller. At above rated wind

speed, the turbine power is regulated by reducing the rotor speed. Since in this study no controller was coupled with HAWC2, the rotor speed was varied through changing the synchronous frequency of the induction generator manually similar to what has been done in the work of Galinos [7]. The MATLAB script finds the revolution averaged power from HAWC2 output for each wind speed and if the power exceed the rated power then MATLAB reduces the rotor speed and rerun the HAWC2 simulation for that wind speed until the power is less than the rated power.

It is worth noting that rated wind speed is not predefined to the optimizer, instead, it is determined as the lowest wind speed that the turbine achieves the rated power. The optimizer is free in choosing which wind speed corresponds the rated power hence the rated wind speed becomes free parameter determined as an outcome of the optimization.

The bound constraints are simple upper and lower limits on all the design variables. These constraints are used to limit the design space and to prevent the optimizer from choosing in extreme values of design variables.

4.4 Design Variables

Design variables are the variables that can be changed by the optimizer to change the value of the objective function and the constraints. Parameters, on the other hand, are constant values that are fixed for a given optimization problem and cannot be changed by the optimizer. The values of these parameters although being fixed, affect the value of the objective function and the constraints. For the optimizer to be able to enhance an initial turbine design, design variables and parameters need to be chosen adequately to describe the geometry and operation of the turbine. Note that both design variables and constant parameters are needed to describe the turbine design adequately.

The type and number of design variables depend on the objective function and constraints as well as on the complexity and detail level of the design. In this study, design variables and parameters and will be divided into aerodynamic, structural, and operational. This study uses 12 design variables for the coupled aerodynamic and structural optimization. These variables are listed in Table 4.1.

Table 4.1: Design variables used in coupled aerodynamic and structural optimization.

Design variable	**Symbol**	**Unit**
Chord length at roots	c_1	[m]
Chord length at the equator	c_2	[m]
Maximum rotor radius	R	[m]
Rotor Height	H	[m]
Maximum rotor radius location	a	[-]
Tip speed ratio below rated speed	λ	[-]
Zone 1 material thickness at roots	$t_{1\,root}$	[m]
Zone 1 material thickness at the equator	$t_{1\,equa}$	[m]
Zone 2 material thickness at roots	$t_{2\,root}$	[m]
Zone 2 material thickness at the equator	$t_{2\,equa}$	[m]
Zone 3 material thickness at roots	$t_{3\,root}$	[m]
Zone 3 material thickness at the equator	$t_{3\,equa}$	[m]

To understand the context of the design variables in the optimization problem, we need first to look at how the turbine is parametrized regarding its planform shape, material thickness topology, and rotor speed profile. The platform (outside) shape of the rotor is parametrized as a modified Troposkien shape. The modified Troposkien shape definition is taken from Paraschivoiu Equation 3.79 [47] which is:

$$\eta = \sin\left[\frac{\pi}{2}\left(\frac{1 \pm \xi}{1 \pm a}\right)\right] \tag{4.12}$$

Where η and ξ are the normalized radius and height respectively. The (+) sign is for $\xi \in [-1, a]$ and the (–) sign is for $\xi \in [a, 1]$.

$$\eta = \frac{r}{R}, \qquad \xi = \frac{h}{H/2} \tag{4.13}$$

where r is the radius of the rotor at any height h.

Modified Troposkien shape is similar to ideal Troposkien but differs in the maximum radius location which occurs below the mid-height of the rotor. The maximum radius location is determined by the value of a (G/T_0 in Paraschivoiu notation [47]). Larger values of a corresponds to lower maximum radius and when $a = 0$ then the ideal Troposkien is recovered.

Figure 4.4 shows rotor outside shape of modified Troposkien with a maximum radius of 60.5 m, rotor height of 143 m, and a =0.33. Figure 4.4 shows also the DeepWind [62] rotor which has same radius and height. The dotted lines in Figure 4.4 indicate the location of root sections. In this study , the root sections extent as a percentage of total blade length is kept fixed at 14.6% and 10.8% for the lower and upper roots respectively. These values are chosen based on the root extent in DeepWind rotor.

As shown in Figure 4.4, the rotor blade is divided into two sections, the root, and the equator. Having only two sections, root and equator means that the rotor blade has only two different structural properties and chord lengths. Namely, one value for the two root sections (upper and lower) and another value at the equator section. This parameterization is chosen primarily to reduce the total number of design variables and also to make the optimization problem simpler. It is worth noting that this parametrization is the same as the one used in DeepWind turbine with the exception that the current parametrization allows for different chord lengths at the equator and root. DeepWind has the same chord length for root and equator sections.

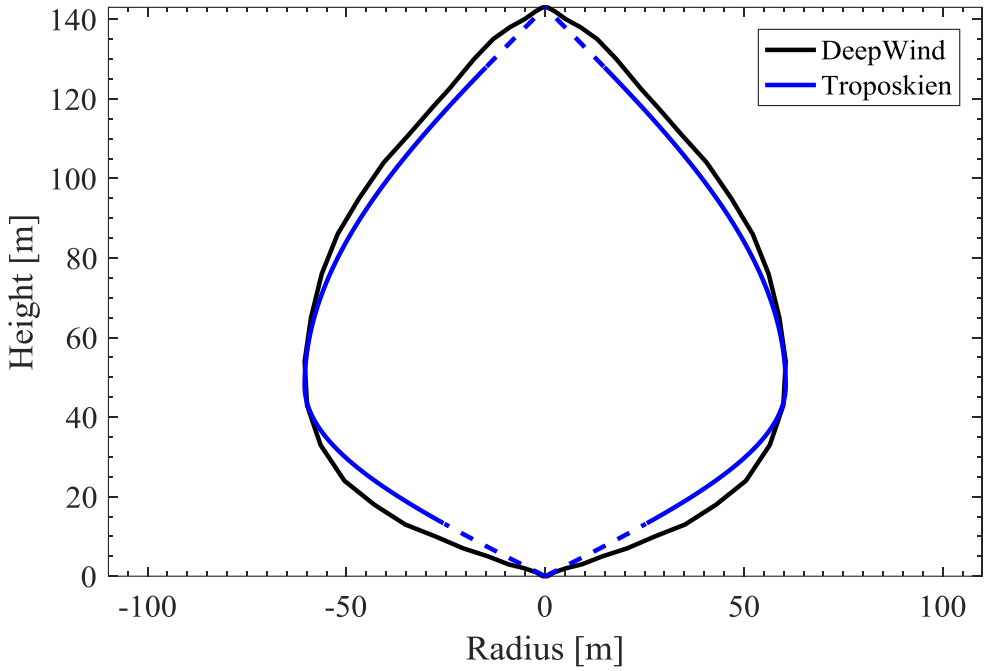

Figure 4.4: Rotor outside shape for both DeepWind and modified Troposkien. Dotted lines show the locations of root sections.

Figure 4.5 shows the blade airfoil internal thickness structure, material topology, and the different zones of the structural design variables. The different zones of material thickness are the same for root and equator sections. As shown in Figure 4.5, the two shear web locations are fixed at 10% and 85% of chord length from the airfoil leading edge. The reason for moving the shear webs away from the airfoil center is to increase the edgewise stiffness of the blade to avoid the edgewise instability that is reported in [7], [62], and observed in this study as well.

The material used for zone 1 is uni-axial glass fiber while all other zones including the shear webs are tri-axial glass fiber. The difference between the two materials is that former has main strength along the fiber direction with off fiber direction strength being only moderate while the latter has similar strength in all directions. The shear web material thickness is not changed independently but is set equal to the thickness of zone 2.

The airfoils used for root and equator sections are the NACA 0025 and NACA 0018 respectively. These airfoils are fixed during optimization and are not changed. The aerodynamic performance of the turbine is influenced by the choice of the airfoil, thus several airfoils need to be explored to find the best aerodynamic performance. However, due to the added computational cost of this approach, it was not implemented as part of this study. The author believes that there are better choices of airfoil than what is used in this study. Airfoils other than the symmetric NACA airfoils for VAWT applications have been explored in other studies and shown to yield better performance [63]–[66].

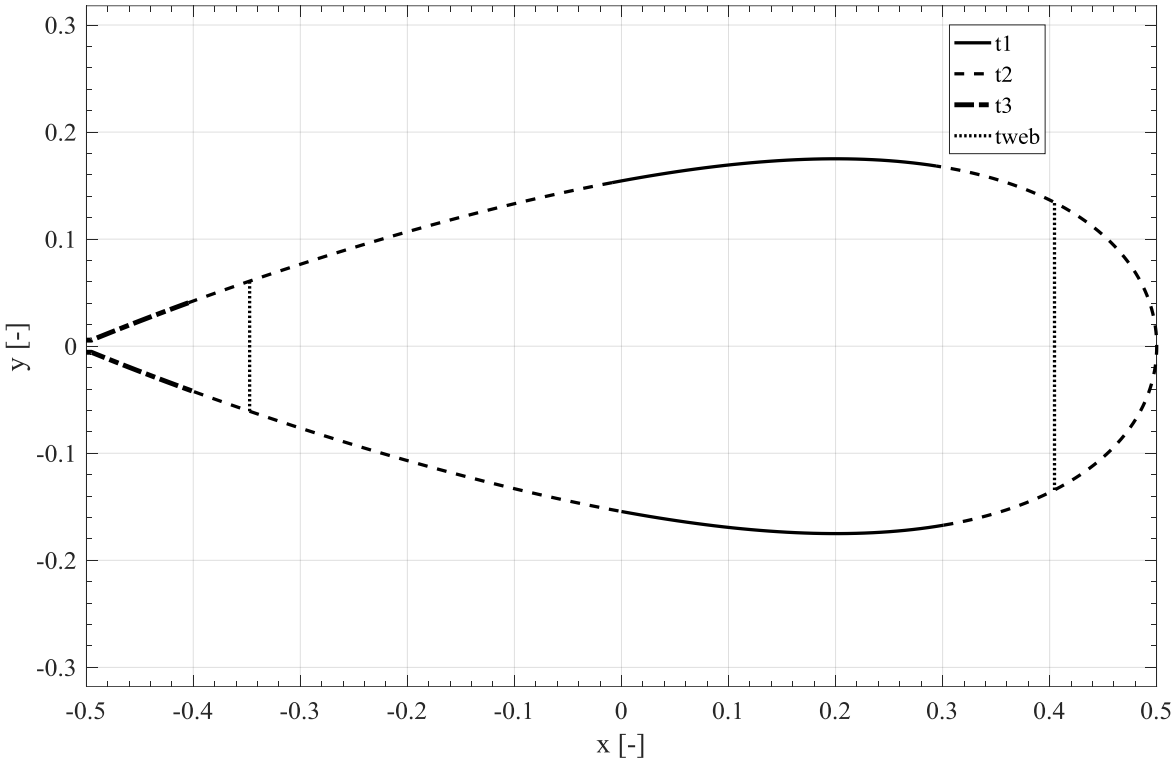

Figure 4.5: Blade airfoil internal thickness structure showing the material topology and the different zones of the structural design variables.

The distribution of blade mass and stiffness along the blade length considered in this study is stepwise distribution. An example of the mass per unit length distribution along the blade length is shown in Figure 4.6. The corresponding stiffness values and material thicknesses follow the same distribution as shown in Figure 4.6.

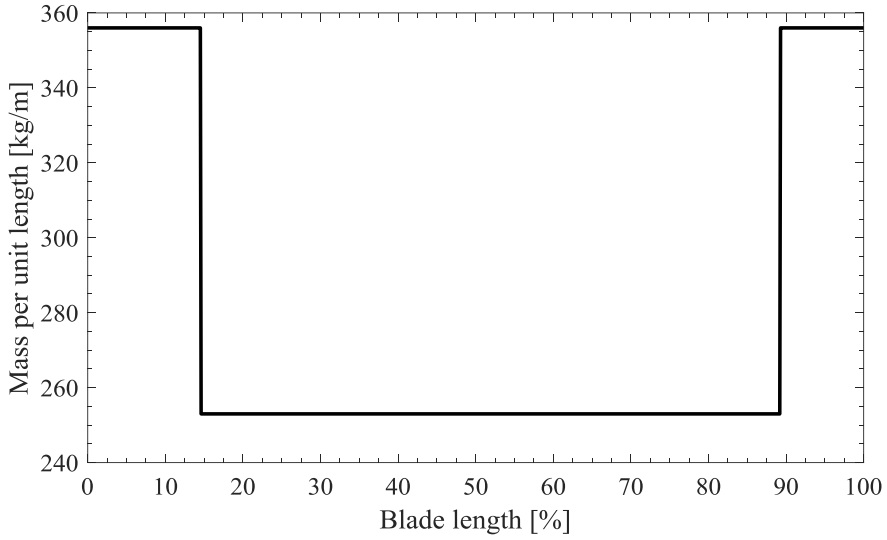

Figure 4.6: Example of the blade mass per unit length distribution along the blade length.

$$\lambda = \frac{\omega R}{V} \tag{4.14}$$

From equation (4.14) we can see that the rotor speed varies linearly with wind speed. This linear dependency continues up to the wind speed that gives mean power larger than the rated power P_{rated}. After that, the rotor speed is changed so that the output power remains constant at P_{rated} as described in section 4.3. A typical rotor speed variation with wind speed is shown in Figure 4.7.

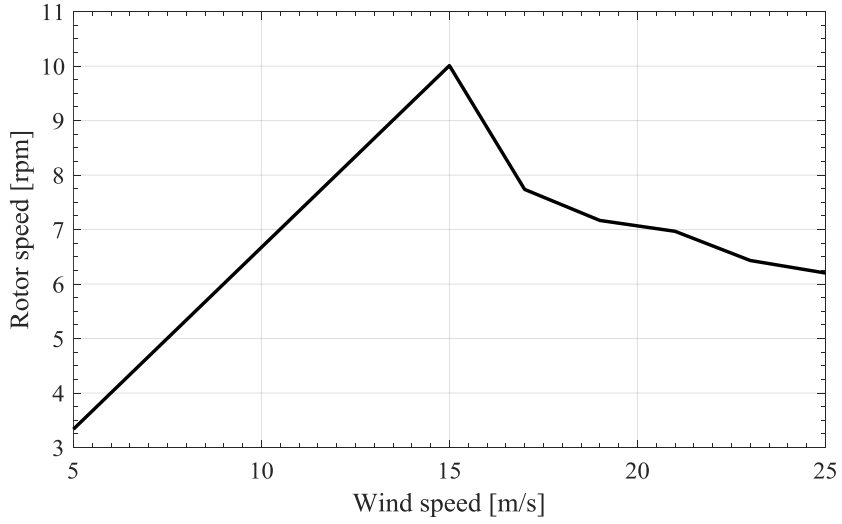

Figure 4.7: Example of rotor speed variation with wind speed.

Note that the first six variables in Table 4.1 are aerodynamic variables whereas the last six are structural variables. In sequential optimization, AEP is maximized by changing the first six variables only, while mass is minimized by changing the last six variables. In coupled optimization, all the twelve variables are used simultaneously. More description of the optimization cases is given in section 4.6.

It is noteworthy that the structural properties of all the turbine components (tower, generator, and support platform) except the blades are taken to be as defined in [7]. Notice that the tower height is allowed to change in this study as a consequence of changing rotor height, but the tower structural cross-sectional properties remain the same as the tower stretches or contracts.

4.5 Optimization workflow

The optimization workflow is the way that the optimization module (MATLAB optimizer) receives and passes different data from and to the analysis module (HAWC2 and BECAS). It describes the sequence of running various functions inside the analysis module and how the output from such functions are passed to the optimizer to update the design variables. Figure 4.8 shows the optimization workflow for a coupled aerodynamic and structural optimization. As seen in Figure 4.8, MATLAB defines the optimization problem, establishes the data flow between HAWC2 and BECAS, converts the raw output data of HAWC2 to quantities that are useful in obtaining the objective function and constraints, and of course, uses the optimization algorithm to improve the design according to the objective function.

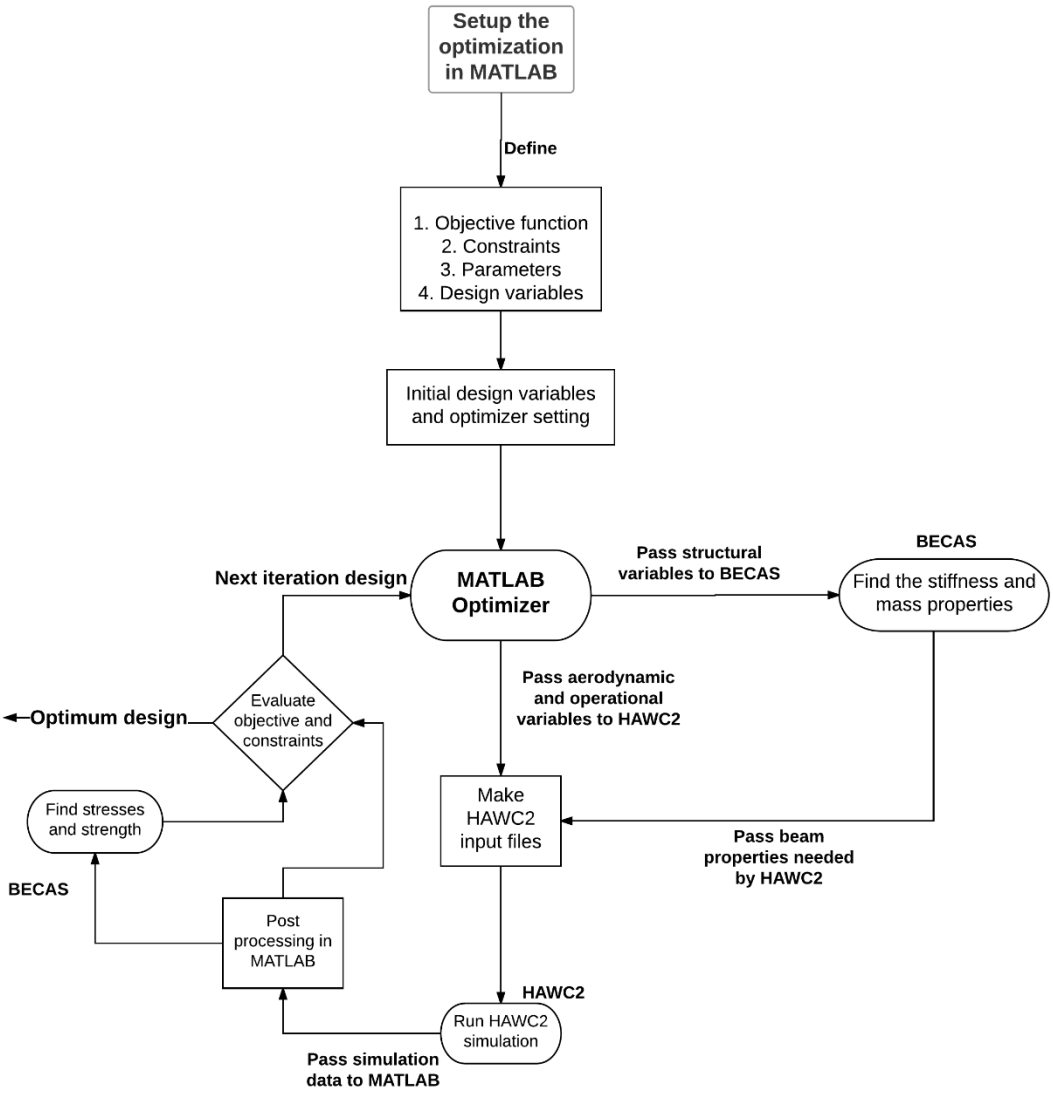

Figure 4.8: Coupled optimization workflow and data flow between MATLAB, HAWC2, and BECAS.

4.6 Optimization Cases

The next chapter presents the different optimization cases examined in this study. Here, we list these optimization cases. The optimization case produces an optimum turbine using the framework described in this chapter. Each optimization case has something different in the optimization setup. This difference leads to a different optimum turbine for each of the cases. The coupled optimization is an optimization in which the objective function couple the aerodynamic and structural analysis. In this work, the couple optimization uses m_b/AEP objective. The sequential optimization is an optimization in which the aerodynamic aspect of the design is optimized first without any consideration for structural aspect, then the resulting design is optimized structurally by minimizing the mass while keeping the outside shape fixed. In this work, sequential optimization uses two objective functions. The first is to maximize AEP and the second is to minimize m_b. The optimization cases analyzed in this work are:

1. Coupled optimization for a 5MW turbine with 7.5 m/s average wind speed.
2. Sequential optimization for a 5MW turbine with 7.5 m/s average wind speed.
3. Coupled optimization for a 5MW turbine with 10 m/s average wind speed.
4. Coupled optimization for a 3.75 MW turbine with 7.5 m/s averaged wind speed.
5. Coupled optimization for a 2 MW turbine with 7.5 m/s averaged wind speed.

CHAPTER 5

RESULTS AND DISCUSSIONS

In this chapter, the results of turbine optimization are presented. Interpretation and discussion of the results are included in this chapter as well. The organization of this chapter is as follows. First, description of the reference turbine that will be used to compare the results is described. This reference turbine is used to compare the results for 5MW turbine only. Next, a comparison between coupled and sequential optimization of 5MW turbines is presented. After that, a comparison between optimum turbines with a 5MW rating and designed at a location with a mean wind speed of 7.5 and 10 m/s is presented. The coupled optimization approach is used to for both turbines. Finally, results for optimum turbines with 2 and 3.75 MW rating is presented to see the effect of turbine rating on the cost of energy. It is noted here that all the optimized results shown in this chapter are feasible, meaning that they satisfy all the design constraints with no violation.

5.1 Description of the Reference Turbine

To assess the level of improvement of the optimized designs, the optimized results need to be compared against a reference design. The reference design chosen in this study is the modified DeepWind VAWT [7]. DeepWind VAWT was chosen because the shape, airfoil, operation, turbine topology, and distribution of structural properties are comparable to the resulting

optimized designs and hence, the comparison will be meaningful. However, there are slight variations between the turbines that are worth mentioning.

First, for a given maximum radius and height, the planform shape and the frontal area of the turbines are slightly different as can be seen in Figure 4.4. Second, the reference turbine is allowed to produce up to 5.8 MW while the optimized turbine is limited to 5.4 MW. This difference has to do with assumed losses in the turbine drivetrain and generator. Both reference and optimized turbines aim to generate 5MW net electric power. Finally, combination carbon fiber and glass fiber composite material are used for the reference turbine, while glass fiber composites only are used for the optimized turbine. The difference in material leads to an unfair advantage for the reference turbine when the masses are compared since carbon fiber is lighter and has higher strength compared to the glass fiber. For this reason, the reference turbine internal structure materials were redesigned using glass fiber and material topology was changed to be the same as given in Figure 4.5. The new design was obtained via a structural optimization keeping the outside shape and turbine operation fixed at their reference values. The resulting optimized mass was 70.77 tonnes compared with 52.4 tonnes for the reference turbine using carbon fiber. Different material topologies were tried to reduce the mass below 70.77 resulting in a maximum mass reduction of about 6.7%. This reduced mass is not used here for comparison since the internal thickness distribution with blade length that is different from what is used in the current optimization cases. Hence the final new mass used for comparison is 70.77 tonnes. The redesigned reference turbine is used to compare the structural properties and mass results.

It is worth noting that due to the increase in the mass of the reference turbine, gravity and centrifugal stresses have increase on the modified blade. The increase in the stresses caused failure at the lower root of the blade and at 33% blade length location. These failures can be eliminated by a redesign of the internal structure of the blade, but this will be at the expense of

the blade mass. It was decided to keep the blade mass at 70.77 tonnes and not increase it to satisfy failure constraints.

The main geometric properties of the DeepWind turbine are given in Table 5.1 and a schematic of the turbine is given in Figure 5.1.

Table 5.1: Main geometric properties of the DeepWind turbine.

Property	**Value**	**Unit**
Rated electrical power	5	[MW]
Rated rotor speed	0.6231	[rad/s]
Maximum radius	60.5	[m]
Rotor height	143	[m]
Chord at roots	5	[m]
Chord at equator	5	[m]
Swept area	11996	[m^2]
Airfoil at roots	NACA 0025	[-]
Airfoil at equator	NACA 0018	[-]

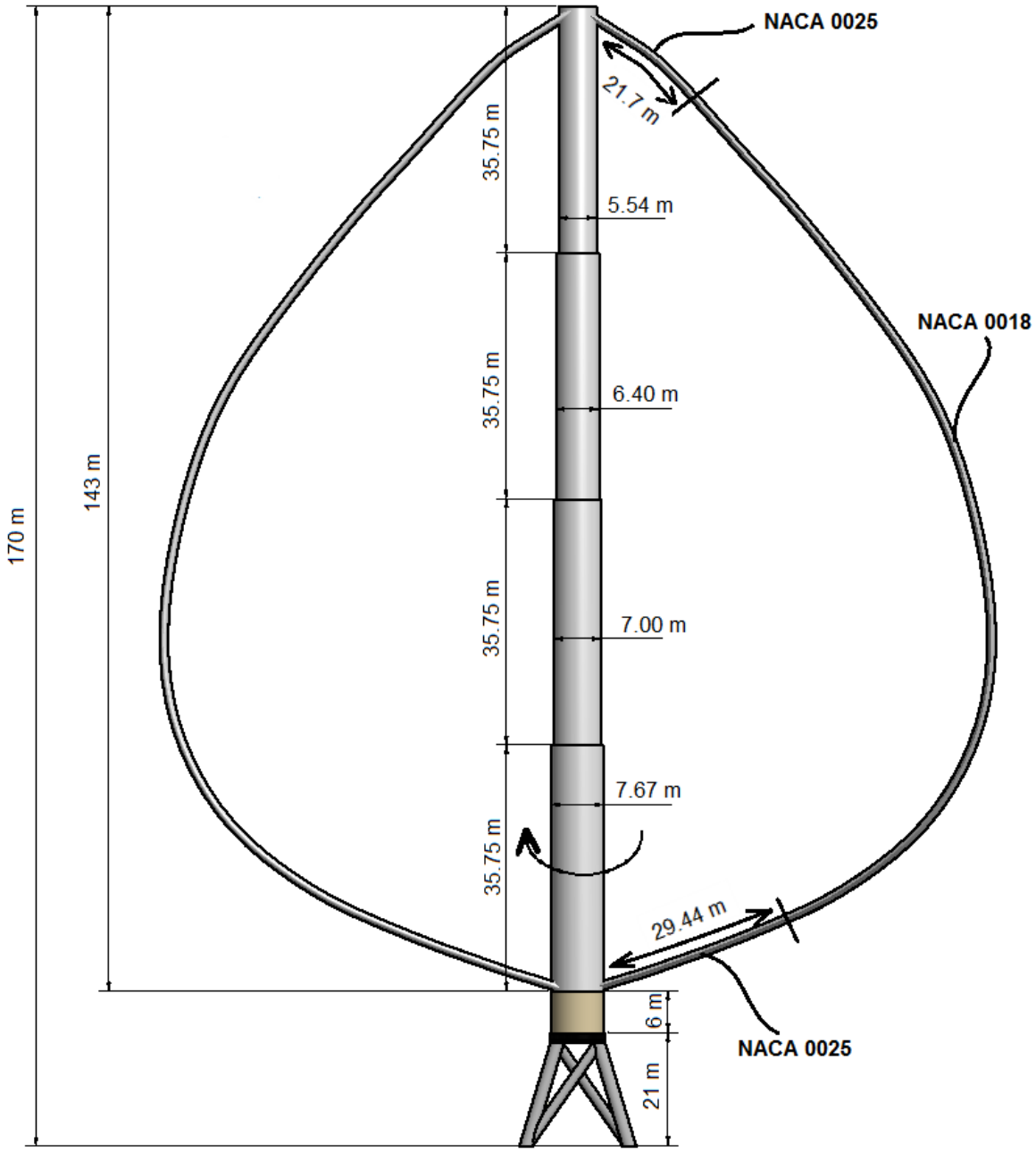

Figure 5.1: Schematic rendering of the DeepWind turbine [6].

5.2 Comparison between Coupled and Sequential Optimization for 5 MW Turbine at 7.5 m/s Averaged Wind Speed

Figure 5.2 shows a comparison between the reference and optimized turbines in terms of m/AEP values in $kg/MW.hr$. The results show that both optimization cases result in a lower m/AEP value compared with the reference turbine. The value of m/AEP is of great importance when comparing turbine designs because lower m/AEP means lower cost of energy which is the ultimate goal in wind turbine design. The reduction in m/AEP value for the optimized designs means that the optimization framework developed in this thesis is successful in its premise, which is to produce VAWT design that is superior in terms of cost of energy while satisfying all constraints. In terms of percentage improvement of m/AEP compared with the reference design, the sequential and coupled optimized turbines have 42.5% and 52.4% relatively lower m/AEP values respectively. These improvements are significant and shows the capability of the current framework. As a reminder, sequential optimization attempts to maximize AEP first at fixed internal thicknesses (aerodynamic optimization) then it minimizes the mass keeping the outside shape of the blade fixed (structural optimization). Coupled optimization on the other hand, minimizes m/AEP directly by coupling the aerodynamic and structural optimization together.

The better results achieved by the coupled optimization compared with the sequential optimization will be explained in some details below, but it suffices to say here that the lower value of m/AEP achieved via coupled optimization illustrates the benefit of incorporating multidisciplinary optimization into the objective function. The benefit is a better value of the desired objective when compared with a sequential design that focuses on a single discipline at a time. The benefit of coupled optimization as suggested by Figure 5.2 is a lower cost of energy. This is achieved by virtue of achieving lower m/AEP value compared with the

sequential design. Incorporating a multidisciplinary objective function like the one used in the coupled optimization seems to give the optimizer better ways to improve the design compared with a single discipline objective function like the sequential optimization. Single discipline optimization approach to a multidisciplinary problem tend to give a sub-optimal solutions as suggested by Figure 5.2.

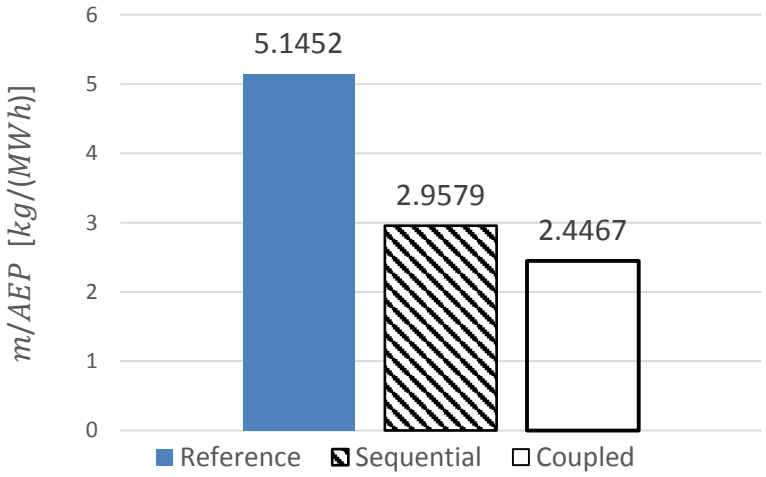

Figure 5.2: Comparison between the reference and optimized turbines in terms of $\boldsymbol{m/AEP}$ values.

To get more insights into the different values of m/AEP for the three turbines, it is helpful to examine the individual values of AEP and blade mass (m). Figure 5.3 shows the different values of AEP in GWh for the reference and optimized turbines. Figure 5.3 shows different trends when compared with the m/AEP trends. For instance, the coupled optimized turbine which has the best m/AEP value, has the lowest AEP value compared with the other two turbine designs. In particular, the percentage change in AEP for the coupled optimized turbine compared with the reference turbine is -30.4% which is a large reduction in the amount of extracted energy. The sequential optimized turbine on the other hand achieves a relative increase of 11.9% in AEP value compared with the reference design. These numbers illustrates the fact that although a certain optimal design might be better in the overall objective (like the

coupled design), some performance aspects (like AEP) of that design might be inferior when compared with a less optimal design (such as the sequential design).

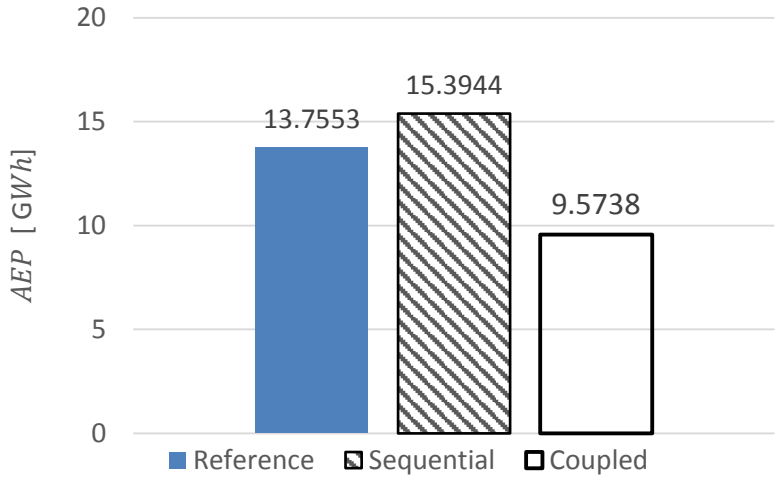

Figure 5.3: Comparison between the reference and optimized turbines in terms of $\boldsymbol{AEP}$ values.

The AEP value comparison shows that the coupled design does not achieve the lowest m/AEP because it generates more energy. The low value of m/AEP cab be attributed to the fact that the resulting structural design is superior compared with other designs. To see this clearly, Figure 5.4 shows a comparison between the blade mass for the three turbine designs. The trend of the mass follows the same trend as for m/AEP, namely, the coupled design has the lowest mass followed by the sequential design and the reference design has the highest mass among all designs. In terms of percentage change in blade mass values, the coupled and sequential designs achieve relative mass reduction of 66.9% and 35.7% respectively.

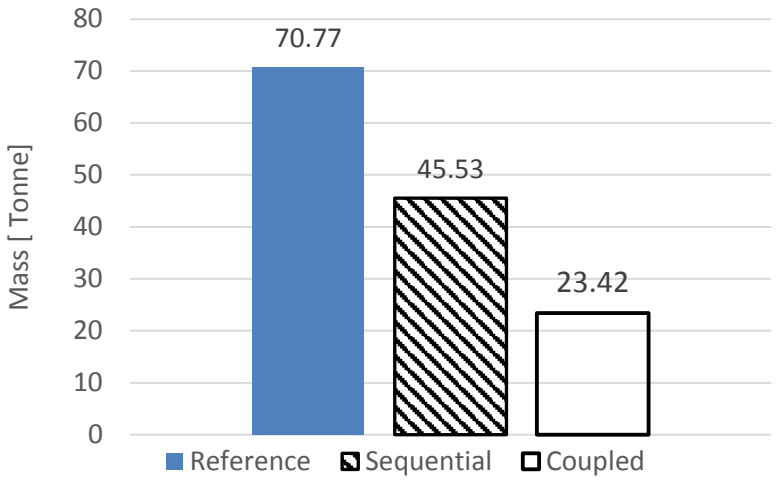

Figure 5.4: Comparison between the reference and optimized turbines in terms of blade mass values.

Comparing the AEP and blade mass values for the optimized turbines show that the main reason for the superiority of the coupled design in terms of m/AEP value is its low blade mass. Having a blade mass of almost half that of the sequential design allows the coupled design to have the best m/AEP value albeit its low AEP value compared with other designs. It is clear that the coupled design is mass biased design, meaning that the design achieves low m/AEP values by focusing on reducing the mass more than increasing AEP. The sequential design on the other hand, is an AEP biased since the design strategy is inclined to increasing AEP more than reducing the blade mass.

The reason for the sequential design to be AEP biased is the that one of its two objective functions is to maximize AEP. Having AEP as an objective function directs the overall design to achieve high AEP value.

The reason for the coupled design to be mass biased is not very clear since the objective function weights AEP and mass in the same way since an increase in AEP has the same effect as a decrease in mass. It could be that constraints might be violated if AEP is increased hence the optimizer chooses a path in which m/AEP is minimized by reducing the mass. Another reason for the optimizer choice could be attributed to the sensitivity of the objective function to different variables. The m/AEP objective function is more sensitive to structural design variables than the aerodynamic design variables. This idea can be illustrated by examining Figure 5.5 which shows the gradient of the m/AEP objective function for all the design variables during a single optimization iterations. In Figure 5.5 the aerodynamic design variables range from 1 to 6 while the structural variables range from 7 to 12 and the ordering follows the order in Table 4.1. It is clear from the figure that the objective function has higher sensitivity to the structural variables compared with aerodynamic variables as evident from the values of scaled gradients. The high sensitivity of the structural design variables leads the optimizer to change the mass in larger proportion compared with AEP. It is worth mentioning here that the idea of the structural variable being more sensitive to changes in m/AEP objective is not a general statement, but it is true for the current optimization.

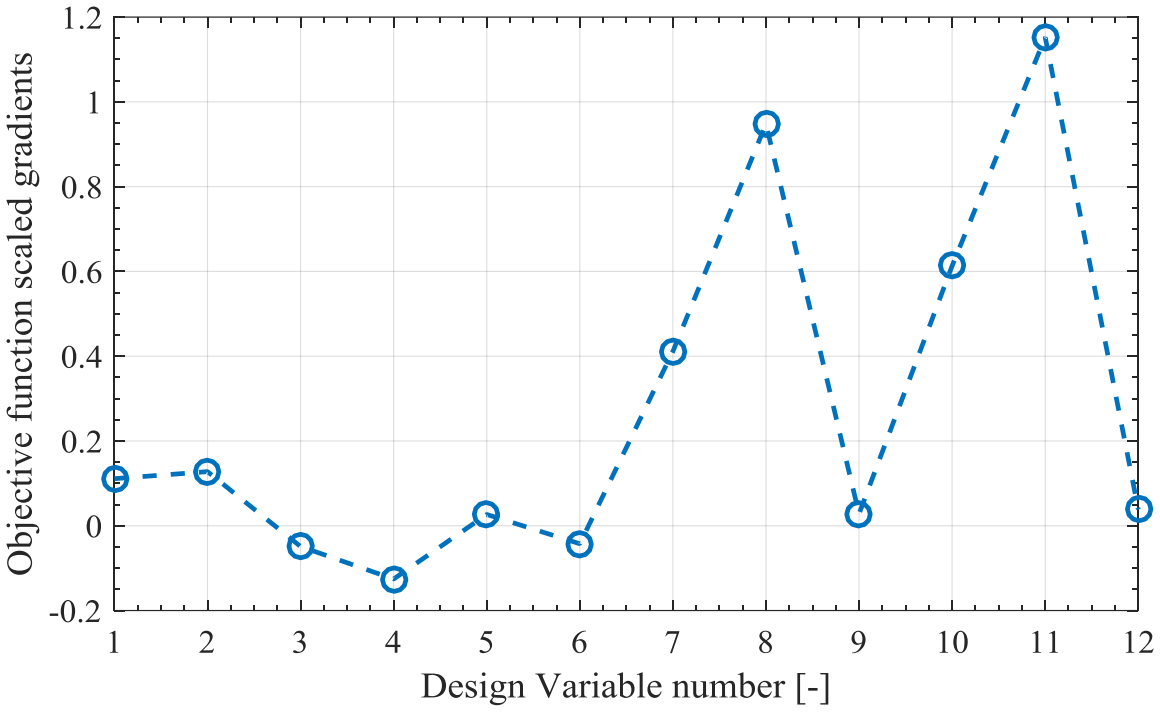

Figure 5.5: m/AEP objective function scaled gradients. Aerodynamic and structural variables range from 1 to 6 and 7 to 12 respectively.

The discussion above focused mainly on the objective function value without looking at the physical design of the turbine. In the discussion below more insights into the design of the turbines are given.

Figure 5.6 shows a comparison between the reference and optimized designs regarding the outer turbine shape. The two figures give some insights into the resulting values of mass and AEP for the optimized turbines. The small size of the coupled optimized turbine together with the short blade length as shown in Figure 5.6 explains the low blade mass and relatively low AEP. On the other hand, the large size of the sequential optimized turbine explains the large AEP value obtained by the turbine. Large frontal area of the sequential optimized turbine allows to capture more power at low wind speeds and this in turn leads to higher AEP value.

Figure 5.7 and Figure 5.8 quantify the main geometric properties which are the diameter, height, blade length, and turbine frontal area for the three turbines.

An interesting point to mention is that even though the sequential optimized turbine has larger frontal area and total blade length compared with the reference turbine, its total blade mass is still lower than the reference blade mass. This illustrates that the sequential optimized turbine uses more efficient structure compared with to the reference turbine. Another point to notice about the shape of the turbines from Figure 5.6 is that the optimized turbines have the maximum radius at nearly half the height which is in contrast with the reference turbine in which the maximum radius is at a lower height. This change in shape could be a reason for the more efficient structural design of the optimized turbines. Note that the DeepWind turbine outer shape was mainly chosen based on minimizing the mean stress resulting from the gravity and centrifugal forces [32] and not the maximum stress resulting from gravity, centrifugal, and aerodynamic forces as in present work.

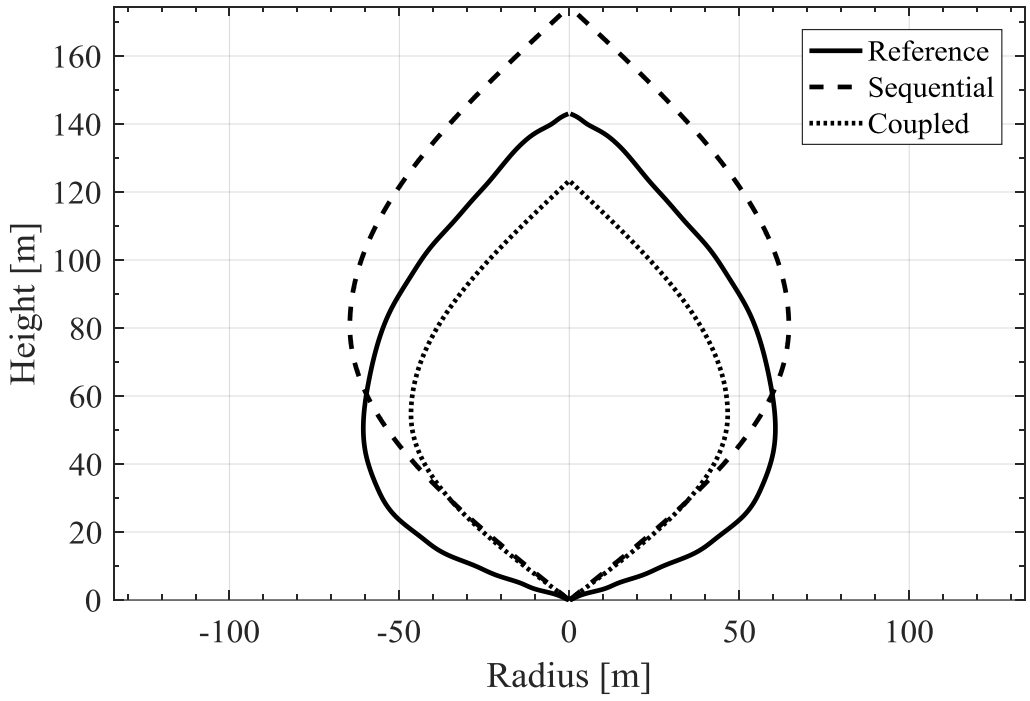

Figure 5.6: Turbine outer shape comparison between the reference and optimized turbines.

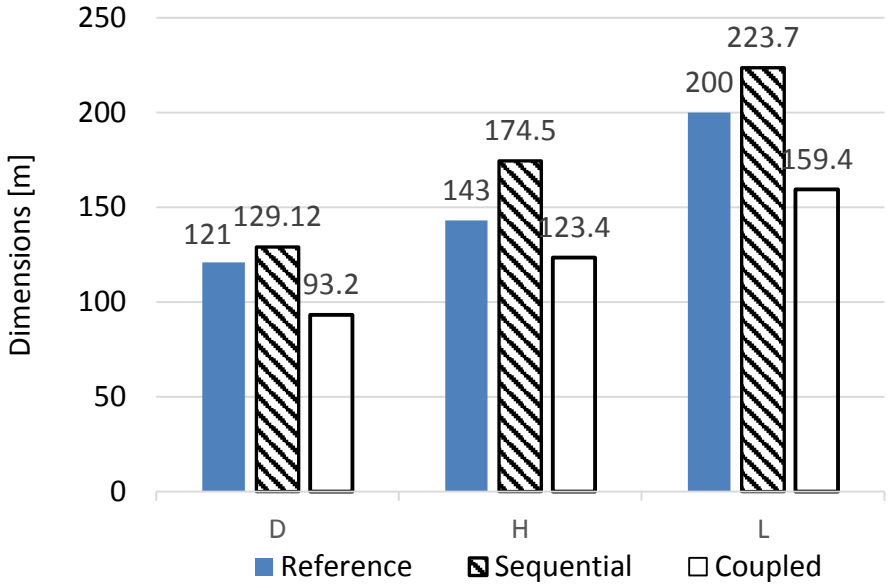

Figure 5.7: Comparison between the reference and optimized turbines in terms of the main turbine geometric properties, diameter (***D***), height (***H***), and total blade length (***L***).

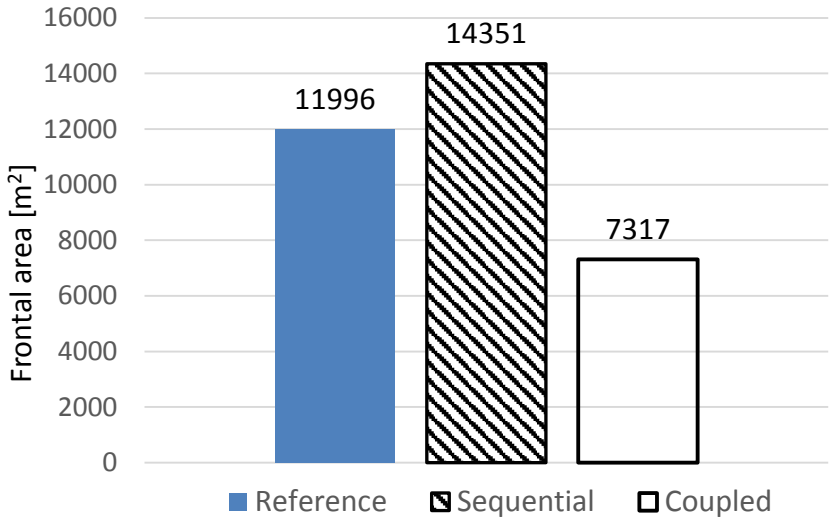

Figure 5.8: Comparison between the reference and optimized turbines in terms of the turbine frontal area.

Another critical design variable to look at is the blade chord length. Blade chord length influences both the aerodynamic performance and the mass of the blade. Figure 5.9 shows a comparison between the blade chord length for the reference and optimized turbines. The first thing to notice is that the optimized designs have different chord length between the root (c1) and equator (c2) section which is in contrast with the reference design which has constant chord along the blade length. The difference in chord length is more prominent in the case of the coupled design, in which the difference between the chord length at the root and equator is significant. The sequential design has a smaller difference between the two chord lengths when compared with the coupled design. Figure 5.9 shows that the optimized designs have larger root chord length compared with the reference design. Regarding the equator chord length, the sequential design has larger chord compared with the reference while the coupled design has chord length which is lower compared with the reference. The reason for the large chord at the root is to minimize the stress, while the choice of equator chord length is based on achieving specific solidity value that the optimizer sees optimal.

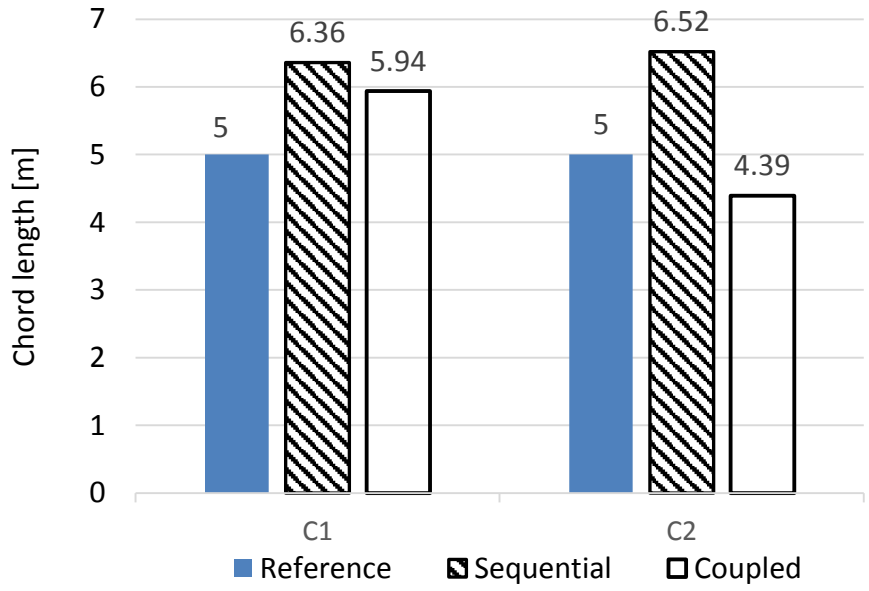

Figure 5.9: Comparison between the root (c1) and equator (c2) chord lengths for the reference and optimized turbines.

Non-dimensional turbine parameters can be useful to make simple general guidelines for the design of the turbine. Comparison between some of the essential non-dimensional parameters of the turbine which are height to diameter ratio (H/D), length to diameter ratio (L/D), equator chord to radius ratio (c_2/R), and tip speed ratio (TSR) at rated wind speed for the reference and optimized turbines are shown in Figure 5.10. The optimized designs have higher (H/D) and (L/D) compared with the reference design The values of (H/D) and (L/D) for both optimized designs are very close to each other with the sequential design having slightly higher values for both quantities. Higher (H/D) and (L/D) for the optimized design means that the turbines contribution to the frontal area from the height is more than the diameter. In addition, due to higher values of (H/D) and (L/D) the shape of the optimized turbines are thinner and more elongated along the vertical axis compared with the reference design.

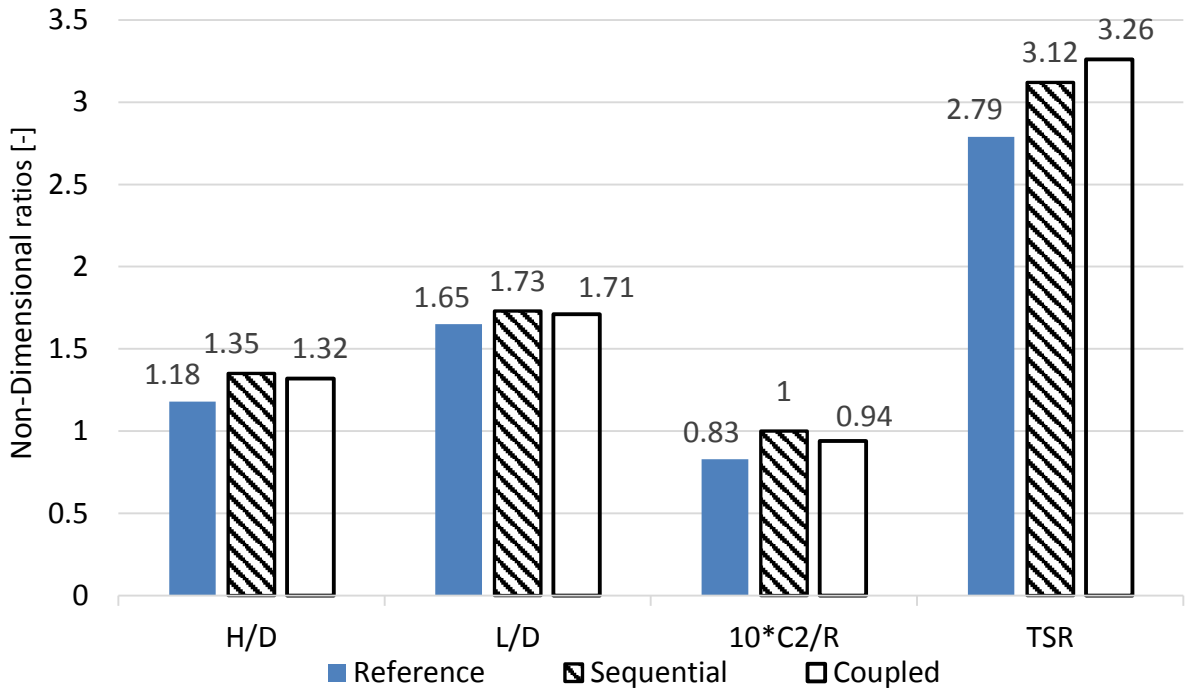

Figure 5.10: Comparison between height to diameter $(\boldsymbol{H/D})$, length to diameter $(\boldsymbol{L/D})$, equator chord to radius $(\boldsymbol{c_2/R})$, and tip speed ratio (TSR) at rated wind speed for the reference and optimized turbines.

In terms of solidity and TSR, Figure 5.10 shows that the optimized designs have higher solidity and TSR than the reference design. In general, higher solidity can achieve better power coefficient than lower solidity as evident in the results shown Figure 5.11 which is taken from Figure 4.11 of reference [47]. Thus the optimizer chooses higher solidity for the turbines to achieve higher power coefficient. Figure 5.10 shows also that TSR for the coupled design is higher than the sequential design. This is mainly a consequence of lower solidity of the coupled design compared with the sequential design. Lower solidity requires higher TSR to achieve maximum power coefficient as shown in Figure 5.11. The optimizer seems to aim to achieve this balance in the design.

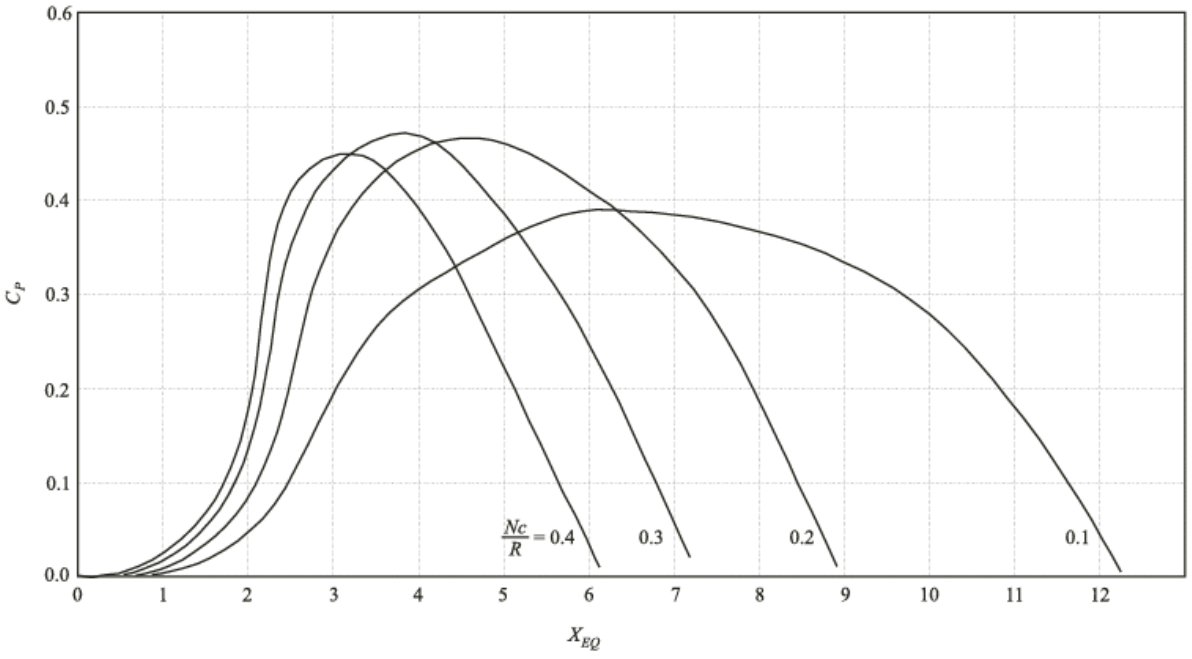

Figure 5.11: Power coefficient $\boldsymbol{C_p}$ versus TSR ($\boldsymbol{X_{EQ}}$) showing the effect of changing solidity on the turbine power coefficient [47].

The power curve shows the power generated by the turbine versus the wind speed, and it is one of the most critical performance plot for a wind turbine. Figure 5.12 shows the power curve for the reference and optimized turbines. The power curve for all the three turbines is very similar since they are controlled using the same logic which is to maximize the power at below rated

wind speeds and keep and power constant at above-rated wind speeds. Figure 5.12 explains the low and high AEP for the coupled and sequential optimized turbines respectively. As can be seen in Figure 5.12, the coupled design develops significantly less power for winds below 15 m/s compared with the sequential optimized and reference turbines. The lower power developed by the coupled design causes the lower AEP value compared with the other two turbines. The sequential design achieves the highest power among all three turbines for below rated wind speeds, i.e. below 13 m/s. the high power of the sequential design in combination with the large frontal area are the reasons for getting the highest AEP value among the three turbines. The rated wind speed (wind speed at which the turbine develops 5 MW) for each turbine can be inferred from Figure 5.12. The rated wind speeds are 13.5 m/s, 13 m/s, and 15 m/s for the reference, sequential, and coupled turbines respectively.

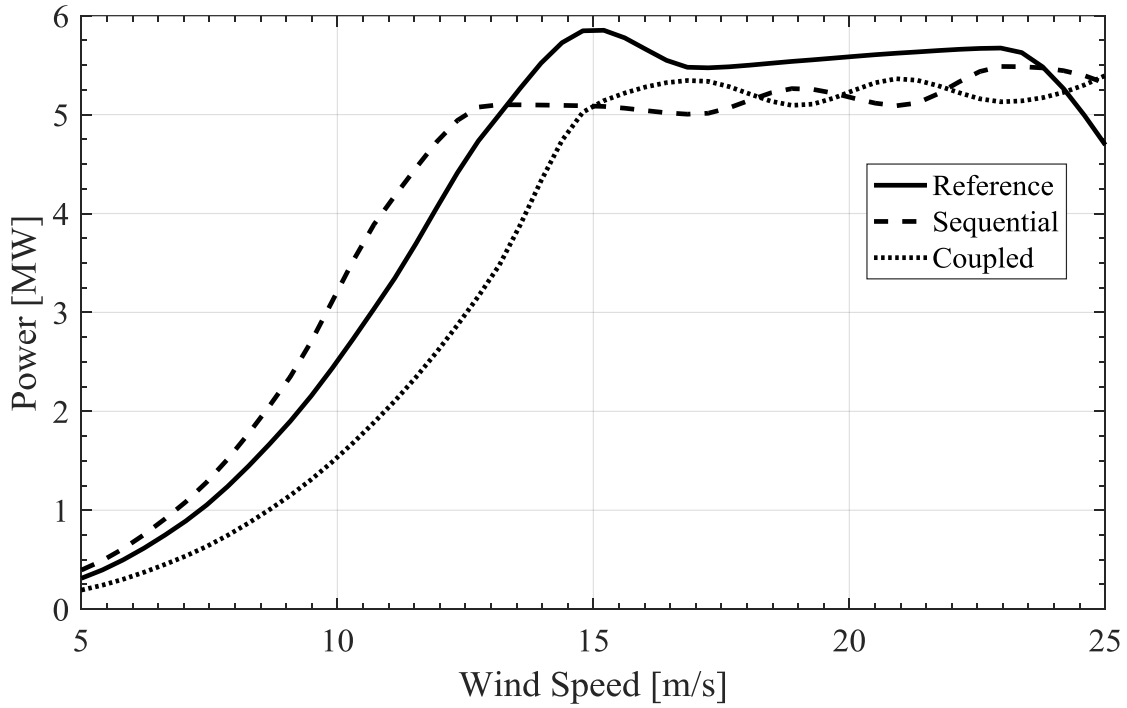

Figure 5.12: Comparison between the power curves for reference and optimized turbines.

Another aspect of the design worth showing is the rotor speed. Rotor speed influences the TSR and determines how the turbine regulates the power at above-rated wind speed. Figure 5.13 shows the rotor speed variation with wind speed for the three turbines. For the optimized

turbines, a linear relationship between the rotor speed and wind speed in the range from cut-in speed until rated wind speed is observed. This linear relation is because the rotor speed is constrained to have a constant TSR in this region of operation. Having constant TSR leads to the observed linear relation. The value of the tip speed ratio is one of the design variables and is chosen by the optimizer in a way to minimize the objective function. It can be seen from Figure 5.13 how the rotor speed is reduced at the above the rated conditions to regulate the power. Although the TSR for the coupled and sequential designs are very similar in magnitude as was shown in Figure 5.10, the rotor speed is very different. The reason for the difference is the different diameters of the coupled and sequential designs. Note that the rotor speed varies inversely with the size of each rotor as shown in Figure 5.13. The difference in diameters is the reason why the sequential design has the slowest rotation speed, while the coupled design has the fastest rotation speed. The rotation speed of the rotor is a significant influence on the design of the turbine drivetrain, so it is worthwhile to study the effect of coupling the design of the drive train with the current framework.

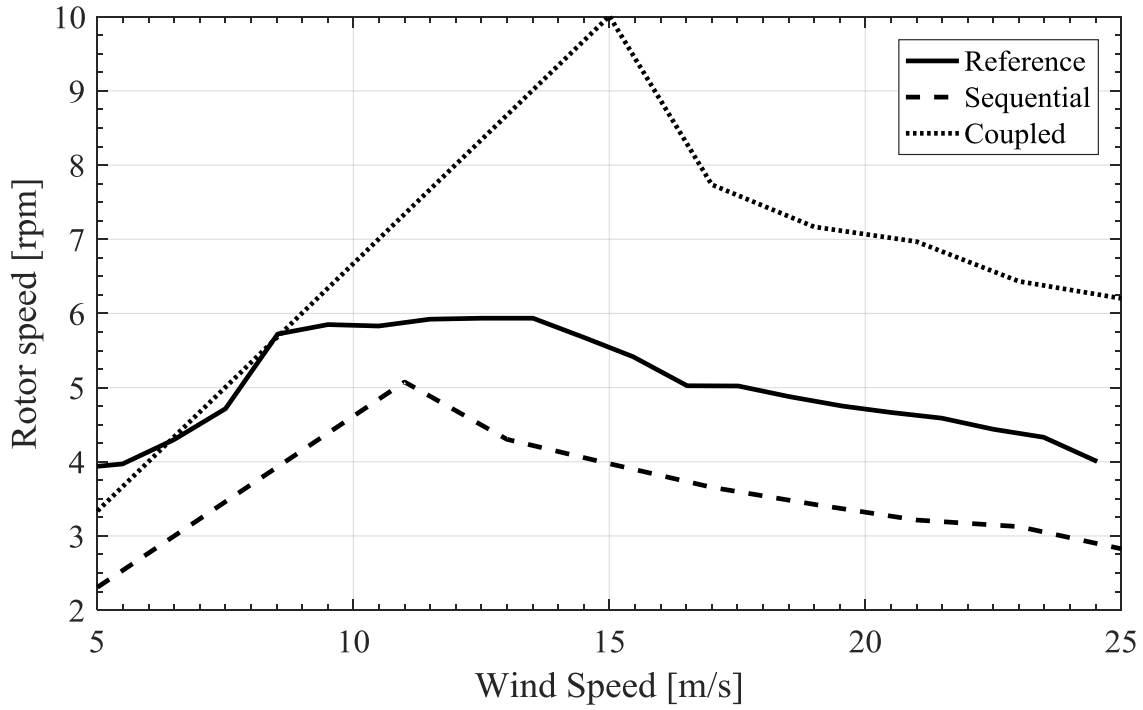

Figure 5.13: Rotor speed in rpm versus the wind speed for the reference and optimized turbines.

Power coefficient C_p versus TSR plot gives an idea about the aerodynamic efficiency of the turbine at different operating conditions. Figure 5.14 shows a comparison of C_p for the reference and optimized turbines. The first thing to note about C_p for the different turbines is that all turbines have very similar power coefficient in terms of its variation with TSR and also in terms of its maximum value. The maximum of C_p occurs at different TSR for each turbine and the reason for this difference can be attributed to the difference in solidity. Table 5.2 shows a comparison of the maximum C_p and the TSR that archives this maximum C_p for reference and optimized turbines. Table 5.2 shows an important observation about the optimum TSR value. We can see from Figure 5.10 that the optimum TSR for sequential and coupled design are 3.12 and 3.26 respectively. At those TSR, the corresponding C_p are 0.328 and 0.336. From these numbers, we can see that the optimizer did not choose the TSR that gives the best C_p, but instead chose a different value that is not optimum in terms of C_p. The reason for this might be that the optimizer terminated at a local minimum and not the true global minimum. Another reason for this is that choosing the TSR which gives maximum C_p might be actually inferior to the objective function which is m/AEP. It is possible that better C_p leads to higher mass or even violates some constraints leading to worse overall m/AEP.

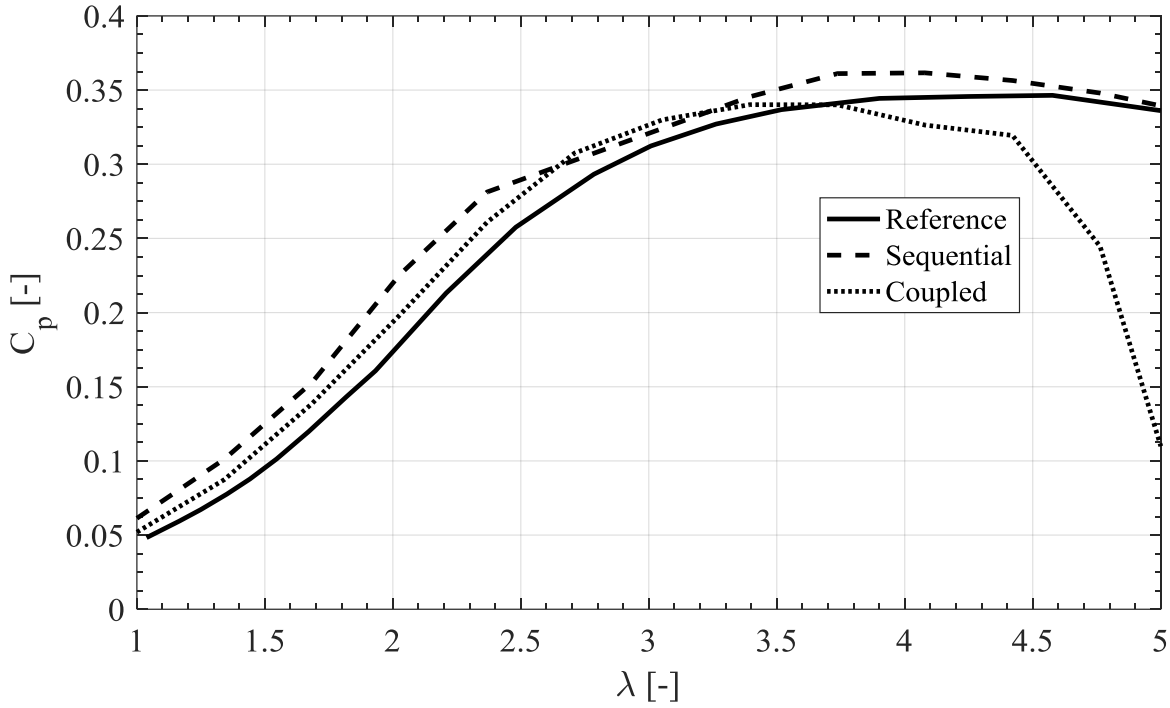

Figure 5.14: Power coefficient versus TSR for the reference and optimized turbines.

Table 5.2: Maximum power coefficient and corresponding TSR for reference and optimized turbines.

Turbine	$C_{p_{max}}$	**TSR**
Reference	0.346	4.58
Sequential	0.362	4.10
Coupled	0.340	3.40

So far, the focus of discussion has been on aerodynamic performance of the optimized turbines. Next, we examine some structural aspects of the design.

The failure index which is given by equation (4.10) (but without the minus one term) is the ratio between the maximum stress and the allowable stress adjusted by a safety factor. The failure index is a function of the blade position since at each position the stress state is different. Figure 5.15 shows a comparison of the maximum failure index versus the normalized blade

length for the reference and optimized turbines. The maximum failure index reported in the figure takes into account all the analyzed wind speeds from 5 to 25 m/s. Figure 5.15 shows that the coupled design has the lowest failure index when compared with the reference and sequential design turbines across the entire blade length. Reference turbine has the highest failure except in between 40% to 55% normalized blade length where the sequential design failure index is the highest. Both optimized designs have failure index less than one everywhere along the blade which means that the designs satisfy the strength constraints. Reference turbine on the other hand has failure index larger than one at a few locations along the blade length, especially near the lower root. One reason for the reference turbine to have failure index larger than the optimized designs could be attributed to the outer shape of the reference turbine. As was shown in Figure 5.6 the reference turbine has very aggressive attachment angle at the lower root which could be a reason for the significant stress.

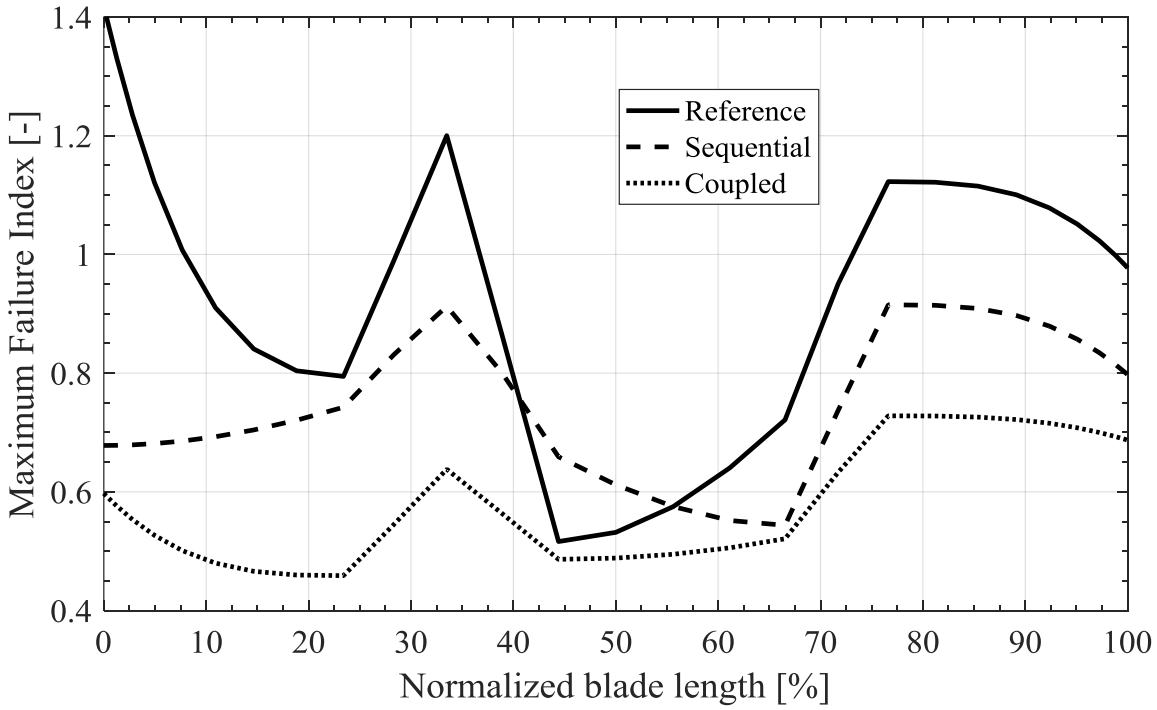

Figure 5.15: Maximum failure index versus the length of the blade for the reference and optimized turbines.

Although the three turbines are different regarding overall dimensions and the blade mass, the failure index functionality with the normalized blade length shows some common features for all three turbines. For instance, all the three turbines have peaks in the failure at 33.5% and 76.6% blade length. To shed some insights about the reason for these peaks, the direction of stress that causes the maximum failure needs to be examined. The direction of stress is with respect to the glass fiber main direction as indicated in Figure 4.2. So we will investigate whether normal or shear stress causes the maximum failure. For this purpose, we will look at seven different locations along the blade. These locations are given in Table 5.3. Table 5.4 lists the maximum failure index with the direction of stress that caused it along with the wind speed at which the maximum failure occurred. Table 5.4 shows that the maximum failure index for the three turbines is not caused only by normal stress along the fiber direction σ_{11} but also due to shear stress σ_{12}. The mode of the maximum failure depends on the location along the blade. For instance, the peaks that is observed in Figure 5.15, which occur at location index 3 and 6, are caused by shear stress as can be seen in Table 5.4. It is interesting to note that for the reference and coupled design turbines, the maximum failure occurs at the wind speed of 25 m/s which is the maximum wind speed for power generation for these turbines. The maximum failure of the sequential design, on the other hand, occurs mostly at a wind speed of 23 m/s.

Table 5.3: location index and corresponding normalized blade length.

Location index	**Normalized length (%)**	**Location index**	**Normalized length (%)**
1	0	5	66.5
2	23.4	6	76.6
3	33.5	7	100
4	44.4		

Table 5.4: Maximum failure index along with the direction of stress that caused the maximum failure and the wind speed at maximum failure for several location along the blade length.

Turbine	Location index	Failure index	Direction of max failure	Wind speed (m/s)
Reference	1	1.42	σ_{11}	25
	2	0.79	σ_{11}	25
	3	1.20	σ_{12}	23
	4	0.52	σ_{11}	25
	5	0.72	σ_{11}	25
	6	1.12	σ_{12}	23
	7	0.98	σ_{13}	25
Sequential	1	0.678	σ_{11}	23
	2	0.743	σ_{11}	23
	3	0.913	σ_{12}	15
	4	0.659	σ_{12}	23
	5	0.544	σ_{11}	25
	6	0.915	σ_{12}	23
	7	0.797	σ_{12}	23
Coupled	1	0.597	σ_{11}	25
	2	0.459	σ_{11}	25
	3	0.638	σ_{12}	25
	4	0.486	σ_{12}	25
	5	0.521	σ_{11}	25
	6	0.728	σ_{12}	25
	7	0.687	σ_{11}	25

Figure 5.16 shows a comparison of the maximum failure index along the main fiber direction (σ_{11}). This plot is similar to Figure 5.15 except that only the failure along the fiber direction is considered (basically the shear failure is ignored in this plot). What is noticeable in Figure 5.16 is the close similarity between the coupled and sequential failure values in contrast with what was observed in Figure 5.15. The large increase in the failure index due to shear stress at 33.5% and 76.6% blade length which is seen in Figure 5.15 does not show up in the normal stress failure index as seen in Figure 5.16. Figure 5.16 suggests that due to lower values of failure index along the main fiber direction it could be possible to design the blade structure based on the normal stress consideration, and then use some composite materials that has better shear strength in order to avoid the large increase in failure index that is seen in Figure 5.15.

From Figure 5.15 and Figure 5.16 we can make two critical comments. The first is about the importance of considering the shear stress in the constraints calculation. As can be seen in Figure 5.15, shear stress can cause the most significant damage along with some length portion of the blade. This observation might be dependent on the type of composite layup used and the topology of the internal thickness distribution in the blade airfoil. The second is about the magnitude of the maximum failure index for the optimized turbines that can be seen in Figure 5.15 which is not very close to 1 for all blade locations. Having room to increase the failure index indicates a potential to lower the mass which lowers the overall cost of energy. The choice of the structural variables by the optimizer seems to be slightly suboptimal, and the reason for this could be either that the optimizer terminated at a local minimum or that it was not able to reduce the mass further without violating some constraints. Let us remember that the optimizer cannot change the structural design for each meter along the blade. the optimizer has only freedom to change the design of the root and equator sections only. So even if there is a potential to decrease the mass along some portions of the blade, the optimizer cannot target that specific location due to the limitation in the structural variables given to the optimizer.

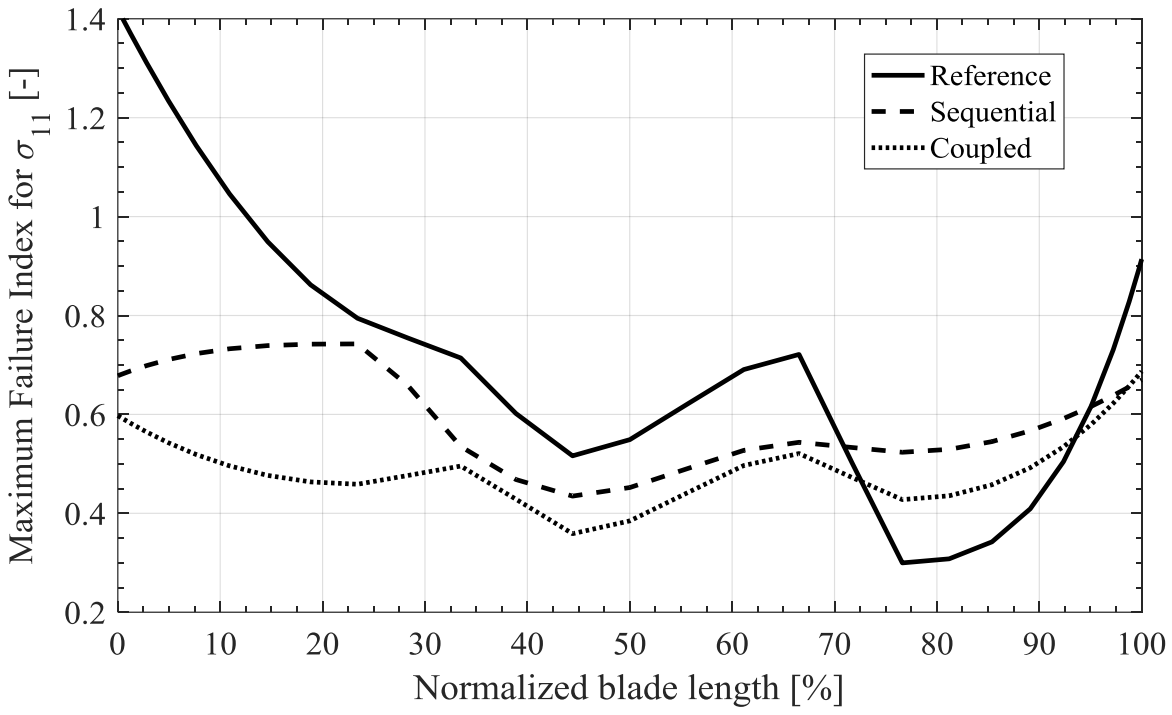

Figure 5.16: Maximum failure index along the main fiber direction ($\boldsymbol{\sigma_{11}}$) versus the length of the blade for the reference and optimized turbines.

To get more insight into the failure index, bending and torsional moments variation for one revolution of the turbine are shown next. The moments' variation for one revolution is shown for all three turbines at 0% and 33.5% blade length and at a wind speed that gave the maximum failure index as given in Table 5.4.

Figures 5.17, 5.18, and 5.19 show comparison between the reference and optimized turbines regarding the flapwise, edgewise, and torsional moments respectively. The moments are shown for a complete revolution of each turbine at the lower root of the blade. Looking at the flapwise moment plot, we can see that the reference has much larger flapwise moment compared to the optimized turbines. The reference turbine also has considerable variation in the moment as it completes the full revolution. The coupled design turbine has the lowest absolute value of the flapwise moment as compared to the other two turbines. In all three turbines, it can be seen that

the maximum absolute value of the moment occurs in the upwind part of the rotation between 60-80 degrees. Edgewise moment plot shows large absolute values of edgewise moment in comparison with the flapwise moment for the three turbines. The variation in the edgewise moment is significant when compared with the flapwise moment. Similar to the flapwise moment, the coupled design turbine has the lowest absolute value of the edgewise moment compared with the other two turbines. Thus the results show that the reference turbine has the largest failure index at the root. This is followed by the sequential design, and then finally the coupled design which has the lowest failure index. This ordering in the failure index can be explained partially by the relative magnitude of the flapwise and edgewise moments that are shown in Figure 5.17 and Figure 5.18. The torsional moment plot shown in Figure 5.19 shows that the reference turbine has drastically different torsional moment when compared with the optimized turbines. The optimized turbines have a small value of torsional moment (almost two orders of magnitude smaller than the flapwise and edgewise moment) while the reference turbine has a considerable larger value as well as variation in its torsional moment. The torsional moment of the reference turbine is still an order of magnitude smaller than the corresponding flapwise and edgewise moments.

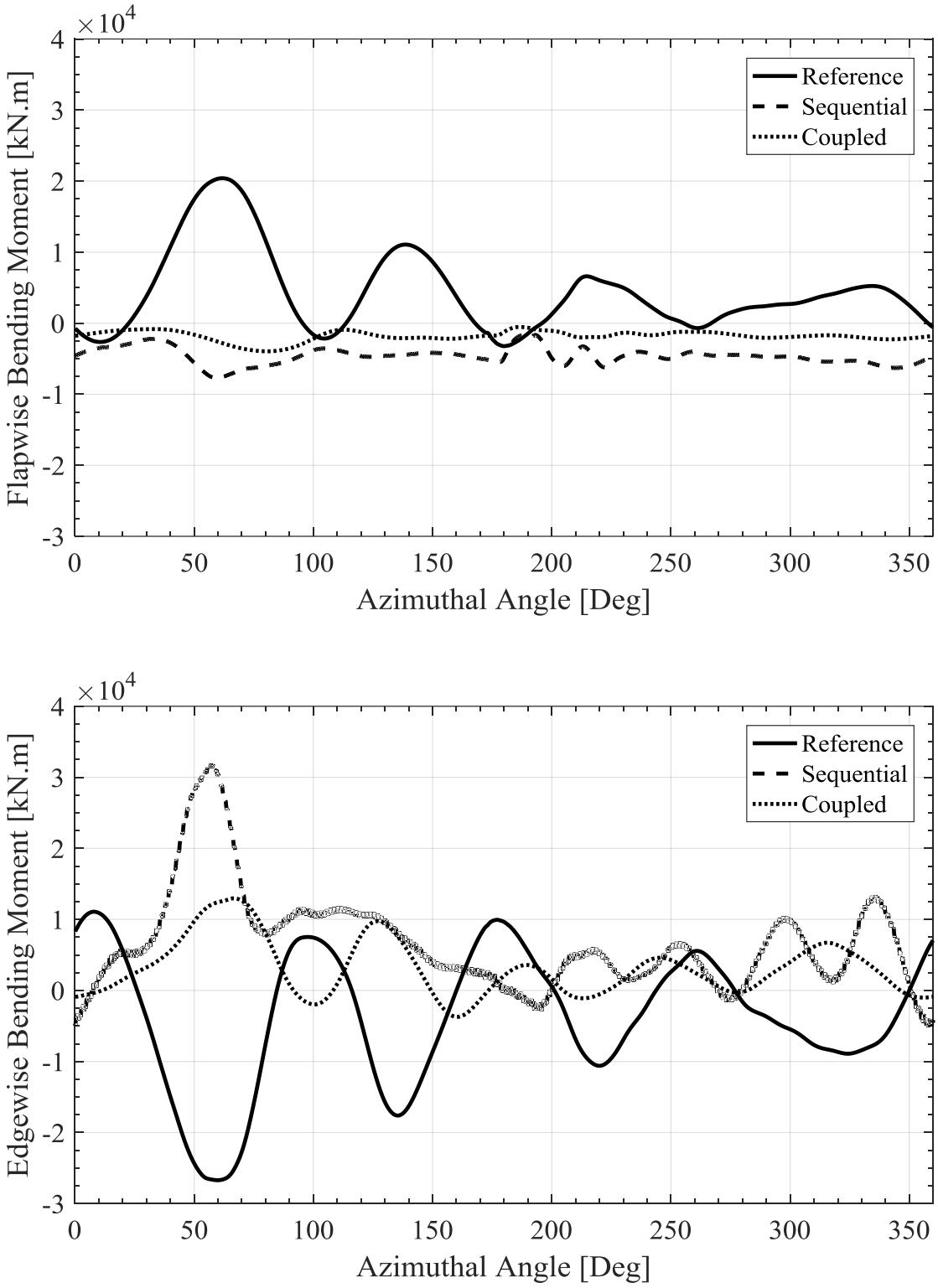

Figure 5.18: Edgewise bending moment variation for a complete revolution at the lower root of the blade for the reference and optimized turbines.

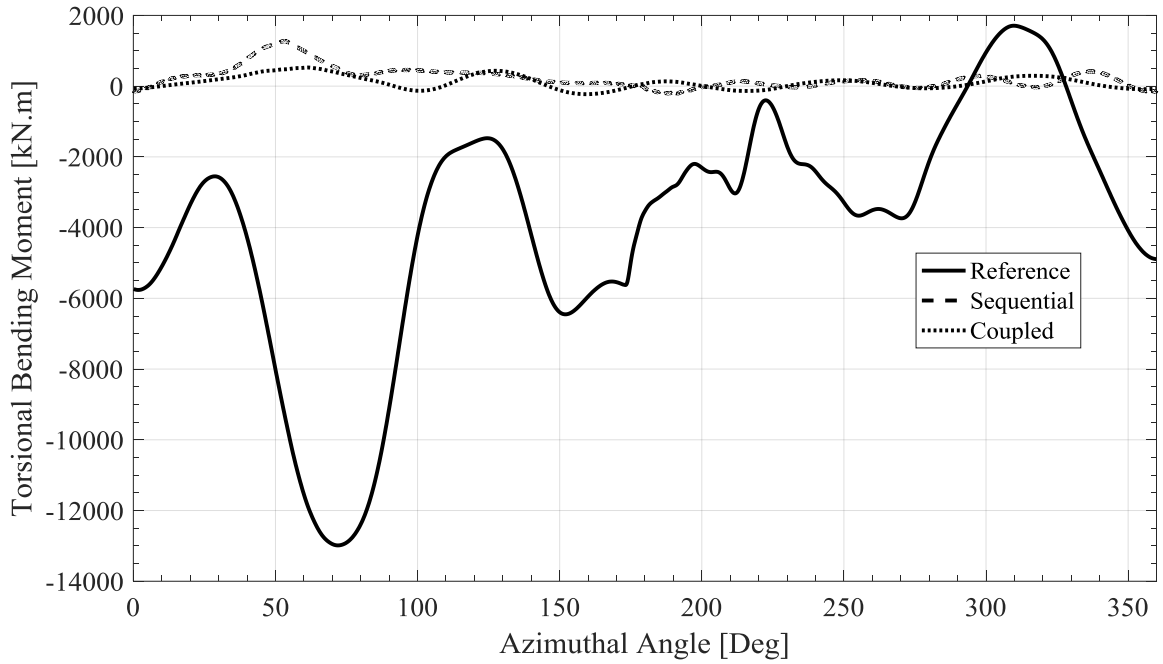

Figure 5.19: Torsional moment variation for a complete revolution at the lower root of the blade for the reference and optimized turbines.

Figures 5.20, 5.21, and 5.22 show comparison between the reference and optimized turbines in terms of the flapwise, edgewise, and torsional moments, respectively .at 33.5% blade length location. At this blade length, the maximum failure index was caused by shear stress as was shown in Table 5.4. Comparing the flapwise and edgewise moments at 33.5% with those at 0% blade length, it can be seen that the value of moments at 33.5% location are lower by an order of magnitude as compared to the moments at the root section. Reference turbine still has the highest flapwise moment. Regarding the edgewise moment, the sequential design turbine has the highest moment followed by the coupled design. The torsional moment at 33.5% location has a similar magnitude to the flapwise and edgewise moments in contrast to what was seen for the root location. The reference turbine has the most significant torsional moment followed by the sequential design and the coupled design. It is the similarity in the order of magnitude between the torsional moment and the bending moments that probably caused the 33.5% location to have a maximum failure due to shear stress.

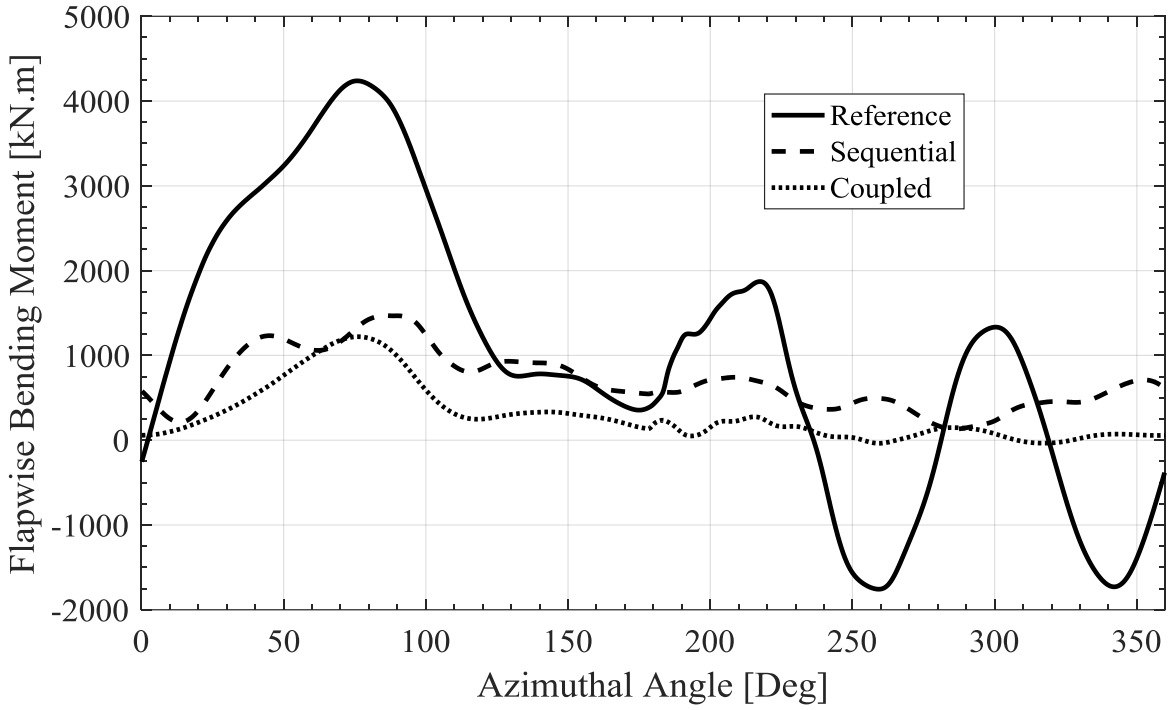

Figure 5.20: Flapwise bending moment variation for a complete revolution at 33.5% blade length for the reference and optimized turbines.

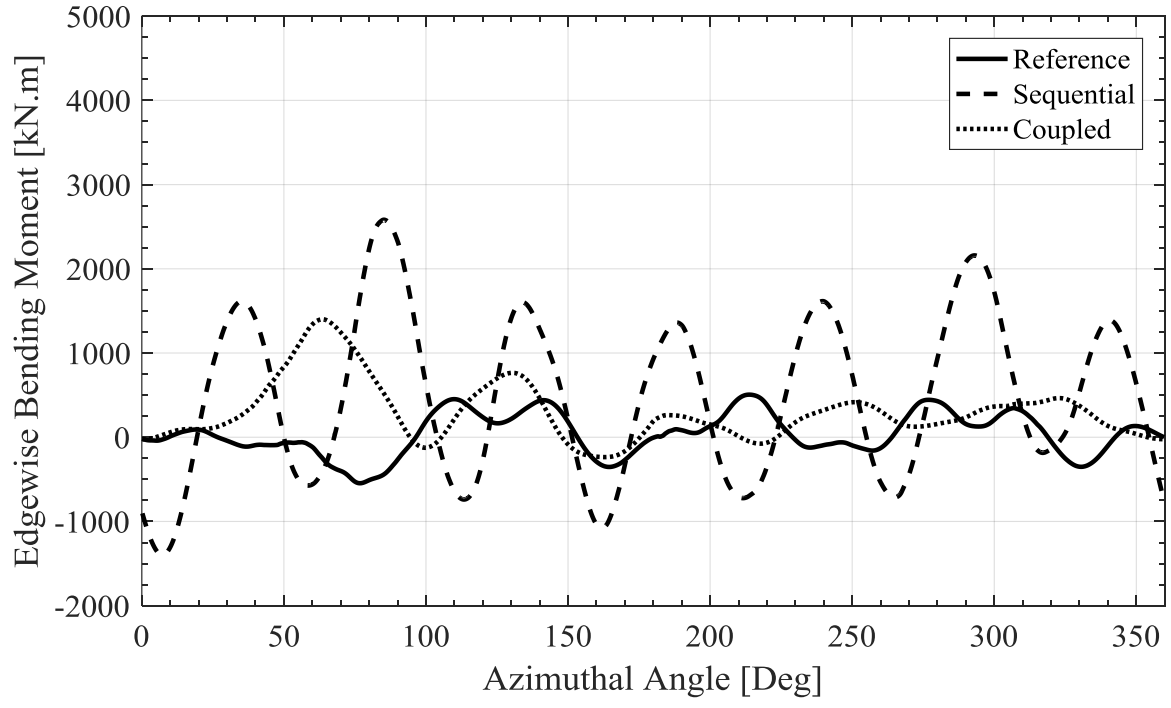

Figure 5.21: Edgewise bending moment variation for a complete revolution at 33.5% blade length for the reference and optimized turbines.

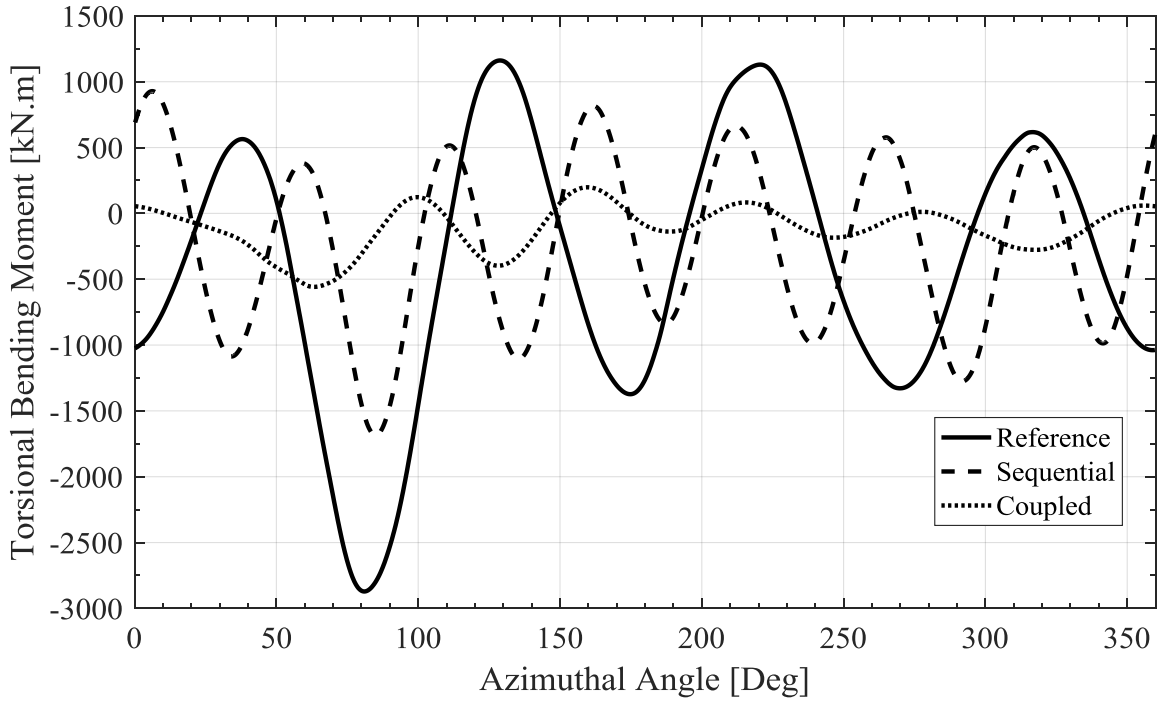

Figure 5.22: torsional moment variation for a complete revolution at 33.5% blade length for the reference and optimized turbines.

It remains in the structural analysis of the turbines to show the internal thickness of blade along the root and the equator section and also to show the cross-sectional properties of the blade that results from the internal thickness.

Table 5.5 shows a comparison between the reference and optimized turbines in the internal thickness of the blade material. For reference to the different thickness, the reader should refer to Table 4.1 and Figure 4.5. From Table 5.5 it can be seen that the reference turbine always has higher thickness as compared to the optimized turbines (except for $t_{3\ equa}$ in which the coupled turbine has the highest thickness). For all the turbines, it can be seen that the thickness at the root for any zone is always larger than the thickness at the equator section. This choice is definitely due to the higher internal loads at the roots that require more

material to handle the stress. Table 5.5 shows also that the optimizer choses larger values of thickness for zone 1 compared with zone 2. This is probably to increase the flapwise stiffness.

Figure 5.23 shows a comparison between the reference and optimized turbines in terms of the blade cross-sectional properties. From Figure 5.23 we can see that the different cross-sectional properties have two unique values, one for the root section and another for the equator section. The root section always has higher values of all cross-sectional properties as compared to the equator section. Regarding the flapwise and edgewise stiffness, we can see that the sequential design has the highest stiffness among the other two turbines. The value of the flapwise and edgewise stiffness at the equator section are very similar when the reference and sequential design are compared, however, the values at the root are very different. It is interesting to note that although the reference turbine uses larger thickness as compared to the sequential design, the sequential design still achieves higher stiffness values. The higher stiffness of the sequential design is probably because the sequential design turbine has larger chord length compared with the reference turbine, therefore the results suggest that it is possible to have higher stiffness values using less material thickness. The coupled design is seen to have the lowest stiffness along the whole blade length when compared with the reference and sequential design turbines. In general, the edgewise stiffness is an order of magnitude larger as compared to the flapwise stiffness. In contrast to the bending stiffness, the reference turbine has the highest torsional stiffness. Torsional stiffness for all turbines is smaller than the flapwise and edgewise stiffness. The variation in mass per unit length of the blade is seen to follow the same trends in the blade total mass, i.e., the coupled design has the lowest linear mass density followed by the sequential design and then the reference design, which is the heaviest amongst all the turbines.

Table 5.5: Comparison between the reference and optimized turbines in the internal thickness of the blade material.

Thickness [mm]	Reference	Sequential	Coupled
$t_{1\ root}$	46.70	20.63	13.32
$t_{1\ equa}$	13.19	11.12	7.56
$t_{2\ root}$	11.27	8.25	6.16
$t_{2\ equa}$	21.41	7.73	5.47
$t_{3\ root}$	13.02	4.44	11.27
$t_{3\ equa}$	5.75	3.01	8.69

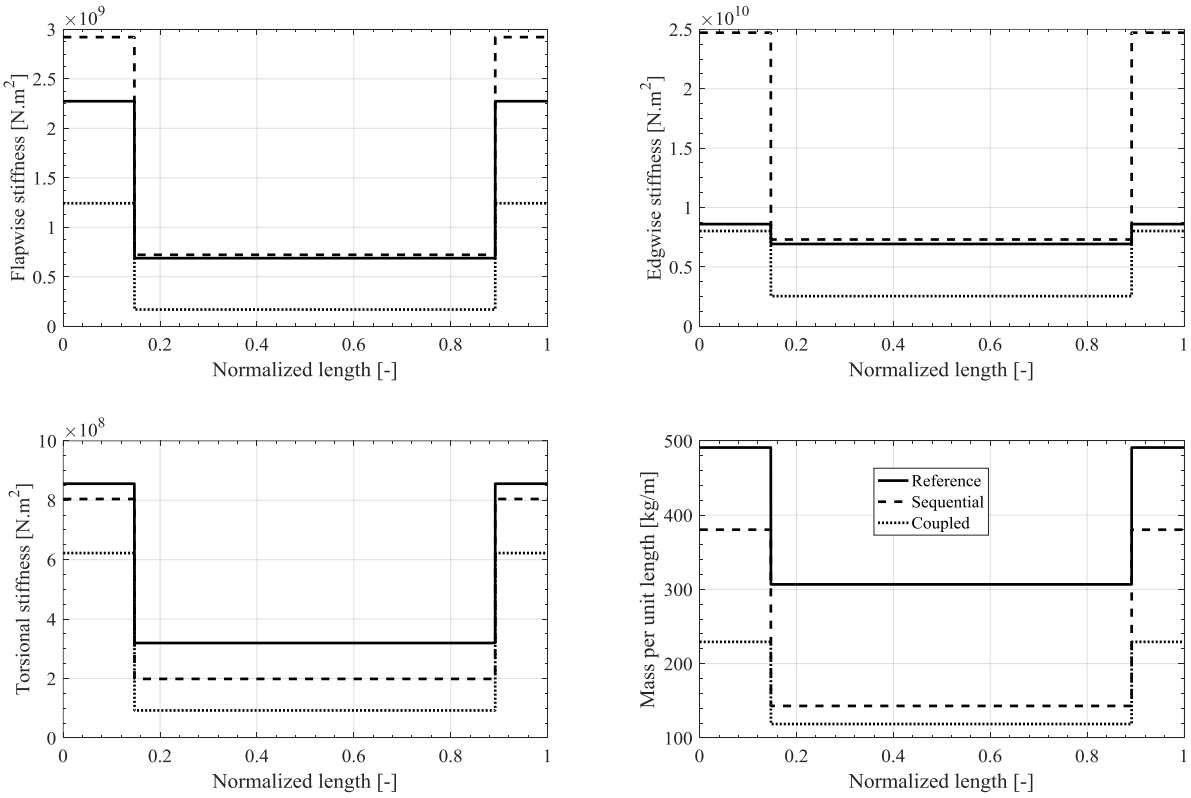

Figure 5.23: Comparison between the reference and optimized turbines in terms of the blade cross-sectional properties.

5.3 Comparison between VAWT Designs for High and Low Wind

In this section, a short comparison between two turbines designed for a 10 m/s and 7.5 m/s annual averaged wind speed. Both turbines are designed using the coupled optimization approach. The two turbines will be referred to in this section as the high and low designs corresponding to the 10 m/s (high wind speed) and 7.5 m/s (low wind speed) respectively. Both turbines are designed to have a rated power of 5MW. The low design is precisely the coupled design presented in the last section. The high design is obtained similarly to the low designed except that when calculating the objective function, the AEP calculation is performed with a Weibull distribution that has 10 m/s averaged wind speed.

Figure 5.24 shows a comparison between the low and high optimized designs regarding m/AEP. In the figure, AEP for both low and high turbines were calculated using wind speed of 7.5 m/s and 10 m/s. Figure 5.24 shows that the values of m/AEP for both turbines are very close to each other and they can be considered the same. Of course, there is a slight advantage of the low design in the high wind setting and advantage of the high design in the low wind setting which is kind of counter intuitive. Nevertheless, the variation is small and can be considered practically negligible as it is less than a percent.

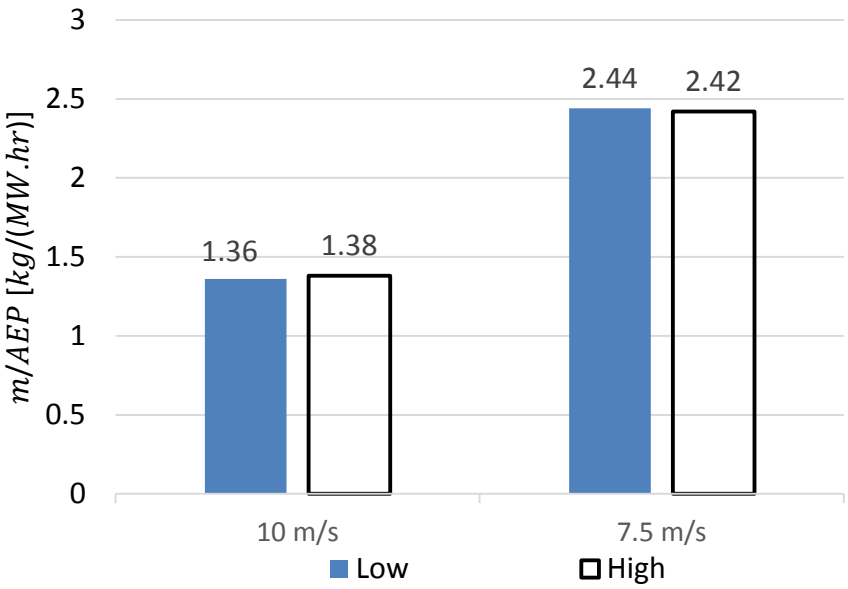

Figure 5.24: Comparison between the low and high optimized turbines in terms of $\boldsymbol{m/AEP}$

Comparison of the component of m/AEP, namely AEP and blade mass is shown in Figure 5.25 and Figure 5.26. We can see form Figure 5.25 that the high design have always higher AEP than the low design. In particular, for a 7.5 m/s average wind speed, the high design has about 4% higher AEP compared with the low design. For the case of 10 m/s average wind speed, the high design achieves 2% higher AEP compared with the low design. In terms of the blade mass, Figure 5.26 shows that the high design has higher blade mass than the low design (about 3% more). Comparing Figure 5.25 and Figure 5.26 we can see that the optimizer tries to balance the increase in blade mass by increasing AEP for the high design to keep the ratio f m/AEP relatively constant in comparison with the low design. No real benefit is seen when a turbine is designed for high wind speed compared when it is designed for low wind speed. There is slightly higher AEP that can be obtained, but at the cost of slightly higher blade mass.

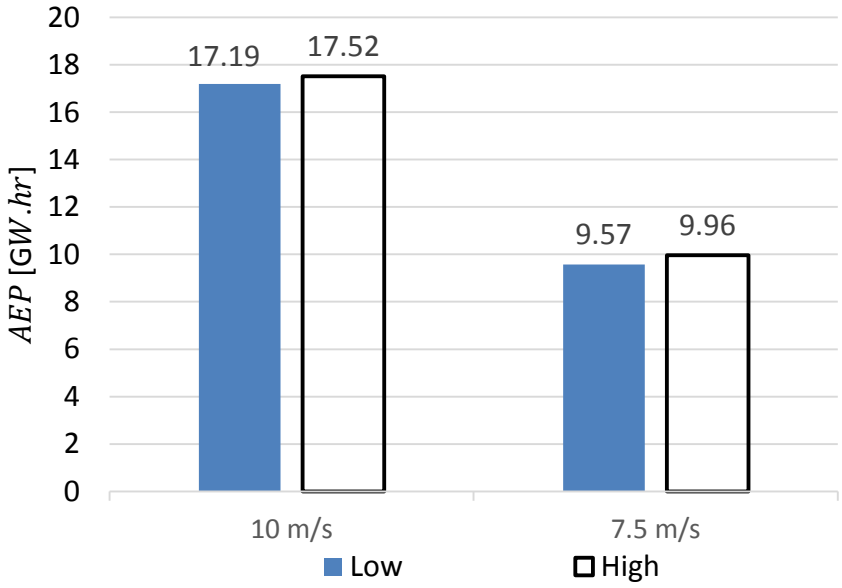

Figure 5.25: Comparison between the low and high optimized turbines in terms of ***AEP***

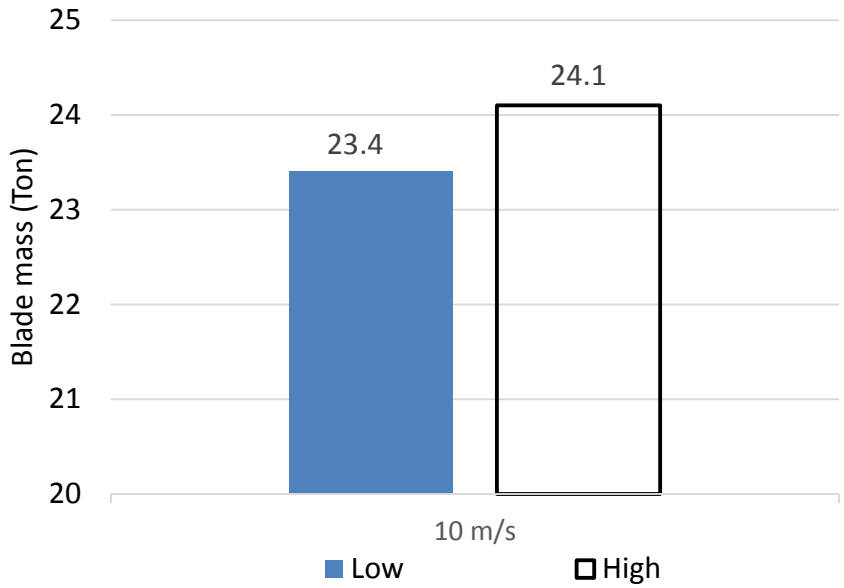

Figure 5.26: Comparison between the low and high optimized turbines in terms of blade mass.

Figure 5.27 shows a comparison between the low and high designs regarding the outer turbine shape. Figure 5.27 explains the increase in AEP for the high design. The increase in AEP can be seen as a result of increasing the turbine height and diameter which results in an increase in the frontal area. This increase in the frontal area for the high design was accompanied by an increase in the blade mass due to the increase in the total blade length. Figure 5.27 shows that the low and high designs have the same Troposkien shape when it comes to the location of maximum radius.

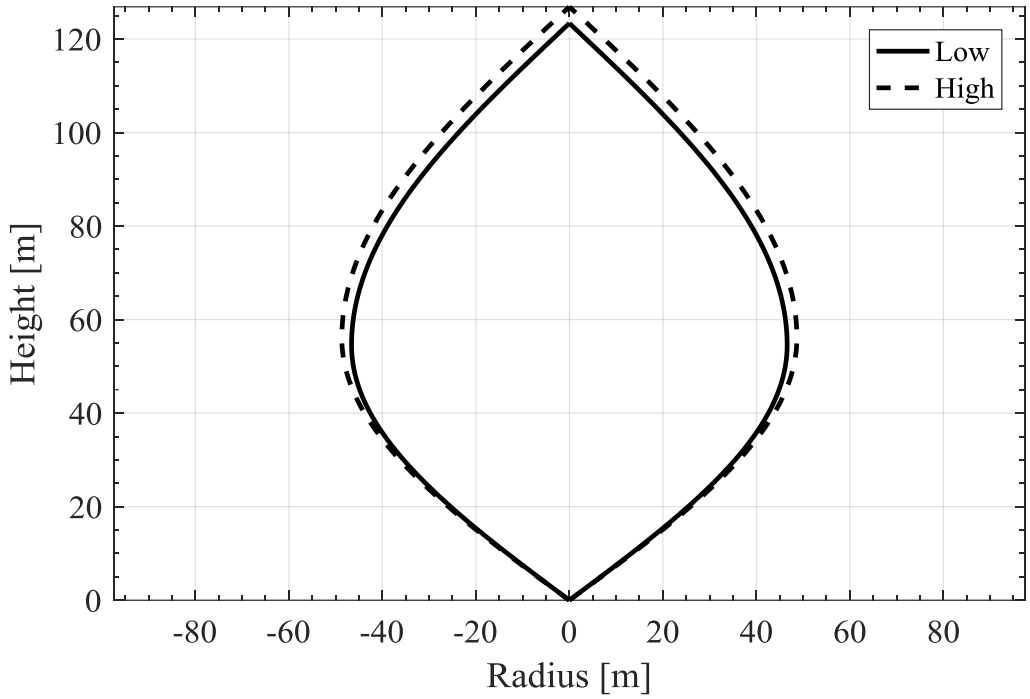

Figure 5.27: Turbine outer shape comparison between the low and high optimized turbines.

5.4 Comparison between 2, 3.75, and 5 MW Designs

In this section, a comparison between optimized designs that have 2, 3.75, and 5MW power ratings is presented. The primary objective of this comparison is to see how the optimized designs are scaled for different rating and how the m/AEP objective varies for different power ratings. The optimized designs were obtained using the coupled approach. The 5MW design is precisely the same as the coupled design presented in section 5.2.

Figures 5.29, 5.30, and 5.32 show m/AEP, AEP, and blade mass comparison between optimum designs with different power rating. Figure 5.29 shows that as the power rating of the turbine decreases, m/AEP value decreases as well indicating an advantage to using smaller

rating turbines to achieve a lower cost of energy. For instance, the 2MW and 3.75MW designs achieves 25.7% and 9.8% reduction in m/AEP compared with the 5MW design respectively. AEP for smaller rating turbine is smaller compared with the 5MW design as can be seen in Figure 5.30. This is of course expected since with the decrease in turbine power rating there is also an associated decease in overall dimensions of the turbine. The blade mass follows AEP trends with power rating, i.e., the blade mass decreases as the power rating decreases as can be seen in Figure 5.30. As the power rating of the turbine is decreased, the optimizer balances the decrease in AEP with an even larger decrease in the blade mass in order to drive the ratio m/AEP to be small quantity.

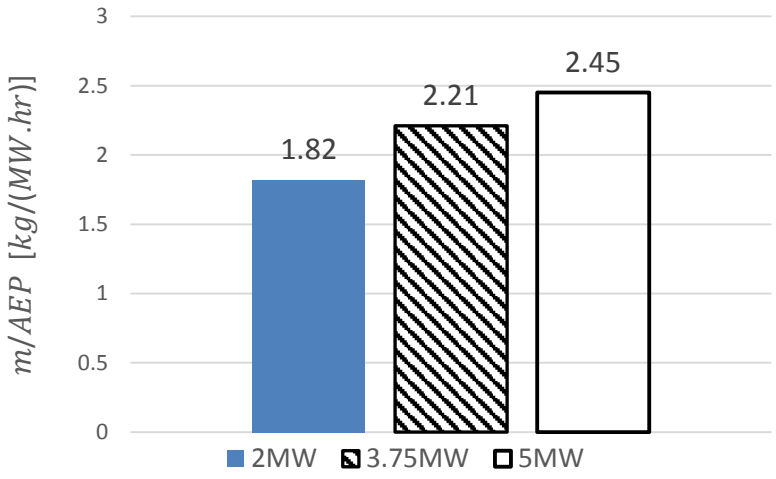

Figure 5.28: Comparison between the optimized designs with different power rating in terms of $\boldsymbol{m/AEP}$ values.

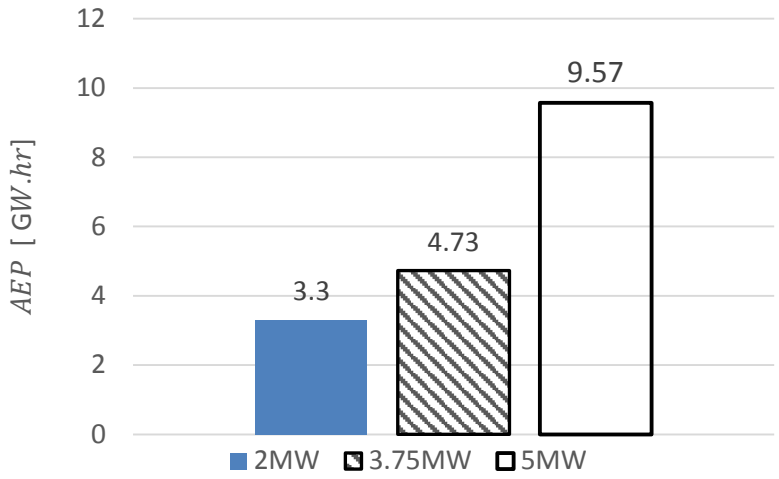

Figure 5.29: Comparison between the optimized designs with different power rating in terms of ***AEP*** values.

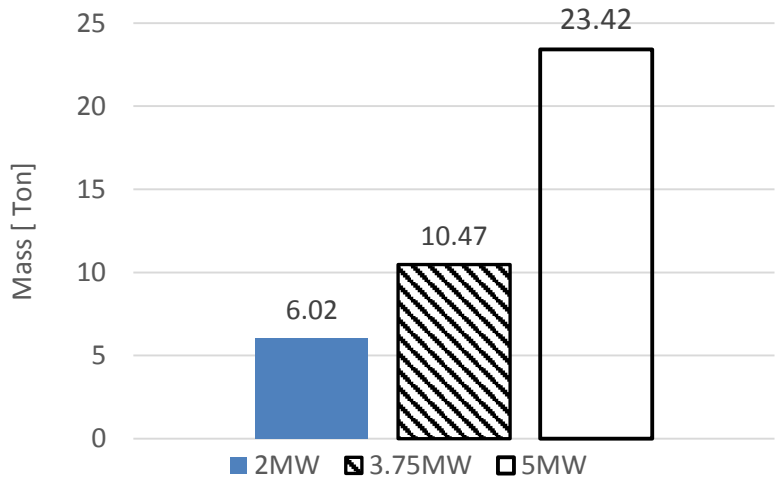

Figure 5.30: Comparison between the optimized designs with different power rating in terms of blade mass values.

Figure 5.31 shows the outer shape of the optimized designs. The figure shows that the optimizer chooses to decrease the size of the turbine as the power rating decreases to reduce the blade mass as much as possible. It is interesting to notice from Figure 5.31 that the frontal area of the turbine does not scale linearly with power rating but instead scales exponentially. It seems that the optimizer prefers to decrease the mas more that increasing AEP as was observed in an earlier section. This trend can be seen to persist for this optimization case as well.

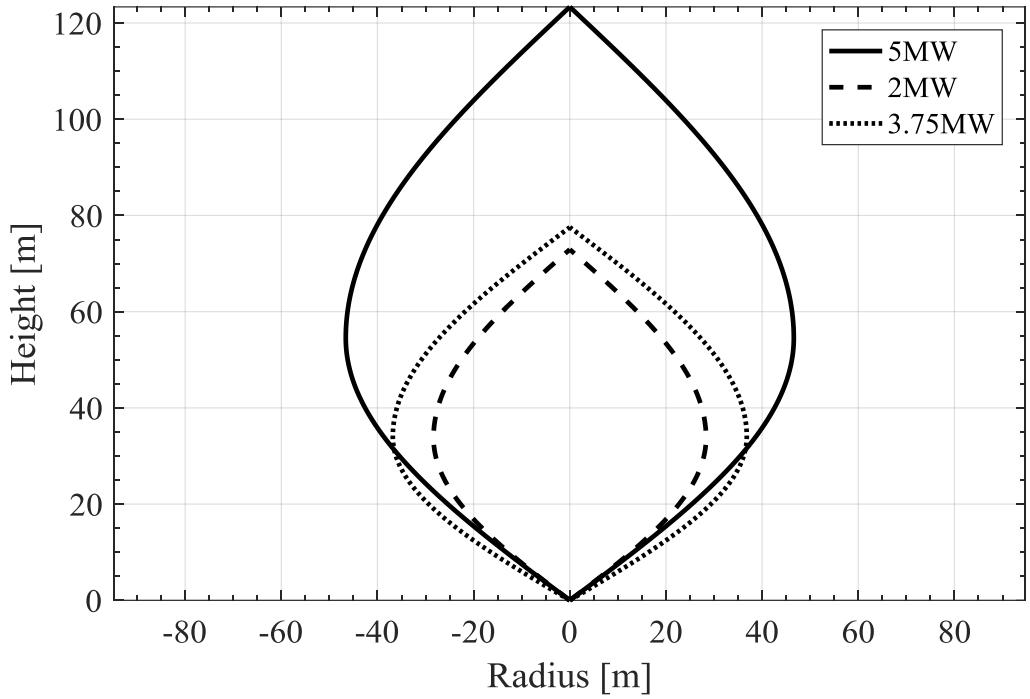

Figure 5.31: Turbine outer shape comparison between optimized designs with different power rating.

A quantity that is worth looking at is the capacity factor. Capacity factor is defined as the ratio between the turbine AEP and the energy obtained if the turbine produced continuously the rated power for a whole year. Figure 5.32 shows the capacity factor for the three different power rating turbines. Figure 5.32 shows that the 5MW designs is superior in terms of the capacity factor while the 3.75 MW has the lowest capacity factor. Since the three turbines operate at the same wind resource (7.5 m/s annual averaged wind speed) and they have roughly the same aerodynamic efficiency (power coefficient for below rated wind speed are very similar) then the reason for capacity factor differences is mainly due to the frontal area of the turbine. The frontal area of the 3.75MW design seems to be smaller than what is supposed to be, and this can be inferred from Figure 5.31. Small frontal area means that less energy can be generated at any given wind speed and that is why the 3.75MW designs has a low capacity factor. It is worth to mention here that the objective is to minimize m/AEP, hence the optimizer might sacrifices the capacity factor by lowering the mass to achieve overall all low m/AEP.

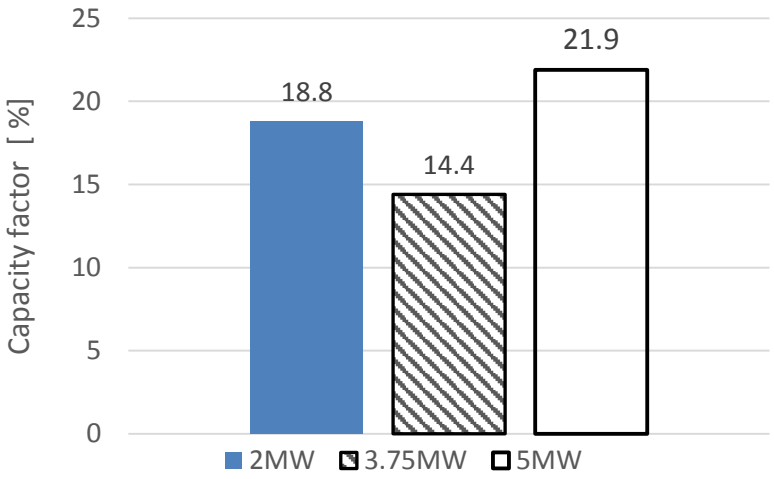

Figure 5.32: Comparison between the optimized designs with different power rating in terms of the capacity factor.

CHAPTER 6

CONCLUSIONS AND RECOMMENDATIONS FOR FUTURE RESEARCH

In this final chapter, the important conclusions of this study are presented followed by recommendations for further research in the area of VAWT optimization.

6.1 Conclusions

This study presents a coupled aerodynamic and structural optimization framework for vertical axis wind turbines. The primary objective is to find a turbine design that minimizes the cost of energy. The framework presented uses simulation tools that were developed at Technical University of Denmark (DTU Wind Energy). These tools includes HAWC2 and BECAS codes and were employed to obtain the aeroelastic response of the turbine. A MATLAB interface was developed to communicate between the different simulation tools and to perform the optimization. Vertical axis wind turbine designs with low blade mass to annual energy production ratio (m/AEP) is achieved using the optimization formulation presented in this thesis. Since the (m/AEP) ratio directly relates to the cost of energy for a turbine, minimizing (m/AEP) yields designs with low cost of energy.

Several optimum designs are obtained using the present optimization framework. Some designs are obtained by coupling the aerodynamic and structural variables employing a single

multi-disciplinary objective function. This design approach is referred to as the coupled design method. Other designs were obtained by sequentially varying the aerodynamic and structural variables by employing a sequence of single discipline objective functions. This design approach is referred to as the sequential design method. The coupled design methodology are used to design 2, 3.75, and 5 MW VAWTs whereas the sequential methodology are used to design a single 5 MW VAWT. In addition, the coupled methodology are used to compare VAWT designs using low (7.5 m/s) and high (10 m/s) annual averaged wind speeds.

The sequential design was obtained by first maximizing AEP, while keeping the internal structure of the blade fixed, and then minimizing the mass while keeping the outer shape of the blade fixed. The coupled optimization on the other hand, combines both objectives into one which is to minimize the ratio m/AEP.

The DeepWind 5MW concept design was used as a reference to compare the optimized 5MW designs and to see the level of improvement the optimization framework can achieve relative to the reference turbine.

Comparison between reference, sequential, and coupled 5MW designs show that the optimization framework can reduce m/AEP relative to the reference value by 52.4% and 42.5% for coupled and sequential designs respectively. The coupled design achieve the low m/AEP value by reducing the blade mass more than increasing AEP. On the other hand, the sequential design weights AEP more than blade mass hence the reduction in m/AEP comes from increasing AEP with higher proportion compared with blade mass. In terms of the overall design of the turbine, coupled and sequential designs have higher solidity, tip speed ratio, and height to diameter ratio compared with the reference design. Extended height to diameter ratio obtained by the optimized designs indicates that the frontal are the turbine is enlarged by increasing the height more than the diameter. Structurally, the optimized designs archives

lower failure index compared with the reference design and have smaller bending moments at the lower blade root. It was concluded that the coupled optimization approach is more mass biased due to the higher sensitivity of the structural design variables on the objective function m/AEP compared with aerodynamic variable sensitivities. This difference in objective function variable sensitivities makes the optimizer mass biased when it comes to minimize m/AEP ratio. Since the overall objective of the design is to find the lowest possible m/AEP, it is concluded that the coupled optimization approach is better compared with the sequential optimization approach.

The designs for 7.5 m/s and 10 m/s annual averaged wind speed have very similar characteristics. The only small difference is that the high wind design has slightly higher mass and AEP compared with a low wind design. The m/AEP for both turbines are very close from each other indicating that for a 5MW turbine designed using the coupled optimization scheme, annual average wind speed choice does not change the overall design.

The effect of the power rating of the turbine on m/AEP was investigated by designing a 2MW and 3.75 MW using the coupled optimization and comparing the results with the 5MW coupled optimized design. The results show that m/AEP decreases with the decrease in power rating meaning that the 2MW has the lowest m/AEP value overall. This reduction in m/AEP was achived by tremendous decrease in the blade mass that allows the 2MW designs to have small m/AEP albeit its low AEP. On the other hand, the capacity factor comparison for the different power rating turbines show that the 5MW design archives the highest capacity factor among the other two lower power rating turbines.

6.2 Recommendations for Future Research

In this section, recommendations to enhance the capabilities of the current optimization framework are highlighted that requires furthur explorations and research with the primary objective to achieve the lowest possible cost of energy.

Use of different blade airfoil

In this thesis, NACA 4-digit symmetric airfoils were the only airfoil type used for the turbine blade. Specifically, NACA0018 and NACA0025 were used for the equator and chord sections respectively. Other types of airfoils need to be used to enhance the aerodynamic efficiency and increase AEP. Adding the airfoil type as a design variable can also help identify the best airfoil for each turbine design but at an added computational cost. Choosing from a set of airfoils implies discrete design variable which needs to be handled by other than gradient-based optimizers. It is also possible to make the airfoil type a continuous variable if for example the thickness to chord ratio is chosen as the driver for changing the airfoil type and in addition, the airfoil polars are calculated from a code like XFOIL.

Extent of root and equator sections

In this thesis, two main blade sections were used, the root and equator sections. The location of the root and equator sections were fixed by constraining the lower and upper roots extension to be always 14.6% and 10.8% of the total blade length respectively regardless of the blade shape and total length. These fixed values were chosen based on the DeepWind blade and might not be the optimum choice for all designs. Making the extent of the root and equator sections a design variable might help in reducing the mass and improving the overall aerodynamics of the design.

Incorporation of fatigue constraints

Ultimate strength was used in this thesis as the primary structural constraint. Fatigue analysis needs to be considered and included in the constraints. Fatigue constraints might influence the structural design which will lead to changes in the blade mass. also, fatigue analysis will give a good estimate of the lifetime of the blade which is necessary information to know in designing real turbines.

Inclusion of dynamic response

Mode shapes and frequencies for the optimized designs have not been analyzed in this thesis. Analysis of the mode shapes and frequencies are essential in avoiding resonance especially that all optimized designs presented have variable rotor speed operation. A constraint can be set to have a margin between any mode frequency and the harmonics of the rotor rotation frequency. In this way, the possible catastrophic resonance can be avoided making the design more robust.

Addition of minimum constraints for capacity factor or AEP

Optimum designs obtained using the coupled approach give low values of m/AEP which is desirable outcome. However, AEP values were rather low. It might be a good idea to impose a minimum constraint on the capacity factor or AEP to force the optimizer to look in the regions of design space where moderate to high values of AEP is a possibility. This approach might actually produce designs with even lower m/AEP than what was obtained in this thesis. Another suggestion is to reformulate the objective function so that the blade mass and AEP can have different weights. This approach can also limit the optimizer bias to lower the blade mass without increasing AEP.

Topology optimization

Only one topology and configuration was considered in this work which is a two-bladed Darrius VAWT. Different topologies worth investigations since they might produce designs with better cost of energy. Such topologies include but not limited to: three bladed Darrius, straight bladed VAWT with two and three blades, and Darrius VAWT with support struts near the roots. In addition, the use of guy wires to enhance the structural integrity and stability of the tower can be investigated. Different topologies can also be considered for the design of the internal thickness distribution of the blade. Different material distribution can be considered that focus on strengthening the shear and tensile strengths where they are needed inside the blade. Shear webs can be given the freedom to be angled instead of being only vertical.

Global optimization

In this work, the optimization algorithm used is a local optimization method. When using local optimization method, there is no guarantee that the solution obtained is the global minimum in the design space. Using global optimization algorithm might give designs with better objective overall. Multi-start method (choosing multiple starting design vector) with local optimizer might be an excellent way to see whether the optimizer reported a local or a global minimum. As the design space gets larger and larger, the number of local minima will probably increase as well warranting the use of global optimization algorithm. Global optimization algorithm comes at a higher computational cost compared with local optimization especially if non-gradient methods are used.

System-level optimization

Realistic design of wind turbine needs to incorporate the design of the tower, drivetrain, generator, and controller in addition to the blade design. Incorporating all these subcomponents

also requires a cost model that takes into account the change of the total cost of the turbine due to changes in the subcomponent design. Performing system level optimization requires careful choice of the design space with proper turbine parametrization. The cost model is also a necessity especially if the cost of energy is the objective function chosen for optimality condition. Computational cost is expected to grow hugely due to the increase in the design space and the addition of new types of analysis tools required to capture all subcomponent responses.

REFERENCES

[1] Frankfurt School-UNEP Center, "Global Trends in Renewable Energy Investment 2018," 2018.

[2] Global Wind Energy Council, "Global Wind Report," 2018.

[3] L. Fried, S. Shukla, S. Sawyer, and S. Teske, "Global Wind Energy Outlook 2016," Global Wind Energy Council, 2016.

[4] H. J. Sutherland, D. E. Berg, and T. D. Ashwill, "A Retrospective of VAWT Technology," Sandia National Laboratories, Albuquerque, New Mexico, SAND2012-0304, 2012.

[5] B. C. Owens, "Theoretical Developments and Practical Aspects of Dynamic Systems in Wind Energy Applications," Ph.D. dissertation, Texas A&M University, 2013.

[6] M. J. Fowler *et al.*, "Hydrodynamic Module Coupling in the Offshore Wind Energy Simulation (OWENS) Toolkit," presented at the ASME 2014 33rd International Conference on Ocean, Offshore and Arctic Engineering, San Francisco, California, USA, 2014, p. V09BT09A027.

[7] C. Galinos, "Study of Design Load Cases for Multi-Megawatt Onshore Vertical Axis Wind Turbines," Master Thesis, DTU Wind Energy, 2015.

[8] D. Marten *et al.*, "Validation and comparison of a newly developed aeroelastic design code for VAWT," in *35th Wind Energy Symposium*, Grapevine, Texas, 2017.

[9] U. S. Paulsen *et al.*, "1st DeepWind 5 MW Baseline design," *Energy Procedia*, vol. 24, pp. 27–35, 2012.

[10] F. Savenije, "S4VAWT Floating vertical axis wind turbines with pitched blades," Netherlands, ECN-M—16-049, 2016.

[11] M. Barone and J. Paquette, "Vertical-axis wind turbine revisited: A sandia perspective." Sandia National Laboratories, 2012.

[12] A. Ning, R. Damiani, and P. Moriarty, "Objectives and Constraints for Wind Turbine Optimization," in *51st AIAA Aerospace Sciences Meeting including the New Horizons Forum and Aerospace Exposition*, 2013.

[13] S. Andrew Ning, R. Damiani, and P. J. Moriarty, "Objectives and Constraints for Wind Turbine Optimization," *J. Sol. Energy Eng.*, vol. 136, no. 4, pp. 041010-041010–12, Jun. 2014.

[14] G. S. Bir, "User's Guide to PreComp (Pre-Processor for Computing Composite Blade Properties)," National Renewable Energy Laboratory, Golden, Colorado, NREL/TP-500-38929, Jan. 2006.

[15] L. J. Fingersh, M. M. Hand, and A. S. Laxson, "Wind turbine design cost and scaling model," National Renewable Energy Laboratory, Golden, Colorado, NREL/TP-500-40566, Dec. 2006.

[16] J. Jonkman, S. Butterfield, W. Musial, and G. Scott, "Definition of a 5-MW reference wind turbine for offshore system development," National Renewable Energy Laboratory, Golden, Colorado, NREL/TP-500-38060, 2009.

[17] W. Xudong, W. Z. Shen, W. J. Zhu, J. N. Sørensen, and C. Jin, "Shape optimization of wind turbine blades," *Wind Energy*, vol. 12, no. 8, pp. 781–803, Nov. 2009.

[18] P. Fuglsang and K. Thomsen, “Cost optimization of wind turbines for large-scale offshore wind farms,” Risø National Laboratory, Roskilde, Risø-R-1000, 1998.
[19] P. Fuglsang and K. Thomsen, “Site specific design optimization of wind turbines,” in *1998 ASME Wind Energy Symposium*, 1998.
[20] D. O. Yu, H. M. Lee, and O. J. Kwon, “Aerodynamic shape optimization of wind turbine rotor blades considering aeroelastic deformation effect,” *J. Mech. Sci. Technol.*, vol. 30, no. 2, pp. 705–718, Feb. 2016.
[21] T. Ashuri, M. B. Zaaijer, J. R. R. A. Martins, G. J. W. van Bussel, and G. A. M. van Kuik, “Multidisciplinary design optimization of offshore wind turbines for minimum levelized cost of energy,” *Renew. Energy*, vol. 68, pp. 893–905, Aug. 2014.
[22] G. Hayman, B. Jonkman, and R. Murray, “AeroDyn.” [Online]. Available: https://nwtc.nrel.gov/AeroDyn.
[23] J. Jonkman, “FAST.” [Online]. Available: https://nwtc.nrel.gov/FAST.
[24] F. Zahle, C. Tibaldi, C. Pavese, M. K. McWilliam, J. P. A. A. Blasques, and M. H. Hansen, “Design of an Aeroelastically Tailored 10 MW Wind Turbine Rotor,” *J. Phys. Conf. Ser.*, vol. 753, no. 6, p. 062008, 2016.
[25] “HAWC2 info,” *http://www.hawc2.dk*. [Online]. Available: http://www.hawc2.dk/HAWC2-info. [Accessed: 05-May-2017].
[26] J. P. Blasques and R. D. Bitsche, “BECAS an Open-Source Cross Section Analysis Tool,” presented at the EWEA 2012, Copenhagen, 2012.
[27] C. Bak *et al.*, “The DTU 10-MW Reference Wind Turbine.” DTU Wind Energy, 2013.
[28] F. Zahle, C. Tibaldi, D. R. Verelst, R. Bitche, and C. Bak, “Aero-Elastic Optimization of a 10 MW Wind Turbine,” presented at the 33rd Wind Energy Symposium, 2015.
[29] M. K. McWilliam, F. Zahle, C. Pavese, and J. P. Blasques, “Multi-fidelity Optimization of Horizontal Axis Wind Turbines,” presented at the 35th Wind Energy Symposium, 2017.
[30] C. L. Bottasso, F. Campagnolo, and A. Croce, “Multi-disciplinary constrained optimization of wind turbines,” *Multibody Syst. Dyn.*, vol. 27, no. 1, pp. 21–53, Jan. 2012.
[31] T. J. Carrigan, B. H. Dennis, Z. X. Han, and B. P. Wang, “Aerodynamic Shape Optimization of a Vertical-Axis Wind Turbine Using Differential Evolution,” *Int. Sch. Res. Not. Renew. Energy*, vol. 2012, p. e528418, Jan. 2012.
[32] U. S. Paulsen, H. A. Madsen, J. H. Hattel, I. Baran, and P. H. Nielsen, “Design Optimization of a 5 MW Floating Offshore Vertical-axis Wind Turbine,” *Energy Procedia*, vol. 35, pp. 22–32, Jan. 2013.
[33] V. Kumar, M. Paraschivoiu, and I. Paraschivoiu, “Low Reynolds Number Vertical Axis Wind Turbine for Mars,” *Wind Eng.*, vol. 34, no. 4, pp. 461–476, Jun. 2010.
[34] G. Bedon, M. Raciti Castelli, and E. Benini, “Optimization of a Darrieus vertical-axis wind turbine using blade element – momentum theory and evolutionary algorithm,” *Renew. Energy*, vol. 59, pp. 184–192, Nov. 2013.
[35] R. Sheldahl, “Comparison of field and wind tunnel Darrieus wind turbine data,” Sandia National Labs., Albuquerque, NM, 1981.
[36] G. Bedon, M. Raciti Castelli, and E. Benini, “Optimal spanwise chord and thickness distribution for a Troposkien Darrieus wind turbine,” *J. Wind Eng. Ind. Aerodyn.*, vol. 125, pp. 13–21, Feb. 2014.
[37] G. Bedon, U. Schmidt Paulsen, H. Aagaard Madsen, F. Belloni, M. Raciti Castelli, and E. Benini, “Computational assessment of the DeepWind aerodynamic performance with different blade and airfoil configurations,” *Appl. Energy*, vol. 185, Part 2, pp. 1100–1108, Jan. 2017.
[38] I. Paraschivoiu, O. Trifu, and F. Saeed, “H-Darrieus wind turbine with blade pitch control,” *Int. J. Rotating Mach.*, vol. 2009, 2009.

[39] L. Song, H.-Z. Liu, and Z.-X. Yang, "Orthogonal Analysis Based Performance Optimization for Vertical Axis Wind Turbine," *Math. Probl. Eng.*, vol. 2016, p. e6241360, Feb. 2016.
[40] A. Bianchini, G. Ferrara, and L. Ferrari, "Design guidelines for H-Darrieus wind turbines: Optimization of the annual energy yield," *Energy Convers. Manag.*, vol. 89, pp. 690–707, Jan. 2015.
[41] M. Jafaryar, R. Kamrani, M. Gorji-Bandpy, M. Hatami, and D. D. Ganji, "Numerical optimization of the asymmetric blades mounted on a vertical axis cross-flow wind turbine," *Int. Commun. Heat Mass Transf.*, vol. 70, pp. 93–104, Jan. 2016.
[42] A. Shires, "Design optimisation of an offshore vertical axis wind turbine," *Proc. Inst. Civ. Eng. - Energy*, vol. 166, no. 1, pp. 7–18, Feb. 2013.
[43] M. Schelbergen, "Structural Optimization of Multi-Megawatt, Offshore Vertical Axis Wind Turbine Rotors," Master Thesis, TU Delft, 2013.
[44] B. Roscher, "Structural Optimization Of A Vertical Axis Wind Turbine With Aeroelastic Analysis," Master Thesis, Technical University of Denmark (DTU), Denmark, 2014.
[45] B. Roscher, C. S. Ferreira, L. O. Bernhammer, H. A. Madsen, D. T. Griffith, and B. Stoevesandt, "Combined structural optimization and aeroelastic analysis of a Vertical Axis Wind Turbine," in *33rd Wind Energy Symposium*.
[46] I. PARASCHIVOIU, "Double-multiple streamtube model for studying vertical-axis wind turbines," *J. Propuls. Power*, vol. 4, no. 4, pp. 370–377, Jul. 1988.
[47] I. Paraschivoiu, *Wind Turbine Design: With Emphasis on Darrieus Concept*, 1st ed. Canada: Polytechnic International Press, 2002.
[48] K. R. Dixon, "The Near Wake Structure of a Vertical Axis Wind Turbine," Ph.D. dissertation, Technical University of Delft (TU Delft), 2008.
[49] C. Ferreira, "The near wake of the VAWT," Ph.D. dissertation, Technical University of Delft (TU Delft), 2009.
[50] J. Murray and M. Barone, "The Development of CACTUS, a Wind and Marine Turbine Performance Simulation Code," presented at the 49th AIAA Aerospace Sciences Meeting, Orlando, Florida, 2011.
[51] D. Marten, M. Lennie, G. Pechlivanoglou, C. N. Nayeri, and C. O. Paschereit, "Implementation, Optimization, and Validation of a Nonlinear Lifting Line-Free Vortex Wake Module Within the Wind Turbine Simulation Code qblade," *J. Eng. Gas Turbines Power*, vol. 138, no. 7, pp. 072601-072601–10, Dec. 2015.
[52] D. Marten, "QBlade v0.95 Guidelines for Lifting Line Free Vortex Wake Simulations." TU Berlin, 2016.
[53] B. Owens, J. Hurtado, J. Paquette, D. Griffith, and M. Barone, "Aeroelastic Modeling of Large Offshore Vertical-axis Wind Turbines: Development of the Offshore Wind Energy Simulation Toolkit," presented at the 54th AIAA/ASME/ASCE/AHS/ASC Structures, Structural Dynamics, and Materials Conference, Boston, Massachusetts, 2013.
[54] T. J. Larsen and A. M. Hansen, *How 2 HAWC2, the user's manual*. Roskilde: Risø National Laboratory, 2015.
[55] H. Madsen, T. Larsen, L. Vita, and U. Paulsen, "Implementation of the Actuator Cylinder flow model in the HAWC2 code for aeroelastic simulations on Vertical Axis Wind Turbines," presented at the 51st AIAA Aerospace Sciences Meeting including the New Horizons Forum and Aerospace Exposition.
[56] C Simão Ferreira and H Aagaard Madsen and M Barone and B Roscher and P Deglaire and I Arduin, "Comparison of aerodynamic models for Vertical Axis Wind Turbines," *J. Phys. Conf. Ser.*, vol. 524, no. 1, p. 012125, 2014.
[57] "HAWC2 online course." Technical University of Denmark (DTU), 2013.

[58] J. P. A. A. Blasques, “Optimal design of laminated composite beams,” Ph.D. Thesis, Technical University of Denmark (DTU), Denmark, 2011.
[59] J. P. Blasques and M. Stolpe, “Multi-material topology optimization of laminated composite beam cross sections,” *Compos. Struct.*, vol. 94, no. 11, pp. 3278–3289, Nov. 2012.
[60] “User’s Manual for BECAS - a cross section analysis tool for anisotropic and inhomogeneous beam sections of arbitrary geometry,” DTU Wind Energy, 2015.
[61] A. R. Parkinson, R. Balling, and J. D. Hedengren, *Optimization methods for Engineering design*. Brigham Young University, 2013.
[62] D. R. Verelst, H. Aagaard Madsen, K. A. Kragh, and F. Belloni, “Detailed Load Analysis of the baseline 5MW DeepWind Concept,” Technical University of Denmark (DTU), DTU Wind Energy Report Number E-0057, 2014.
[63] F. Saeed, I. Paraschivoiu, O. Trifu, M. Hess, and C. Gabrys, “Inverse Airfoil Design Method for Low-Speed Straight-Bladed Darrieus-Type VAWT Applications,” *Wind Eng.*, vol. 35, no. 3, pp. 357–367, Jun. 2011.
[64] C. S. Ferreira and B. Geurts, “Aerofoil optimization for vertical-axis wind turbines,” *Wind Energy*, vol. 18, no. 8, pp. 1371–1385, Aug. 2015.
[65] D. Ragni, C. S. Ferreira, and G. Correale, “Experimental investigation of an optimized airfoil for vertical-axis wind turbines,” *Wind Energy*, vol. 18, no. 9, pp. 1629–1643, Sep. 2015.
[66] C. Simao Ferreira, M. F. Barone, A. Zanon, R. Kemp, and P. Giannattasio, “Airfoil optimization for stall regulated vertical axis wind turbines,” in *33rd Wind Energy Symposium*, 0 vols., American Institute of Aeronautics and Astronautics, 2015.

VITAE

Ali Salman Alhamaly was born in Dammam Saudi Arabia on January 16, 1992. Upon graduation from high school in 2009, Ali attended Saudi Aramco College Degree Program for non-Employees to complete his college education in mechanical engineering. He attended Virginia Tech from 2010 to 2014 and graduated with major in mechanical engineering in addition to minors in mathematics and physics. In 2014 he joined Saudi Aramco as a full time employee working in Dhahran. Ali entered the graduate school program of King Fahd University of Petroleum and Minerals (KFUPM) in 2015 as a part-time student aiming to get a Master of Science degree in mechanical engineering. His research in the master program was about wind turbine design and optimization. Ali earned a Master of Science degree from KFUPM in May 2018.

Address: 6491 18D- An Nasirah
Al Qatif 32641-3350
Saudi Arabia